

博士学位論文

超薄分子組織化膜技術の新潮流

— "有機化無機ナノ粒子" と
"高分子トポロジー化学" への展開 —

埼玉大学 大学院理工学研究科 博士後期課程
理工学専攻
物質科学コース

孟 起

平成 30 年度

Doctoral Thesis

New Trend of Techniques for Ultra-Thin Organized Molecular Films

- Developments into "Organ-Modified Inorganic
Nanoparticles" and " Topological Chemistry of Polymers" -

Graduate School of Science and Engineering

Saitama University

Qi Meng

March 2019

<< Contents >>

Chapter 1. General Introduction	1
1.1 Background	2
1.2 Heat-Registrant Nanodiamond Layers	6
1.3 Topological Polymers	10
1.4 This Study	13
Chapter 2. Materials and Methods	16
2.1 Nanodiamond Preparation	16
2.2 Types of Modified Agents Used in This Study and Their Modification Reaction	16
2.3 Aggregated Particle Size Evaluation of Dispersion Medium	20
2.4 Formation of Single Particle Layer on the Water Surface	20
2.5 Transferring of Organized Particle Layer onto Solid Substrate and Its Evaluation	21
2.6 Preparation and characterization of organo-modified ND	24
2.7 Formation of monolayer on the water surface and estimation of structure and morphology of transferred films	34
2.8 Morphological observation and elucidation of organo-particle arrangement in the integrated layers	34
2.9 Topological Polymers	35
2.10 Structural Estimations of Topological Polymers	35
Chapter 3. Correlation Between Nanodispersion of Organo-Modified Nanodiamond in Solvent and Condensed Behavior of Their Organized Particle Films	38
3.1 Abstract	38
3.2 Evaluation and Calculation of Surface Modification Ratio	39
3.3 Dispersion Behavior of Organo-Modified ND in Polar and/or Nonpolar Solvents	42
3.4 Formation of Single Particle Layers on the Water Surface of Organo-Modified NDs	49
3.5 Characterization of Morphology and Arrangement of Organized Particle Films of Organo-Modified ND on Solid Substrate	52
3.6 Relation between Condensation Behavior at Air/Water Interface and Dispersibility in Solution of Organo-Modified ND	58
3.7 Conclusion	60

Chapter 4. Thermal stability of ordered multi-particle layers of long-chain phosphonate-modified nanodiamond with superior heat-resistance	62
4.1 Abstract	62
4.2 Solid-State Structure and Monolayer Formation of Organo-Modified ND	63
4.3 Multi-Particle Layer Structure of Organo-Modified ND	68
4.4 Discussion	73
4.5 Conclusion	81
Chapter 5. Topological "Interfacial" Polymer Chemistry–Dependency of Polymer "Shape" on Surface Morphology and Stability of Layer Structures when Heating Organized Molecular Films of Cyclic and Linear Block Copolymers of n-Butyl Acrylate–Ethylene Oxide–	83
5.1 Abstract	83
5.2 Monolayer Formation of Topological Polymers at Air/Water Interface	85
5.3 Monolayer Morphology of Topological Polymers on Solid Substrate	94
5.4 Molecular Arrangement of Topological Polymers in Multilayers	99
5.5 Conclusion	104
Chapter 6. Concluding Remarks	106
References and Notes	110
Publications	128
Acknowledgements	134

1. General Introduction

In 1987, the Nobel Prize for Chemistry awarded to the "Contribution to the Development of Supramolecular Chemistry " was based on high evaluation to an academic paper published in 1967, which summarized the complex formation of crown ethers and metal ions. Subsequently, supramolecular chemistry such as cyclodextrin, calixarene, inclusion compound, development of drug delivery system, rotaxane molecule necklace, etc. progress smoothly, and the Nobel Prize in chemistry has been given "Molecular Machines" including catenane etc. in 2016, again. Research of Langmuir-Blodgett (LB) films in which molecules are organized in the same plane at the air / water interface, which are ordered and layered on a solid substrate in a layered manner is one area of such supramolecular chemistry in a broad sense. In this Doctoral thesis, author first indicate the LB film study of "organo-modified inorganic nanoparticles" with organic chain-modified on the surface of nanoparticles as a new development of LB film research. That is to say, it is an example that tried to develop not only surfactants and organic molecules but also inorganic nanoparticles as a technology capable of arrangement, integration, and the layering of inorganic nanoparticles. Here, author have also described "nanodispersion of organo-particles in general organic solvents" as the "preparation process problems of monolayers". Next, author introduce the application to the topological polymers, which is the new trend of current synthetic chemistry of functional polymers. Here, even if the constituent components are the same, it is touched upon the differences in structure and physical properties,

which are indicated by "monomolecular layer state" by polymer groups of different "shapes" such as cyclic, linear, polycyclic, and branched types. In particular, the order maintenance properties of cyclic and linear polymers under heating was simulated, mimicking the heat resistance of bacteria called "thermophilic bacteria".

1-1. Background

Energy production *via* petrochemistry [1] remains the dominant approach used around the world amidst developments in solar power generation and as some countries and local governments (turn away from or shy away from or resist) the use of nuclear power plants [2]. Petrochemistry has produced gasoline [3], gas [4], lubricant oil [5], resin [6], etc. (Figure 1-1). Although oil supply problems [7] have persisted for a long time, the utilization of natural resources will continue for a while owing to the improvement of mining technology [8]. Like gasoline, the polymer industry is significantly affected by changes in crude oil prices. Alternatives to biomass polymers, including poly(L-lactic acid) [9], have been studied for a long time. The lubricant industry is very different in terms of its ripple effect. In the automotive industry, applications such as precision machinery, grease, domestic permeable lubricating oil spray, etc., are versatile. A representative example of a solid lubricant is molybdenum sulfide (MoS) [10]. Normally, particles with a diameter in the order of submicrons are used. What is currently drawing attention is the utilization of nanoparticle systems in the single nanometer

regime. Introducing nanoparticles with a single-digit nanosized diameter into lubricant base oil may smoothen the surface after friction action and reduce the friction coefficient [11, 12]. Previously, Y. Xu, *et al.* reported the synthesis and tribological studies of nanoparticle additives for pyrolysis of bio-oil formulated as diesel fuel [13]. B. Zhao, *et al.* also reported oil-soluble polymer brush grafted nanoparticles as effective lubricant additives for friction and wear reduction [14].

On Apr. 28–29, 2017, an event was held at the Centre national de la recherche scientifique in France, where monomolecular automobiles (nanocars) competed, launching the so-called nanocar race. [15]. An undulating Au substrate surface was utilized as a racing course, and electric pulses from the probe of a scanning tunneling microscope or molecule deformation [16] were used. These molecules traveled along the 100 nm route for 38 h. It was a very innovative and pioneering academic competition. Essentially, if the object moved, friction always occurs. One of the biggest obstacles to the realization of a molecular nanomachine [17] is the friction problem. It is probable that the nanoworld would be impossible in a world with extreme friction. When an object is miniaturized, the ratio of surface area to the volume significantly increases. If this ratio increases, the values of friction significantly increase. By simple calculation, the friction acting on a sphere with a diameter 1 nm reaches 10 million times that of a sphere with a diameter 1 cm [18]. Therefore, if nanometer-sized molecules are designed, there is a possibility that stable driving of molecular motion is restricted by increased friction. However,

if the target corresponds to particles at a single nanometer scale like a nanosphere, then the "rolling force" of the molecule itself is induced. This raises the possibility that the influence on macroscopic friction property has been also induced, resulting in super hierarchical and cooperative extension of mechanical nanobearings by the nanoforce.

In addition, it is well known that nanodiamond (ND) particles [19] have been synthesized by detonation method from the explosion itself [20]. The minimum first-order particle size uniformly corresponds to approximately 5 nm. Utilization of ND as an abrasive in an aqueous dispersion system is known because of its high Mohs hardness (10) and the existence of a water nanolayer on the ND surface [21]. Studies on ND as a lubricant candidate [22] are relatively few owing to its restricted behavior in aqueous systems. The organo-surface modification method [23] is a powerful technique that can be used to attain nanodispersion [24] of water-based fine particles in general organic solvents. Now, there are some important and relative reports about self-assembled diamond-based composite materials and LB film application [25-28]. Previously, dispersion media of several organo-modified NDs have been used as the spreading solution for monolayer (single particle layer) on the water surface [29-31]. However, all of these cases involve the use of a low concentration system as the dispersion medium. Further, the relationship between condensation/expansion behavior [32, 33] of a single particle layer at the air/water interface and the dispersion ability in the organic solvent as a middle concentration system has never been discussed.

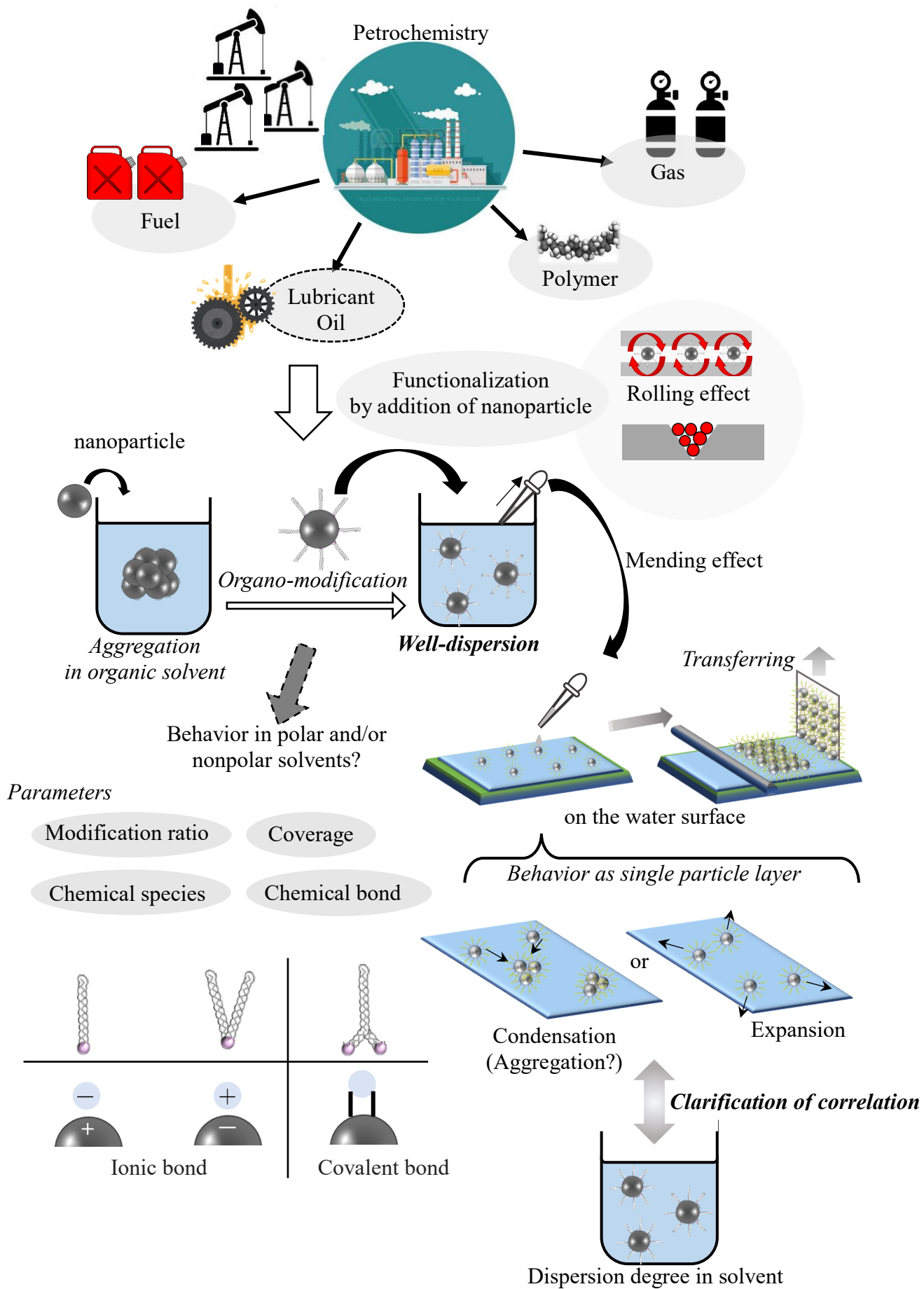


Figure 1-1. Research strategy of Chapter 3.

1-2. Heat-Resistant Nanodiamond Layers

Almost all molecular functions are derived from molecular structure, and the molecular arrangement and packing structure of formed molecular groups are caused by intermolecular interactions [34]. Examples of "layered organization" [35] in nature include graphite [36], natural clay minerals [37], cell membranes [38], β -sheets of proteins [39], surfactants [40], and lamellae of crystalline polymers [41]. These structures are important because of the physical properties that arise through functionalization based on exfoliation [42] and interlayer electron/signal transfers [43, 44]. Most crystalline long-chain compounds with a carbon chain length of about C_{14} or more form layered structures [45]. A sub-cell structure formed in the *ab*-plane [46] and a layered structure along the *c*-axis direction [47] are the bases of structure formation, even if the material does not have highly oriented organization, such as liquid crystals [48] or LB films [49-51]. The main factor responsible for forming layered structures is the van der Waals interaction between alkyl chains [52]. The reflection by X-ray diffraction based on the in-plane packing of phase-aligned long-alkyl chain groups is enhanced [53], and these periods are called "short spacings" [54]. On the other hand, these layered structures are supported by van der Waals interactions between alkyl chain ends. In particular, the double layer structure, which is a superposition of bilayers with head-to-head and tail-to-tail arrangements, has a structure in which long alkyl chains are adjacent. Further, the polar groups at the other end face each other, and the structure is often supported by the interaction between

the terminal CH₃- groups in the layers, which occurs in a narrow contact region. Heating creates disorder in the layered structure, and the structure can no longer be supported by van der Waals interactions because the molecular mobility improves. In the case of liquid crystals, the in-plane structure becomes disordered earlier and is equivalent to the state in which only the layer structure is maintained. In the case of LB films, there are examples in the literature, such as order-disorder transitions in the high temperature region of J-aggregate dye LB films [55, 56]. Also, there is example that the layered structure maintenance characteristics are derived from the molecular form of topological polymers having the same constituent components [57]. Multilayered structures can also be successfully obtained in the layer-by-layer technique [58]. M. Morga et al had reported that the obtained structures by LBL are of well-defined coverage and properties [59]. Evaluation of the maintenance characteristics of layered structures in high-temperature environments and improving these characteristics are driving functional manufacturing inspired by the natural world. Maintaining biological structures in severe environments also guarantees that electronic materials and advanced devices will not lose their performance characteristics, even due to heat generation from the deterioration of batteries. Therefore, the ability of a layered structure comprising organic molecules to withstand high temperatures is important for next-generation materials development. Although electrical conduction is due to electron transfer, heat conduction is a phonon electromotive phenomenon arising from lattice vibrations. Therefore, it often does not receive the focus of chemists.

However, thermal management, including thermal dissipation and heat transfer in industrial fields, is an important research subject. For example, thinning of optical displays and the development of mobile displays have seen technological innovation in recent years. However, even though the displays of mobile devices have become smaller and thinner, the miniaturization of batteries has not occurred at the same pace. As general device users may have experienced, mobile devices tend to generate heat due to battery deterioration, and batteries do not last long. The effect that technological innovations on thermal management will have on next-generation industries is immeasurable.

ND [60], which is an inorganic nanoparticle and one type of nanocarbon material, is known as a functional material having a uniform particle diameter [61] and excellent thermal conductivity [62]. In addition to the unique properties of nanocarbon materials, ND also possesses a high refractive index [63] and antibacterial properties [64]. The dispersion properties of functional nanoparticles are often focused on in research. The achievement of a well-dispersed state with a small particle aggregation size improves the properties of the solvent and resin containing it, and imparts particle function [65, 66]. The surfaces of many oxide inorganic nanoparticles are universally terminated with hydroxyl groups [67], and in particular, ND is stabilized by the surface of the outermost layer being covered with a nano-adsorption layer of water [68]. Although many nanoparticles are hydrophilic and well-dispersed in an

aqueous medium [69], their dispersibility in an organic solvent or an organic polymer matrix is inherently low.

On the other hand, the technique of integrating nanoparticles [70] having a large surface area into a sheet is a low-cost and highly efficient means of replacing only the outermost layer of the target material with a functional surface. The two-dimensional integration characteristics of nanoparticles are different from their dispersion and aggregation characteristics, and environment/characteristic control is needed in this technique [71]. However, these two characteristics can be attained simultaneously by organo-modification of the surface of inorganic particles [72]. Previous studies have focused on organo-modification of nanoclay [73], zirconia [74], zinc oxide [31], magnetic nanoparticles [30], and ND [29]. Further, formation of single particle layers and nanocomposite preparation with crystalline polymers has also been studied. Long-chain carboxylic acids [29-31, 74] and long-chain quaternary ammonium [73] cations have been used as modifiers in previous work.

1-3. Topological Polymers

A large amount of research in the field of polymer science is currently focused on effecting changes in the properties of polymers that have different shapes. Polymers having linear, branched, cyclic, and polycyclic forms are all being investigated [75, 76]. The effect of differently shaped amphiphilic polymers applied as monomolecular layers to air/water interfaces on the formation and behavior of interfacial molecular films has received considerable attention [77, 78]. In addition, polymers having different shapes that exist in biological systems are of particular interest from a materials properties perspective. For example, the primary components of cell membranes (including those of humans) consist of linear lipid molecules, and the membrane [79, 80] of the single-celled microorganism archaea (a thermophile [81]) consists of cyclic lipids that have excellent heat resistance [82, 83].

The relationship of structure and function for these polymers has been hard to understand based on traditional structural classifications. The concept of primary, secondary, and tertiary structures is a firmly established and well-used concept in almost every area of polymer research [84, 85]. In this context, primary structure refers to the polymer's chemical structure, including molecular weight; secondary structure refers to the conformation adopted by the polymer through intermolecular interactions such as *cis-trans*, *trans-gauche*, and helical conformations; and the tertiary structure refers to a polymer's three-dimensional structure, including crystalline, amorphous, and liquid crystal forms. A "higher-order structure" can exist,

corresponding to the fusion of secondary and tertiary structures, such as occurs in spherulites and phase separations (Fig. 1-2).

A new polymer classification based on higher order polymer shapes has been termed as topological polymer chemistry [86, 87]. Of interest in this paper is the application of topological polymer chemistry to the field of polymer synthesis [88, 89]. Although topological polymers are finding their place in polymer science, understanding the relationship between the chemistry and resulting physical properties is still incomplete. One nice step in this direction is the chemistry of the very thin polymer structures limited by the dimensions of a single molecule. Elucidation of the behavior of polymers built from the same monomers but having different shapes within a single molecular dimension would greatly facilitate the development of topological polymer chemistry of the work discussed in this paper.

Classical classification of polymers

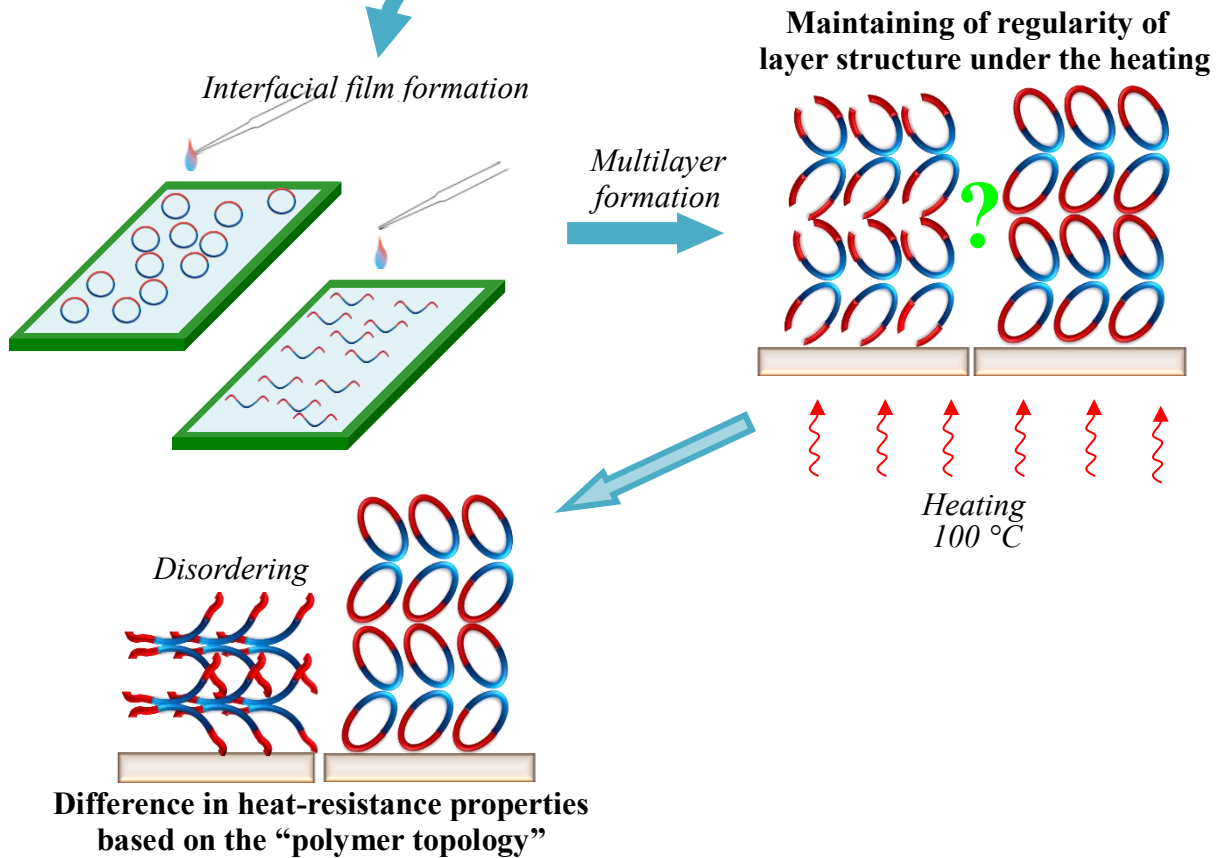
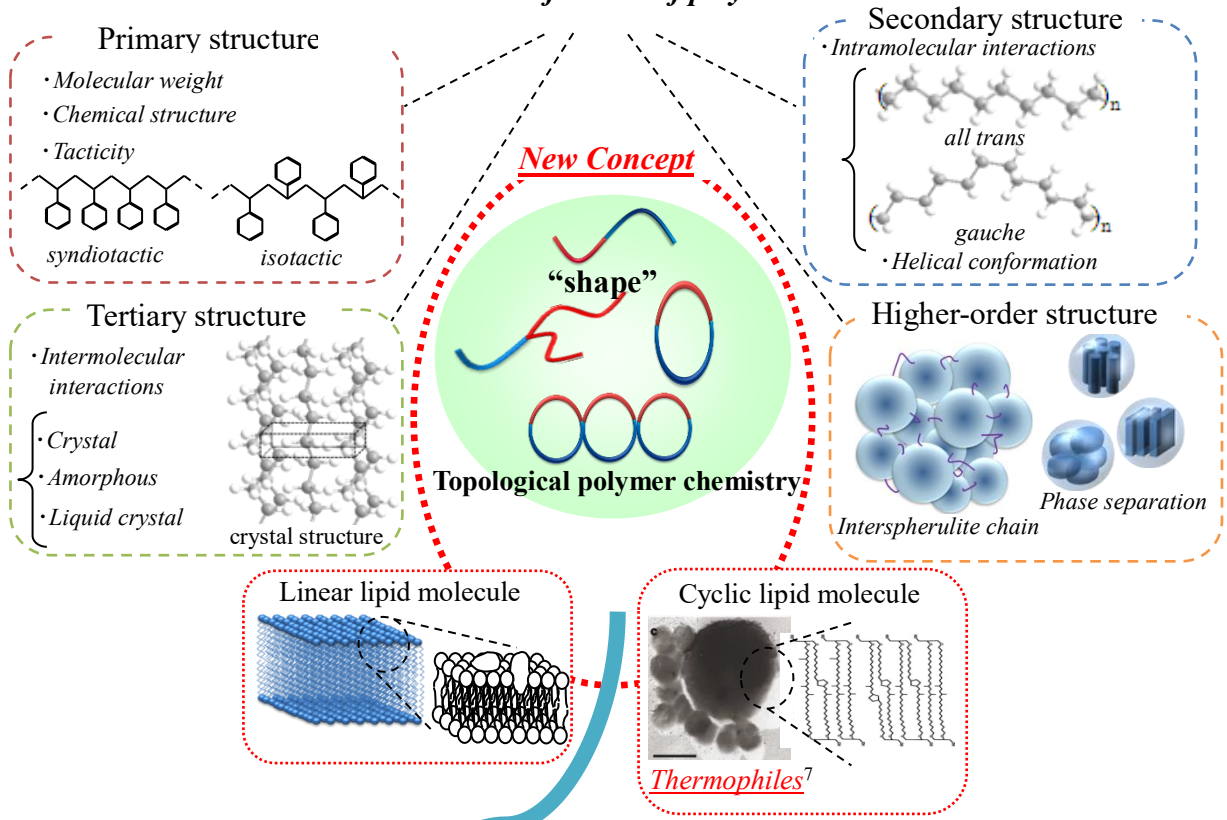


Figure 1-2. Conceptual diagram of topological polymer interfacial chemistry.

1-4. This Study

In this study, as a preliminary effort toward the development of new lubricating oil utilizing inorganic nanoparticles, the impact of organo-modification on nanodispersion behavior in an organic solvent was investigated. Here, several modified agents such as one or two hydrocarbon chain compounds, fluorinated surfactants [90], and carboxylate or phosphonate derivatives [91] are used as surface-treated materials on ND. In these cases, both cationic and anionic ND are utilized [92]. In particular, the study focuses on the surface modification ratio and surface composition and compares the dispersion properties in both polar and nonpolar solvents. Moreover, the relationship between dispersion characteristics in solution and monolayer behavior on the water surface of organo-modified nanoparticle is also discussed. Research on the dispersion behavior of nanoparticles in solution that contributes to the development of new lubricants provides added value that will promote/contribute to tribological research in the future. Therefore, in order to understand the properties of oil film containing nanoparticles formed by the "friction test" (Rotary ball is pressed against the fixed three balls immersed in lubricating oil and it is rotated at high speed, and the abrasion resistance is evaluated from wear marks obtained from this process.) [93], the elucidation of the relationship between the condensation behavior of the interfacial film of organo-nanoparticles and the dispersibility in solution will provide useful information. (Chapter 3)

Also, long-chain phosphonic acid derivatives are adopted as modifier candidates that can

maintain structure under high-temperature conditions. The purpose of this study is to introduce highly functional ND fine particles into a layered structure and evaluate the high-temperature maintenance property of the layered regularity. Understanding the heat-resistant temperature and collapse mechanism may provide useful information for practical applications in future nanodevices (Chapter 4).

Further, three types of amphiphilic block copolymers composed of n-butyl acrylate/ethylene oxide were used [94, 95]. These three copolymers, all synthesized from the same set of monomers, consisted of one ring-shaped and two linear block copolymers. The molecular structure and packing of these polymers at an air/water interface and on solid substrates are of interest to the field of basic polymer science. In this paper, topological polymer chemistry at the air/water interface has been investigated using amphiphilic linear (AB-type diblock and ABA-type triblock) and cyclic block copolymers [96]. In addition, the ability of these three topological polymers to maintain the characteristics of layer regularity under heating were examined (Fig. 1-2). This knowledge could then be applied to the study of the function of thermophilic archaea. Layer structures exist all around us, as biological cell membranes [97], proteins organized into β -sheets [98], in graphite [99], natural clay minerals [100], surfactants [101], and liquid crystals [37]. Of course, LB films [102-104] which include polymer LB film [105, 106], are also layer structures including polymer LB film. Long-chain compounds constituting LB films show a similarity to a layer structure [107] along the *c*-axis and sub-cell

structure [46] in the *ab*-plane at the state of "molecules with low molecular weight", "polymerized macromolecules", "three-dimensional crystal", and "a two-dimensional molecular film". Maintained force of the sub-cell corresponds van der Waals interaction between alkyl chains. Comparison with this lateral interaction, there are tendency of easily disordering by the external effects such as the heating since layer structure is only supported by the interaction between the terminal groups [108]. However, since regularity of layer structure in LB film is generally high, studies on polymer nanosheet [109, 110] and clay nanosheets [111-113] dealing with this ordering are very famous. Work has also been reported on studies of novel polymer nanosheets supported by π - π interactions between carbazole groups [114], polymer nanosphere-layer structures [115, 116], and layered organizations of organo-modified-inorganic nanoparticles [29, 30]. In addition, changes in hydrophobic chain lengths caused by heating have also been investigated as a disordering process effect. (Chapter 5)

2. Materials and Methods

2-1. Nanodiamond Preparation

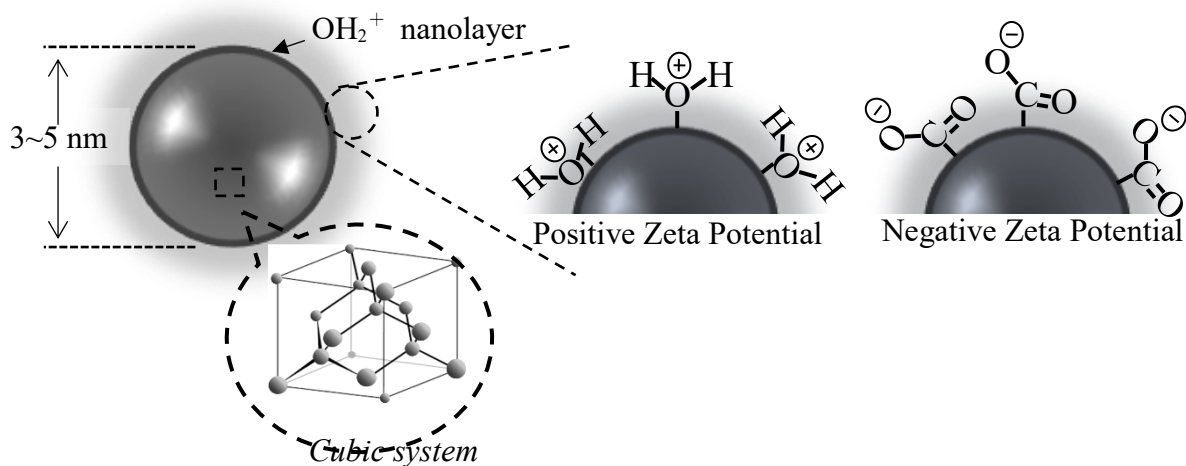
ND (average particle diameter 4.8 ± 0.7 nm, DAICEL Co., Ltd.) prepared by detonation method was used as a sample [117]. The detonation method was performed in a special private facility (owned by Daicel Co. Ltd., Kobe, Japan) by using trinitrotoluene (TNT) and/or 1,3,5-trinitrohexahydro-s-triazine (Research Department Explosive: RDX) explosives as carbon sources. Utilizing the pressure of explosion at that time, it took out soot containing ND and purified this soot to obtain ND. The minimum primary particle diameter of ND at that time is about 5 nm. ND positively charged by protonation to the adsorbed water layer on the ND surface was designated as the positive ND (ζ potential + 38.9 mV, Zetasizer Nano, manufactured by Malvern Instruments), whereas ND in which the $-\text{COO}^-$ group was introduced by blowing CO_2 onto the surface was designated as the negative ND (ζ potential -28.2 mV) (Fig. 2-1(a)).

2-2. Types of Modified Agents Used in This Study and Their Modification Reaction

A long-chain quaternary ammonium bromide with two chains (dimethyl dioctadecyl ammonium bromide, Fig. 2-1(b)) was used as a cationic modifier. On the other hand, stearic acid (Fig. 2-1(c)), stearyl phosphonic acid with bidentate binding (Fig. 2-1(d)) [118], fluorinated carboxylic acid (perfluorododecanoic acid, Fig. 2-1(e)), and fluorinated phosphonic acid with bidentate binding (1*H*, 1*H*, 2*H*, 2*H*-perfluoro-*n*-decylphosphonic acid Fig. 2-1(f))

were used as anionic modifiers. Organo-modification of the ND surface was conducted based on a previous report (Fig. 2-2(a)) [29, 119].

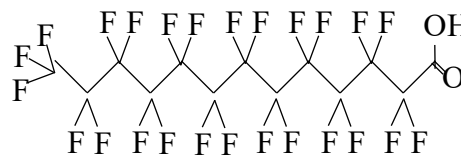
(a) Nanodiamond(ND)



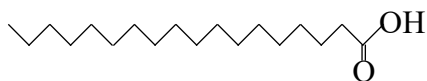
(b) Dimethyl dioctadecyl ammonium bromide



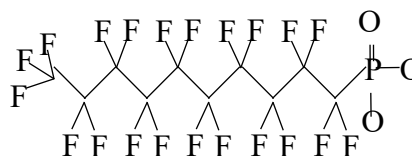
(e) Perfluorododecanoic acid



(c) Stearic Acid



(f) 1*H*, 1*H*, 2*H*, 2*H*-perfluoro-*n*-decylphosphonic acid



(d) Octadecyl phosphonic acid

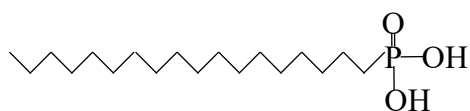


Figure 2-1. (a) Schematic illustration of the structure of nanodiamond covered with a nanolayer of adsorbed water. (b) ~ (f) Chemical structures of organo-modified agents used in this study.

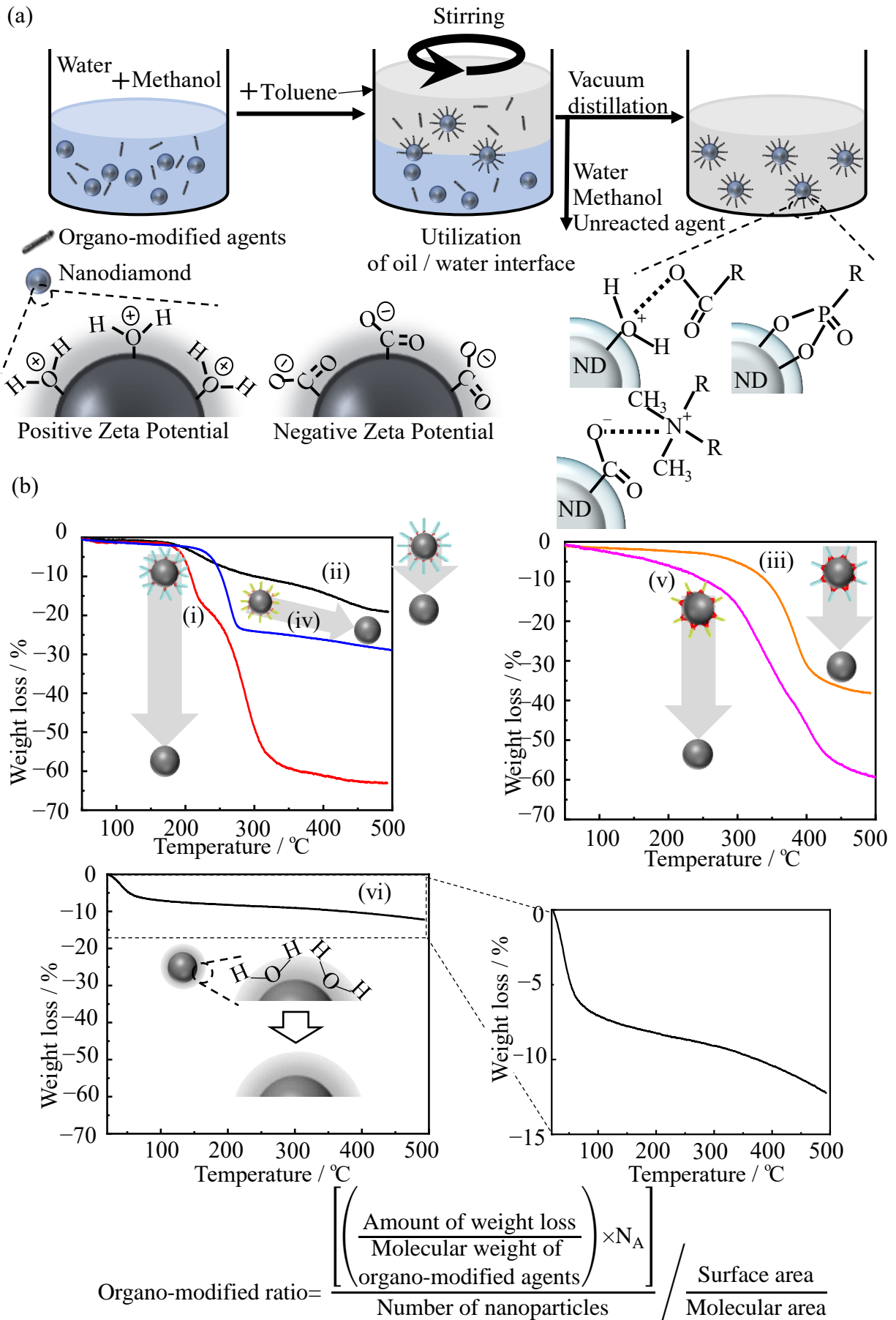


Figure 2-2. (a) Schematic illustration of the organo-modification method. (b) TG curves of (i) DDA-ND, (ii) St-ND, (iii) ODP-ND, (iv) PFD-ND, (v) PFDP-ND, and (vi) neat ND.

2-3. Aggregated Particle Size Evaluation of Dispersion Medium

Dynamic light scattering (DLS) measurements on modified nanoparticles in solution were performed using the Zetasizer Nano (Malvern Instruments). In the DLS measurement, values of the refractive index of ND ($n = 2.42$) and the values of the solvent viscosity (Toluene: 0.560 mPa·s, Hexane: 0.307 mPa·s) at 25 °C were inputted, and the temperature of measuring dispersion medium was also hold constant value of 25 °C. The number of integrations in this measurement was set to 75 times. In this measurement, A He - Ne laser 633 nm was used as a light source, and a photodiode detector was used. The solution concentration was set as 0.01–0.05 wt%. Toluene and *n*-hexane were used as the polar and nonpolar solvents, respectively. With an orientation toward applications in lubricating oil, DDA-ND, which resulted in the highest dispersibility, did not precipitate after more than a week in toluene, in lubricant base oil (fatty acid ester) plus toluene solution, and in fatty acid esthetics.

2-4. Formation of Single Particle Layer on the Water Surface

This dispersion medium was further diluted to a concentration of approximately 1/100 and used as a material for forming a monolayer on the water surface. It was found that nano-dispersion in the organic solvent of ND was attained by organo-modification. This experimental fact indicated that it could be possible to obtain dispersed media of organo-modified ND. In other words, it also means that it is possible to prepare a spreading solution of single particle layer (monolayer) of organo-modified inorganic nanoparticles on the water surface. In this case,

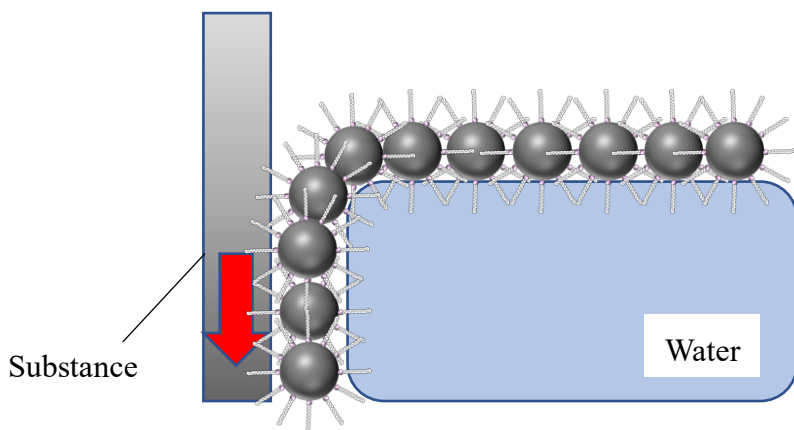
organo-ND/toluene solution (ca. 1.0×10^{-4} M) was spread on ultrapure water (18.2 M Ω cm) to fabricate an interfacial particle layer of organo-modified ND. After the evaporating of toluene during 30 min, π -A isotherms were measured. In order to examine the condensation behavior of the modified fine particles on the water surface, the compression rate was set at 8 cm²·min⁻¹ as a standard, while low-speed compression measurement at 2 cm²·min⁻¹ was also performed. The subphase temperature was controlled at 15 °C by circulating water in thermostat connected to the trough.

2-5. Transferring of Organized Particle Layer onto Solid Substrate and Its Evaluation

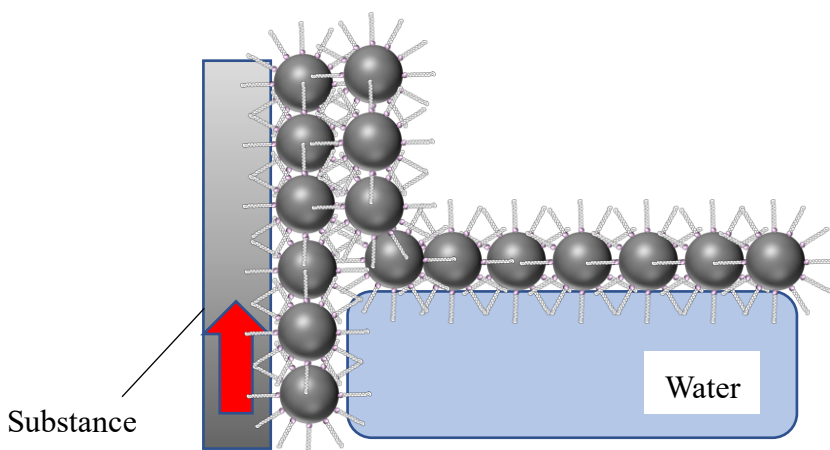
Transfer onto a solid substrate was carried out by the LB method [104, 120-122]. The monolayer was transferred onto the mica substrate by upstroke LB method. Details of the method of the transferring and multi-particle layer formation of the organo-modified particle layer on the solid are shown in Fig 2-3. Morphological observations of monolayer on solid were performed by dynamic force mode (DFM)-atomic force microscopy (*abbrev.* AFM, SII SPA300 module with SPI-3800 probe station). In this case, Si single crystal tip was used as cantilever (spring constant: 1.4 N·m⁻¹). Multilayers were transferred onto glass substrate by alternative up- and downstroke LB method. The layered structures in multilayers were characterized by out-of-plane XRD using a Rint-Ultima III diffractometer (Rigaku Co.). Monochromatized Cu-K α radiation ($\lambda = 0.154$ nm) was generated at 40 kV and 30 mA. In the $\theta - 2\theta$ mode, the samples were scanned by a step-scanning method with a step width of 0.05°

and intervals of 4 s for the diffraction angle 2θ in the range of $0.5\text{--}10^\circ$. The diffracted X-ray beam was monochromatized by a pyrographite monochromatic system and monitored by a scintillation counter. The in-plane spacing of the two-dimensional lattice of organo-modified chains in the same multilayers was determined using an X-ray diffractometer setup with different geometrical arrangements [122, 123] (Bruker AXS, MXP-BX diffractometer; Cu- $K\alpha$ radiation, 40 kV, 40 mA, a special made-to-order instrument) and equipped with a parabolic graded multilayer mirror.

(i) Transferring by down stroke.



(ii) Transferring by up stroke.



(iii) Repeating steps (i) and (ii).

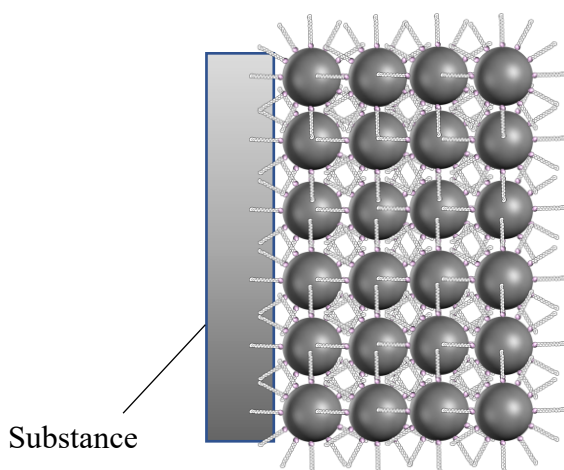


Figure 2-3. Schematic illustration of formation of multi-particle layers on the substance surface of organo-modified ND.

2-6. Preparation and characterization of organo-modified ND

Similarly, ND with a 4.8 ± 0.7 nm particle size (supplied from DAICEL Co. Ltd) was obtained by the detonation method (Fig. 2-4(a)). ND used in this study was formed cubic systems. Octadecyl phosphonic acid (*abbrev.* ODPA) was used as the organo-modifier, and stearic acid (octadecanoic acid, *abbrev.* ODA) was also used for comparison (Fig. 2-4(b)). Figure 2-4(c) shows a schematic illustration of the synthetic method for organo-modified ND. It was expected that the $-\text{OH}$ group on the outermost surface existed as a charged $-\text{OH}_2^+$ group in aqueous solutions. Therefore, the adsorbed water nano-layer on the ND in the reaction system was also positively charged and capable of electrostatic interactions with the phosphonate anions (Fig. 2-4(d)) and the carboxylate anions (Fig. 2-4(e)). Dispersions were prepared by combining an aqueous solution of 5 nm-diameter ND with a methanolic solution of ODPA or ODA (the detailed organo-modification procedure of ND is presented in References 118 and 124). Next, toluene solvent was poured into the dispersed solution with ND while stirring and the organo-modified NDs moved from the aqueous dispersion phase into the toluene phase. Then, CH_3OH , H_2O , and unreacted reagents were removed by evaporation under reduced pressure and decantation method. In addition, the matrix polymer used in the nanohybridization experiment was poly(4-methyl-1-pentene) (PMP); its chemical and three-dimensional structures are shown in Fig. 2-4(f). Although this matrix is a crystalline polymer, PMP is transparent because the density of the crystalline region is as low as that of the amorphous

region. If organo-ND is introduced into this molten matrix and kneaded, the transparency of the obtained composite material can be used to estimate the degree of particle dispersion. If the organo-nanoparticles are dispersed in both the crystalline and amorphous regions and the transparency is maintained, the miscibility between the introduced organo-modified chains and the surrounding organic polymer matrix is improved, and this provides evidence that aggregation of the inorganic particles is suppressed.

The achievement of organo-modification on the ND surface was confirmed by infrared (IR, JASCO Tensor II spectrometer) spectra and thermogravimetry (TG) (Figs. 2-5(a) and (b)). In the IR measurement, the O-H stretching vibration band of ND arising from the surface-adsorbed water nanolayer and the C-H stretching vibration band arising from the organo-modifier ODPA appeared simultaneously in the spectrum of the organo-modified ND (ODPA-ND). Furthermore, confirmation of the band region derived from the phosphonic acid group gives evidence of modification (Figs. 2-5(a) and (b)). In this enlarged IR spectra, the bands of R-P(=O)(-OH)₂ of phosphonic acid is clearly detected at 1116 and 2677 cm⁻¹ (Fig. 2-5(b)), and it has been confirmed the evidence that this functional group is denatured to R-P(=O)(-O-C)₂ by the organo-modification (Fig. 2-4(a)). In this case, the band of 2677 cm⁻¹ disappears due to the disappearance of P-OH, and the P=O band shifts. TG analysis were measured by using an Al-opened pan under the nitrogen atmosphere at 10 °C min⁻¹ heating rate with a SII EXSTAR TG/DTA6200 apparatus. Figure 2-4(b) shows the TG curves of ODA-ND and ODPA-ND. The

thermal degradation onset temperature of ODA-ND (i.e. the starting temperature for desorption of the organic chain) is 155 °C. The desorption temperature of the modified chain of ODP-ND increased to 350 °C. The gradual weight loss at around 100 °C corresponds to the adsorbed water desorption temperature on the ND surface, which is a characteristic inherent to ND. The organo-chain desorption temperature of organo-modified ND with phosphonate was innovatively high.

Nanohybrid formation with an organic polymer matrix was performed as follows. A PMP/organo-modified ND mixture was extruded at 250 °C using a twin-screw extruder (Labo kneader mill, Toshin Co., Ltd.). The organo-modified ND content in the nanohybrid material was 1.0 wt.%. The PMP and its nanocomposite were processed into films with 500 µm thickness between two polyimide sheets (a Kapton 1 HN sheet, Toray-DuPont Co., Ltd.) using a hot press apparatus at 250 °C and 20 MPa for 10 min, followed by quenching to room temperature. As a result, the obtained PMP/organo-ND nanocomposite material indicates transparency. In all these results, it was shown that long-chain phosphonate-modified chains were thermally/mechanically introduced tightly. Before evaluating the maintenance properties of the layered regularity of the organized multi-particulate layers, which is main subject of this study, it was found that the long-chain phosphonate-modified ND had much higher thermal stability than the long-chain carboxylate-modified ND. The preparation method of the polymer-based nanocomposite material shown in Fig. 2-5(c) is called the "melt-compounding method"

[42] and is a simple and highly efficient technique. The only required condition for applying this method is that the organic chain desorption temperature on the nanoparticle surface should be higher than the melting point of the crystalline polymer. When using a crystalline polymer with a high-melting point, like the PMP used as the matrix in this work, nanocomposite preparation with ODA-ND is essentially impossible by this method. It is interesting to evaluate the ordered stability of organized nanoparticles with thermally stable modified chains and their high desorption temperature in a layer structure. By the way, the dispersibility of organo-modified ND can also be evaluated from the measurement of DLS in solution. DLS measurements were performed by Zetasizer Nano made from Malvern Instruments. In this measurement, the particle aggregation size in toluene dispersion medium at 0.01 wt% of stearate-modified ND and stearyl phosphonate-modified ND was evaluated (Fig. 2-7). It is about two orders higher than the concentration of spreading solution of monolayer on water surface. Comparing these two-systems, although the nano-dispersion was achieved in all of them, ODA-ND was a homogeneously distributed aggregation size at 489 nm, and ODPA-ND was coagulation size at about 227 nm though wide distribution. The fact that the bidentate modification shows a higher dispersibility corresponds to a high lipophilicity. Therefore, it is considered that the coverage rate by this type of organic molecule is relatively high.

There is strong bond formation between the ND surface and ODPA (Fig. 2-8). The -OH group at the binding site on the OH-terminated ND surface protonates in solution and exists as

a positively charged $-\text{OH}_2^+$ group. Here, electrostatic dehydration condensation occurs, and a $\cdots\text{P}-\text{O}-\text{C}$ (ND side) bond is formed. Subsequently, proton transfer occurred from the $-\text{OH}$ of the phosphonic acid group, and from the electrostatic dehydration condensation with positively charged $-\text{OH}_2^+$, a bidentate chelate coordination state (μ -oxo type) formed in a self-organizing manner. It is thought that the bidentate bond of this $\cdots\text{P}-\text{O}-\text{C}$ is the cause of the thermodynamically and mechanically strong bond formation.

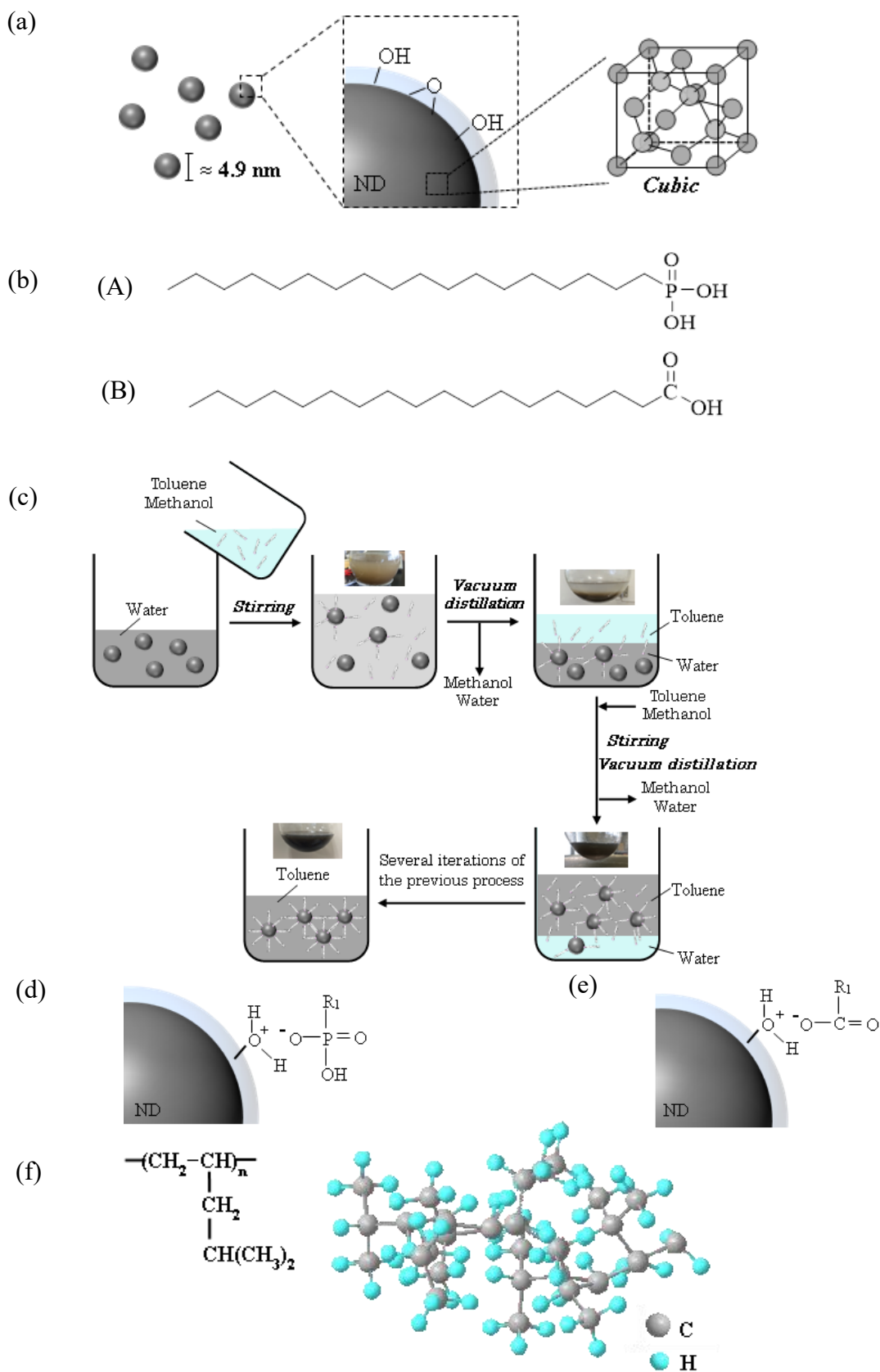


Figure 2-4. (a) Schematic illustration of the structure of ND covered with a nanolayer of adsorbed water. (b) Chemical structure of (A) octadecyl phosphonic acid and (B) octadecanoic acid to modify surface of ND. (c) Formation process of organo-modified ND. Schematic illustration of (d) long-chain phosphonate modification and (e) long-chain carboxylate modification of the outermost surface of ND. (f) Chemical structure of the PMP polymer matrix.

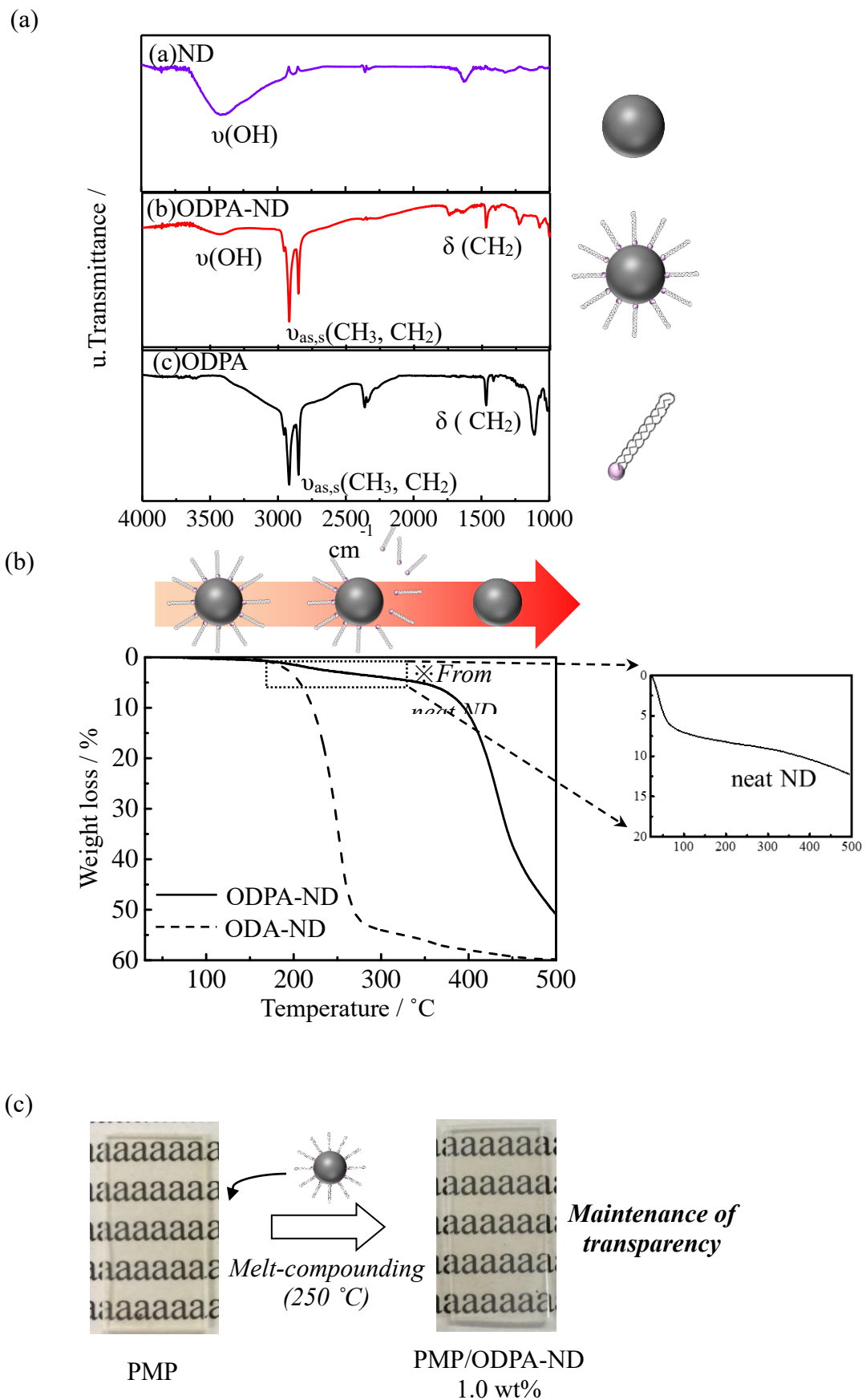
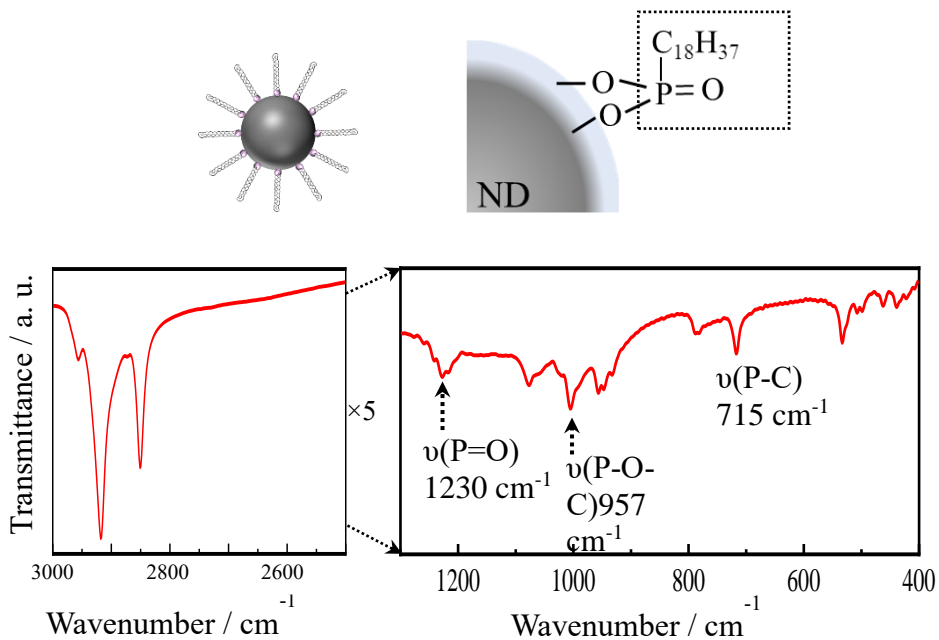


Figure 2-5. (a) IR spectra of ND, ODPA-ND, and ODPA. (b) TG curves of ODPA-ND and ODA-ND. (c) Photographs of pure PMP and PMP/ODPA-ND 1.0 wt.% nanocomposite films.

(a)



(b)

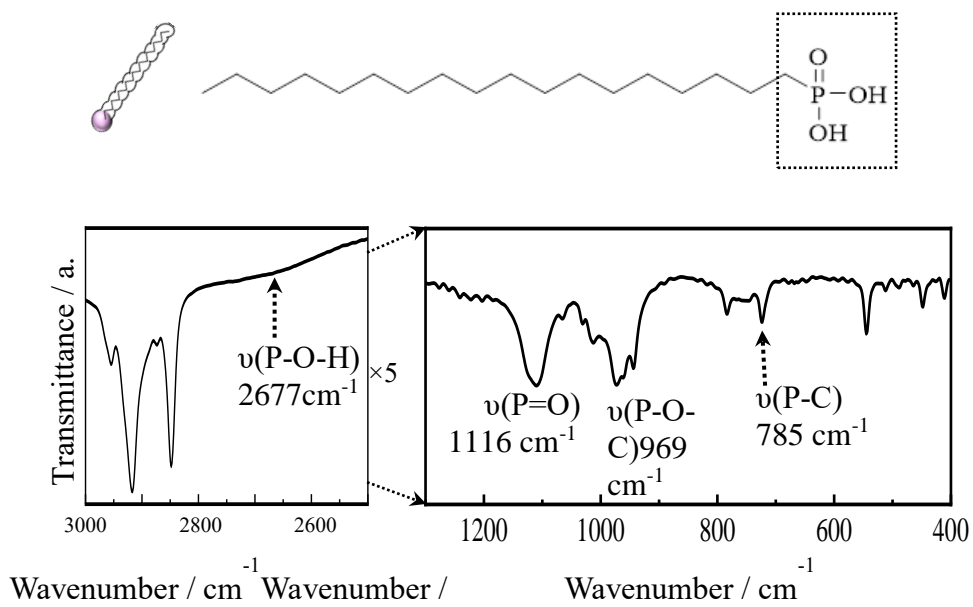


Figure 2-6. Enlarged IR spectra of (a) ODPA-ND and (b) ODPA.

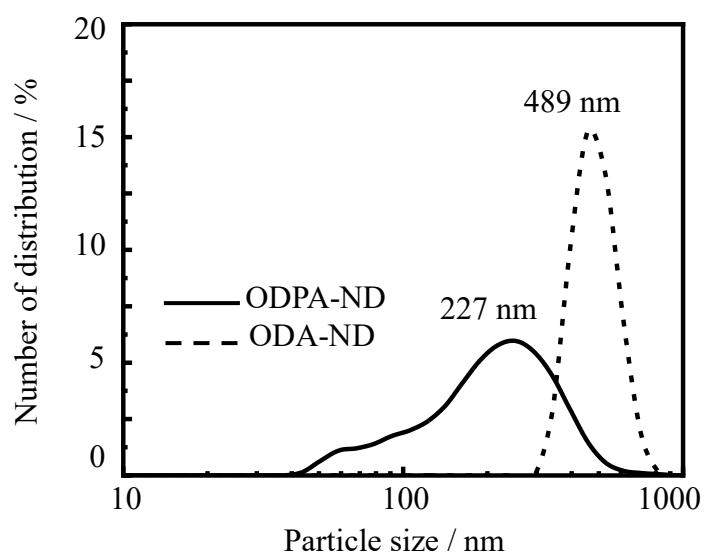


Figure 2-7. DLS curves and schematic illustration of the dispersion state of ODPA-ND and ODA-ND in toluene solvent (0.01 wt%).

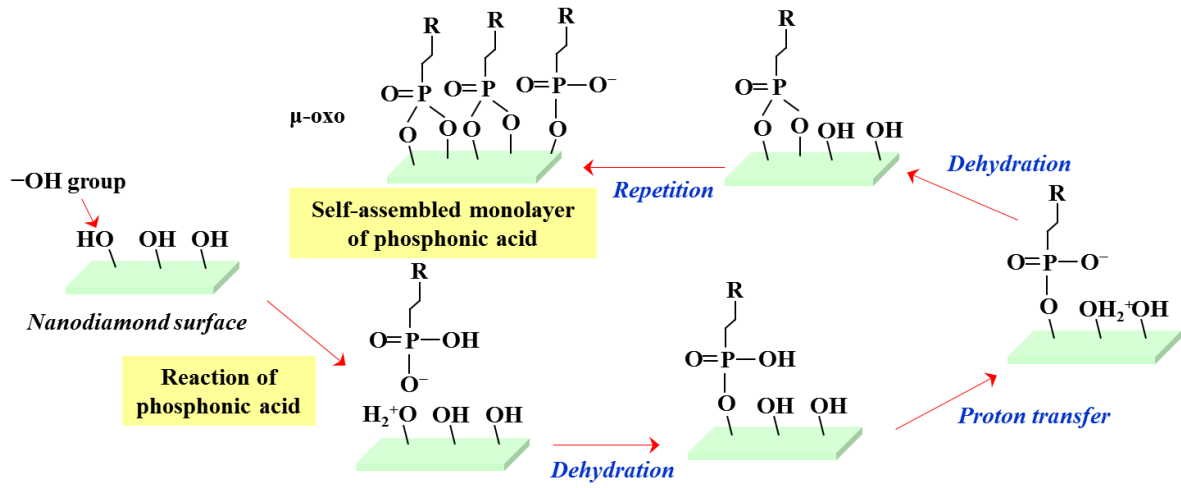


Figure 2-8. Schematic illustration of preparation mechanisms of phosphonate-modified ND.

2-7. Formation of monolayer on the water surface and estimation of structure and morphology of transferred films

It was found that nano-dispersion in the organic solvent of ND was attained by organo-modification. This experimental fact indicated that it could be possible to obtain dispersed media of organo-modified ND. In other words, it also means that it is possible to prepare a spreading solution of single particle layer (monolayer) of organo-modified inorganic nanoparticles on the water surface. In this case, organo-ND/toluene solution (ca. 1.0×10^{-4} M) was spread on ultrapure water (18.2 M Ω cm) to fabricate an interfacial particle layer of organo-modified ND. After the evaporating of toluene during 30 min, π -A isotherms were measured at a constant compression rate of 0.08 mm s $^{-1}$. The subphase temperature was controlled at 15 °C by circulating water in thermostat connected to the trough. LB trough was used to record the π -A isotherms and perform the film transferring to the solid substrate. The samples of AFM and XRD were transferred on mica and glass substrate by LB method at 15 °C.

2-8. Morphological observation and elucidation of organo-particle arrangement in the integrated layers

The surface morphology of single particle layer on solid was observed using an AFM apparatus (DMF mode) with microfabricated Si cantilevers (a spring constant: 1.4 N m $^{-1}$) was used. The long spacings between the particle layers transferred on solid was determined using temperature-controlled out-of-plane X-ray diffractometer (Bruker AXS, D8 Advance; CuK α

radiation, 40 kV, 100 mA) equipped with a graphite monochromator. This apparatus was also used as powder XRD in bulk. The two-dimensional lattice (sub-cell) of the modified-chain on organized particle layer was estimated by using an X-ray diffractometer setup with different geometrical arrangements [122, 123] (Bruker AXS, MXP-BX; CuK α radiation, 40 kV, 40 mA, an instrument specially made to order) and equipped with a parabolic graded multilayer mirror.

2-9. Topological Polymers

Figure 2-9 provides a detailed schematic of the compounds used in this study. The synthesis of cyclic and ABA-type copolymers has been described in previously published papers [94, 95]. AB-type copolymer was synthesized in the same manner. The cyclic copolymer (abbreviated as *c*-BAEO), AB-type (*l*-BAEO) linear block, and ABA-type (*l*-BAEOBA) linear block copolymers were synthesized from ethylene oxide and butyl acrylate. The chemical structure of the cyclic polymer corresponds to an ABA polymer connected at both ends. The molecular weights of all polymers were less than 10,000, which made these polymers freely soluble in chloroform. Monolayers and single-particle layers prepared from chloroform solutions (approximately 10^{-4} M) were formed on distilled water (resistivity was approximately 18 M Ω ·cm).

2-10. Structural Estimations of Topological Polymers

The π -A isotherms were measured using a USI-3-22 film balance at 15, 25, and 35 °C. After evaporation of chloroform from the polymer solutions for 5 min, the π -A isotherms were

recorded at compression speeds of 1.2 and 9.6 cm²/min⁻¹. Then, monolayer films prepared by the LB method at 15 and 20 °C were transferred onto glass for XRD studies, and mica for AFM studies.

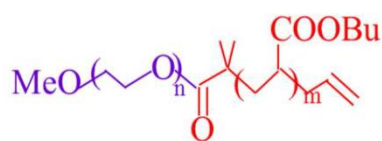
The surface morphologies of the transferred films were observed with an AFM apparatus equipped with microfabricated rectangular Si cantilevers with integrated pyramidal tips used under an applied constant force of 1.4 Nm⁻¹. The spacing between the layers of the polymer structures along the *c*-axis was estimated using an out-of- plane X-ray diffractometer (Rigaku, Rint-Ultima III, Cu *K*α radiation, 40 kV, 40 mA) equipped with a graphite monochromator. The in-plane spacing of the two-dimensional lattice of the films was determined by XRD [122, 123].

Topological polymers

(a)

Linear polymer (AB-type); poly[(butyl acrylate)-*block*-(ethylene oxide)]

(*abbrev. l*-BAEO)



— Mn = **3,000** (Hydrophobic group)

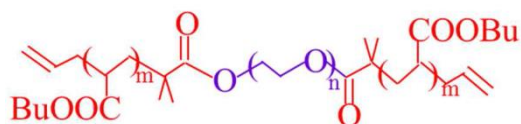
— Mn = **1,800** (Hydrophilic group)

(b)

Linear polymer (ABA-type);

poly[(butyl acrylate)-*block*-(ethylene oxide)-*block*-(butyl acrylate)]

(*abbrev. l*-BAEOBA)

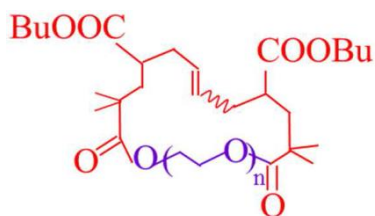


— Mn = **2,400** (Hydrophobic group)

— Mn = **2,600** (Hydrophilic group)

(c)

Cyclic polymer; poly[(butyl acrylate)-*block*-(ethylene oxide)] (*abbrev. c*-BAEO)



— Mn = **4,800** (Hydrophobic group)

— Mn = **2,700** (Hydrophilic group)

Figure 2-9. Chemical structures of (a) *l*-BAEO, (b) *l*-BAEOBA, and (c) *c*-BAEO.

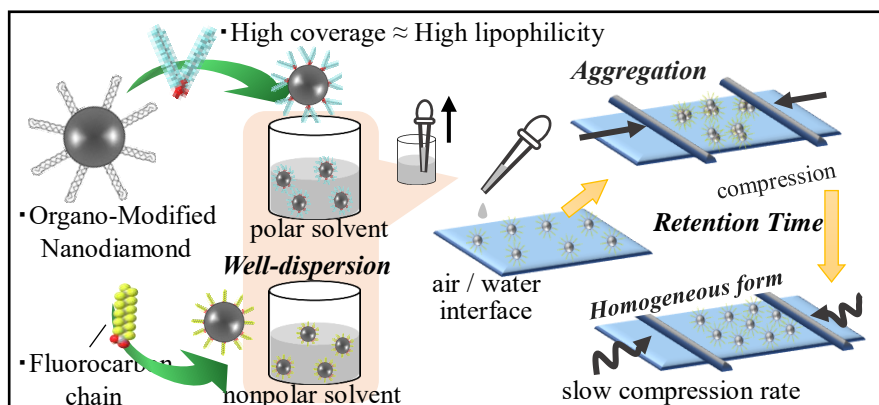
Chapter 3. Correlation Between Nanodispersion of Organo-Modified Nanodiamond in Solvent and Condensed Behavior of Their Organized Particle Films

3-1. Abstract

Organo-nanodiamond (ND) by surface modification using several surfactants has achieved nanodispersion in organic solvent as if these nanoparticles were dissolved. High surface coverage has reduced the aggregated particle size of organo-ND particles in the solvent, and their modification by fluorocarbon chain has achieved nanodispersion in a nonpolar solvent. By using a spreading solvent for single particle layers on the water surface of various organo-NDs of resulting dispersion medium, a close relation was found between the dispersion characteristics of organo-nanoparticles in the solvent and the condensation behavior in their two-dimensional single particle layer. Organo-ND with high dispersion ability in solvent has inferior two-dimensional condensability as a single particle layer. Sufficient retention time is necessary to form a homogeneous single particle layer on the water surface. The reason behind this property was found to be the secondary aggregation of organo-modified nanoparticles at the air/water interface. Since lipophilicized ND is not necessarily stable on the water surface, increasing aggregated particle size and three-dimensionality *were* confirmed in the case where the particle compression rate during two-dimensional integration was relatively fast.

Keywords: Surface Modification, Nanodiamond, Nanodispersion, Single Particle Layer,

Dependency on Compression Rate



3-2. Evaluation and Calculation of Surface Modification Ratio

First of all, it shows the evaluation procedure of the surface modification-rate of ND and the calculation before the indicating of the result of the main subject. The organo-modified NDs are referred to as DDA-ND (cation modified), St-ND (modified with stearate), ODP-ND (modified with stearyl phosphonate), PFD-ND (modified with fluorinated carboxylate), and PFDP-ND (modified with fluorinated phosphonate). The modification rate of ND was estimated from the weight loss due to desorption elimination of the modified chain by TG (Fig. 3(b), The gentle weight loss accompanying the temperature rise of 100 °C or more is due to slight desorption of the adsorbed water nanolayer on the ND surface). This calculation was performed using the value of the limiting area obtained from the π -A isotherms of the modifier molecules with respect to the surface area of the particle. DDA-ND, St-ND, ODP-ND, PFD-ND, and PFDP-ND yielded modification rates of 65%, 35%, >53%, 20%, and 48%, respectively (Table 3-1). Since ODP-ND has particularly high heat resistance among bidentate-type binding modified-chains and exceeds the detection limit of thermal degradation temperature measurement using Al pan, the notation ">53%" was used. The zeta potential values are 2.8, 8.43, 6.1, 18.4, and 0.85 mV for DDA-ND, St-ND, ODP-ND, PFD-ND, and PFDP-ND, respectively; these values were approaching zero (Table 3-2).

Table 3-1. Modification rate of organo-modified NDs estimated by TG.

Sample	DDA-ND	St-ND	ODP-ND	PFD-ND	PFDP-ND
Modification rate [%]	65	35	>53	20	43

Table 3-2. Values of Zeta potential of positive and negative neat NDs and organo-modified NDs.

Sample	ζ Potential [mV]
Positive ND	38.9
St-ND	8.4
ODP-ND	6.1
PFD-ND	18.4
PFDP-ND	0.9
Negative ND	-28.2
DDA-ND	2.8

Modification with Positive ND

Modification with Negative ND

3-3. Dispersion Behavior of Organo-Modified ND in Polar and/or Nonpolar Solvents

Figure 3-1(a) shows a photograph of the photograph of several organo-modified NDs dispersed in toluene solution (0.01 wt%). By visual observation, it is understood that all solutions are in a well-dispersed state without showing precipitation. No precipitation occurred even at a concentration of 0.05 wt%. Figure 3-1(b) shows the results of DLS measurement of toluene solutions (0.01 wt%) with five types of organo-modified ND. The vertical axis is indicated by the number distribution. In the case that the dispersed particle size is large, the resultant scattering intensity is strong even if the number of particles of the corresponding size become small. Therefore, by using expression of "particle number distribution", it is precisely determined number of particles of the specific size that corresponded most exist. As a reference, Fig. 3-2 shows a diagram in which the vertical axis of the corresponding figure is converted to intensity. In the DDA-ND dispersion medium, the aggregated particle size was the smallest and the peak value was 77 nm. The next smaller size sample of particle aggregation in the solution was ODP-ND, with peak-top value of 227 nm. The DLS peak-top values of PFD-ND, St-ND, and PFDP-ND were 472, 489, and 502 nm, respectively. Although PFD-ND has a minute shoulder peak of approximately 200 nm, no significant difference was found in the aggregation size of these three compounds. This result shows that DDA-ND, which has the highest modification rate, two lipophilic chains, and high coverage, is the most dispersible. In other words, the dispersibility of modified-nanoparticles having the highest affinity for the surrounding organic solvent is high. This can explain why ODP-ND has better dispersibility than the other three modified NDs. Comparing the modification rates shown in Table 3-1, it can be seen that the μ -oxo type bidentate bond can achieve higher modification in this surface modification reaction than in ionic monodentate bonding. The difference in aggregate size between ODP-ND and St-ND with the same stearyl lipophilic chain is considered to be the modification rate. The fact that the aggregation sizes of two kinds of fluorocarbon chain-coated

nanoparticles are almost same as the St-ND particle in the solution, regardless of the difference in modification ratio, suggests compatibility with the polar solvent. In other words, the dispersibility of the hydrocarbon-based modified nanoparticles with relatively low modification ratio and the fluorocarbon-based modified nanoparticle group is not so different. This investigation was conducted at concentrations of 0.01–0.05 wt%, but even at a concentration of 0.05 wt%, the stationary nanodispersion state of the modified-ND was retained. Figure 3-1(c) shows the above tendency and the ranking of dispersibility. Here, the ratio (measurement result / ideal particle diameter) of "ideal particle diameter" obtained by adding ND primary particle diameter (5 nm) and modified chain length and the "measurement result" in DLS was calculated (Table 3-3). As a result, it can be decided that the smaller the value of this "ratio", the better the particle dispersibility in the medium [125]. From this quantitative calculation result as well, it is found that the dispersibility of the modified ND with two-hydrocarbons is remarkably excellent at least in the polar solvent. On the other hand, the agglutination size of the fluorocarbon chain-modified ND is relatively large under this condition, and these are inferior in dispersibility.

Next, the dispersion behavior in nonpolar solvent is shown. From the results, three NDs with hydrocarbon-based modified chains were not dispersed in the *n*-hexane solvent. However, it was visually confirmed that the two fluorinated carbon-modified NDs were dispersed in the nonpolar solvent (Fig. 3-3(a)). Figure 3-3(b) shows the DLS curve of the fluorocarbon-modified NDs against the *n*-hexane dispersion medium. The peak values of DLS of PFD-ND and PFDP-ND are 352 and 367 nm, respectively. Both of the modified NDs showed better aggregation size in *n*-hexane than that in toluene by 100 nm or more, suggesting an improvement in dispersibility. Since dipoles cancel each other out when the number of fluorocarbon chains "n" is $n \geq 7$ [126], the fluorocarbon surfactant molecule with low-polarity state and dispersion in nonpolar solvent may be improved. The above findings are summarized schematically in Fig.

3-2(c). It seems that the helical conformation peculiar to fluorocarbons cancels the polarization of the C-F bond and attains a low-polarity state. Therefore, since the miscibility between the modified NDs having low-polarity surface and the surrounding nonpolar solvent is good, the modified NDs easily dispersed.

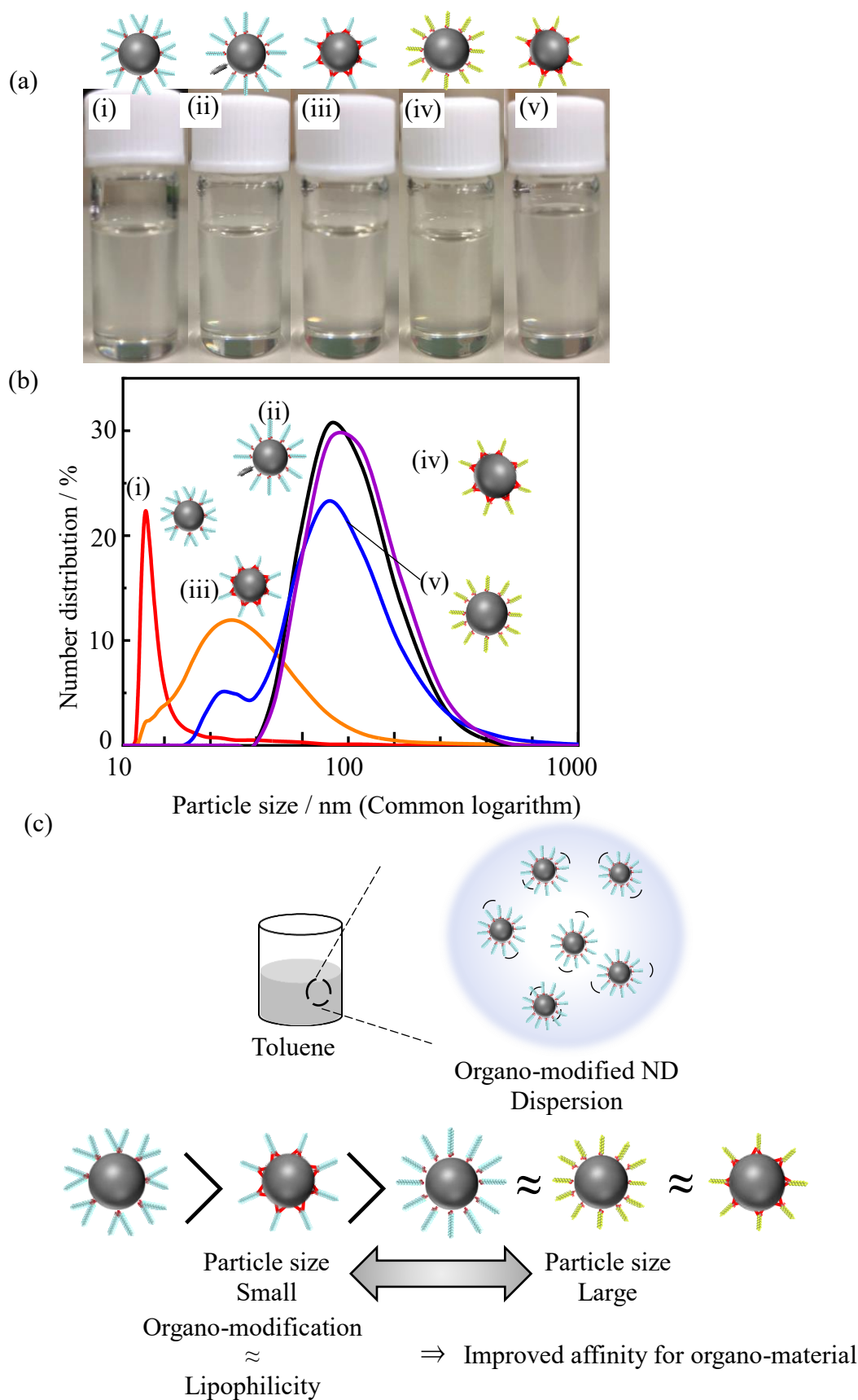


Figure 3-1. (a) Photographs of toluene solution including organo-modified NDs (0.01 wt%). (b) DLS semi-log graphs of toluene solution including organo-modified NDs (0.01 wt%). (c) Schematic illustration of dispersion behavior of organo-modified NDs in polar solution.

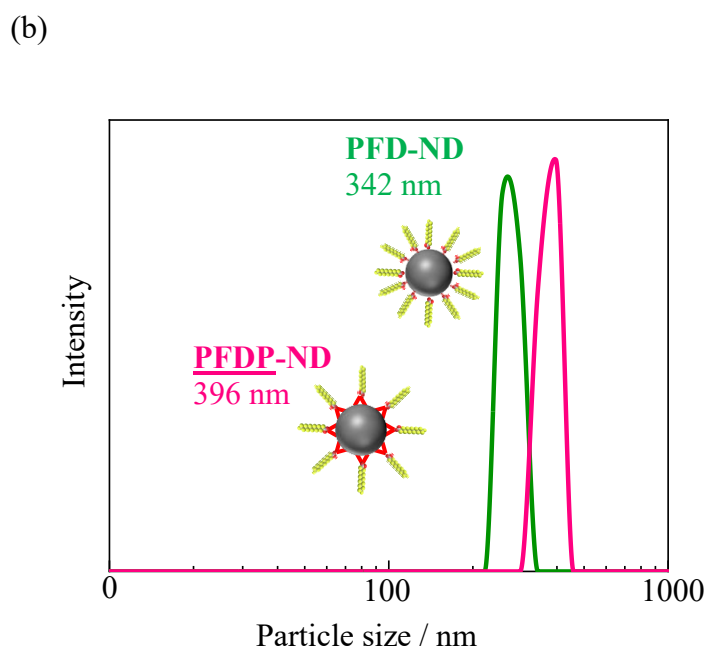
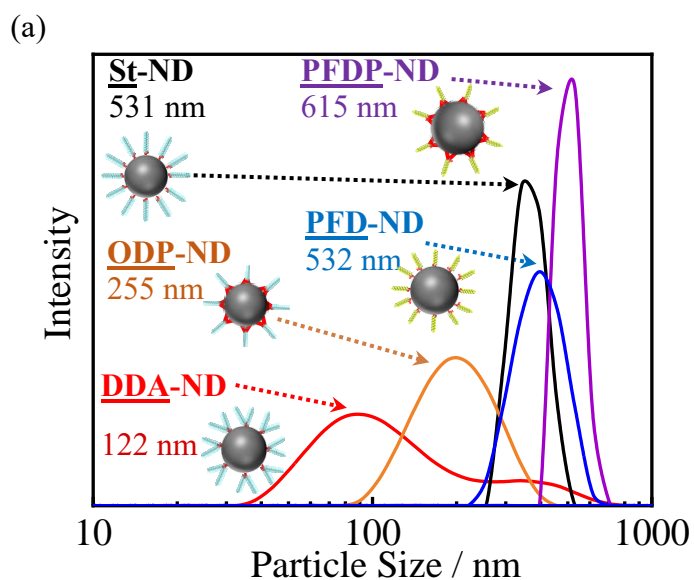


Figure 3-2. DLS curves of (a) toluene solution including organo-modified NDs and (b) *n*-hexane solution including fluorinated organo-NDs (0.01 wt%). Vertical axis corresponds the "Intensity" representation.

Table 3-3. Dispersibility evaluation of organic modified NDs by DLS.

Samples	Equilibrium size [nm]	Observed size [nm]	Ratio (Observed diameter / Equilibrium diameter)
DDA-ND	11	77	7
ODP-ND	11	227	21
St-ND	11	489	44
PFD-ND	8.3	472	57
PFDP-ND	7.7	502	65
PFD-ND (hexane)	8.3	352	42
PFDP-ND (hexane)	7.7	367	48

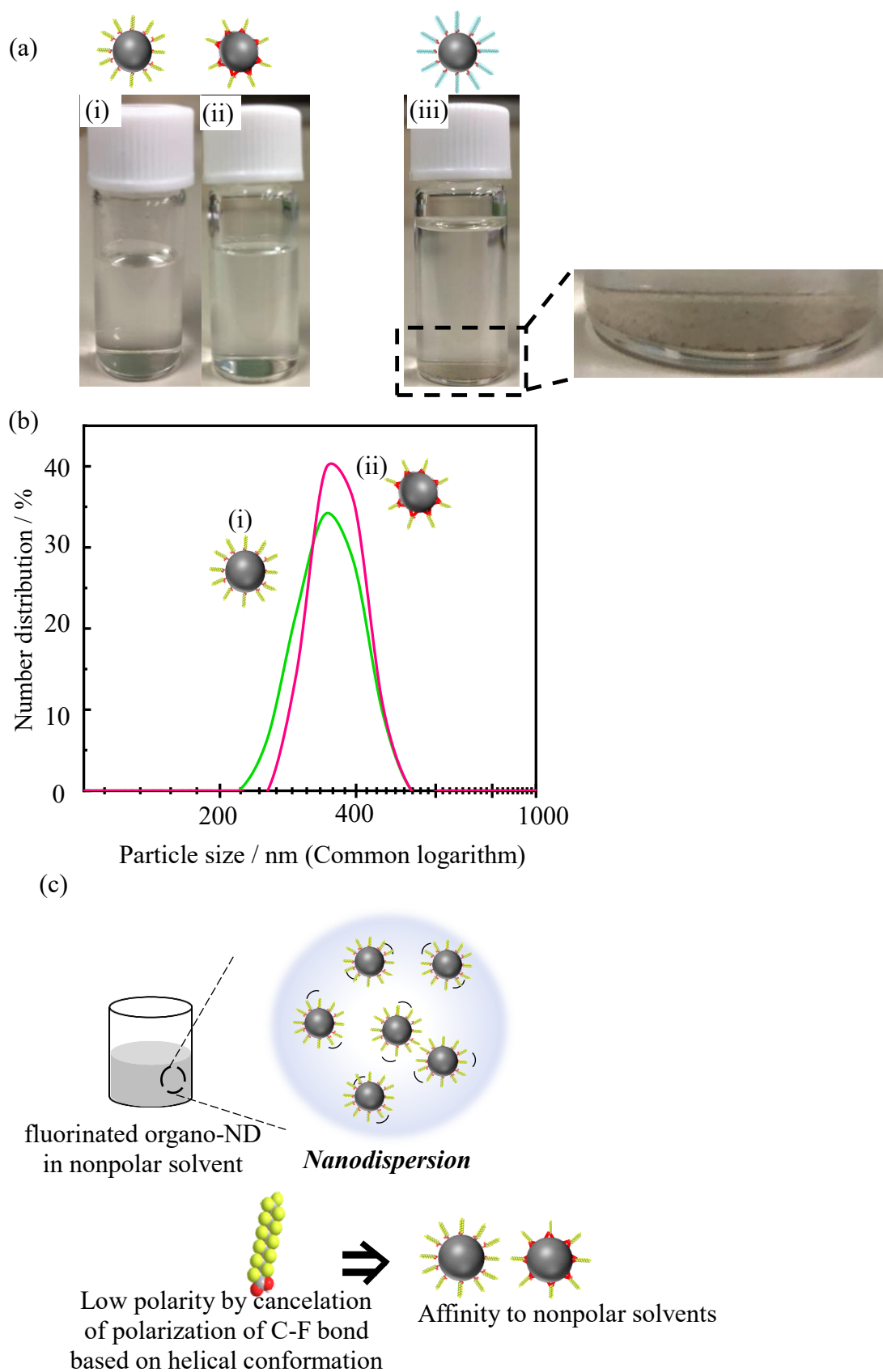


Figure 3-3. (a) Photographs of *n*-hexane solution including organo-modified NDs (0.01 wt%). (b) DLS semi-log graphs of *n*-hexane solution including fluorinated organo-NDs (0.01 wt%). (c) Schematic illustration of dispersion behavior of fluorinated organo-NDs in non-polar solution.

3-4. Formation of Single Particle Layers on the Water Surface of Organo-Modified NDs

Figure 3-4(a) shows a schematic illustration of the formation of single particle layers of organo-modified ND, and the experimental strategy in this case. Since nanodispersion in solution has been achieved, this diluted dispersion medium can be directly used as a spreading solution for a single particle layer on the water surface. In this study, in order to examine the aggregation behavior of the single particle layer, the compression rate dependence was also investigated. In the experiment on the formation of single particle layer, a toluene solution of DDA-ND and ODP-ND, and a hexane solution of PFD-ND, which have excellent dispersibility in solvent, were used. Figure 3-4(b) shows the dependence of the π -A isotherms on the compression rate of the organo-modified ND of the monolayer on the water surface. The horizontal axis value is denoted as the "Trough Area Reduction (%)". This is because the number of modified chains present on a single ND particle is not constant for each particle. Clear compression rate (speed) dependence can be confirmed on these π -A isotherms. Normally, the compression rate dependence cannot be confirmed on the π -A isotherm of low molecular weight surfactant molecule (like a measured-result in Fig. 3-5) because the structure is determined almost immediately after deployment. On the other hand, the compression rate dependence of polymers requiring relaxation time in two-dimensional crystallization is conspicuous (Fig. 2-3(b), [127]). The monolayer on the water surface of organo-modified nanoparticles indicates polymeric behavior in a sense.

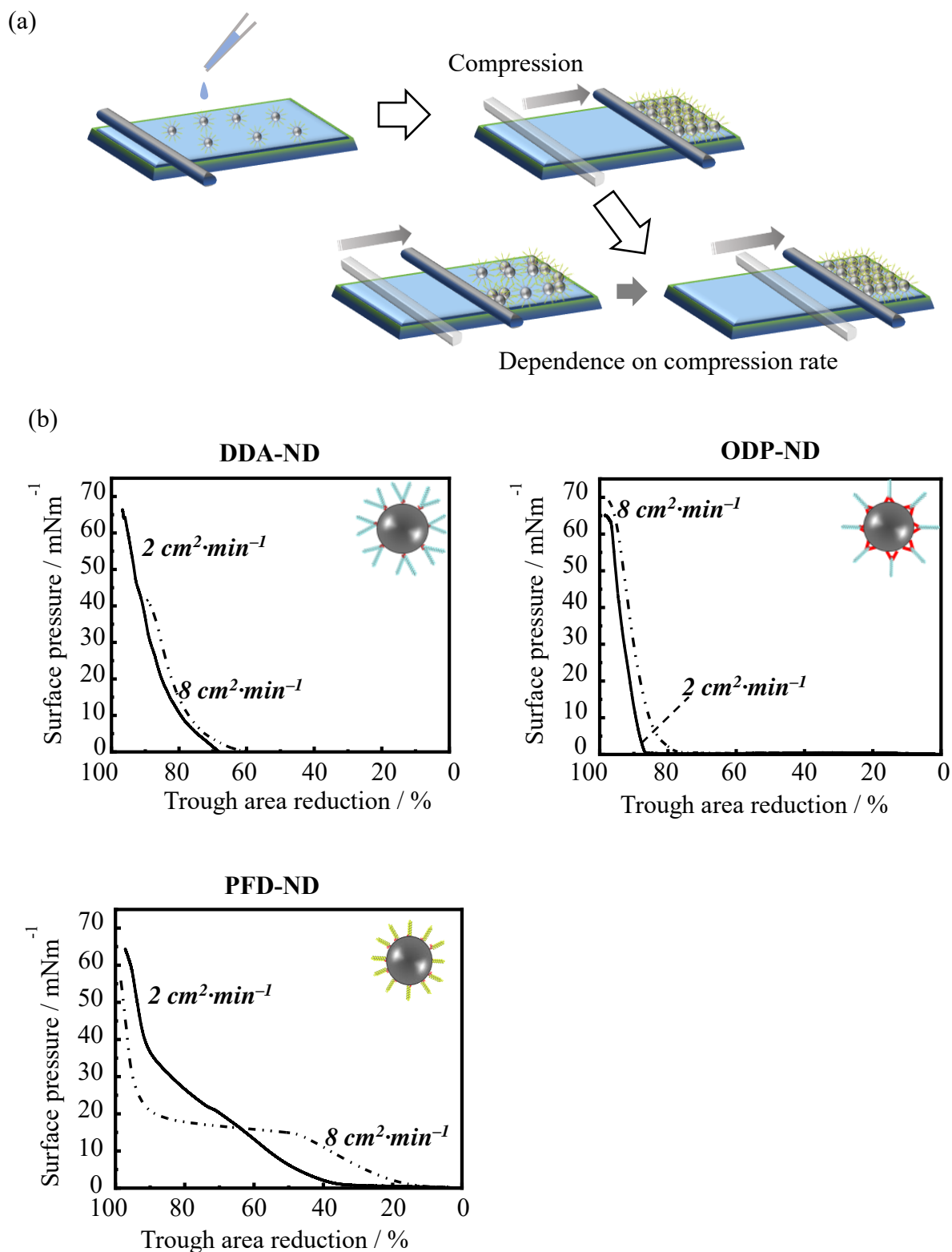


Figure 3-4. (a) Schematic illustration of formation of single particle layers on the water surface of organo-modified ND, and strategy of experiment. (b) π -A isotherms of single particle layers on the water surface of organo-modified ND with different compression rate (solid line: $2 \text{ cm}^2 \cdot \text{min}^{-1}$, dotted line: $8 \text{ cm}^2 \cdot \text{min}^{-1}$).

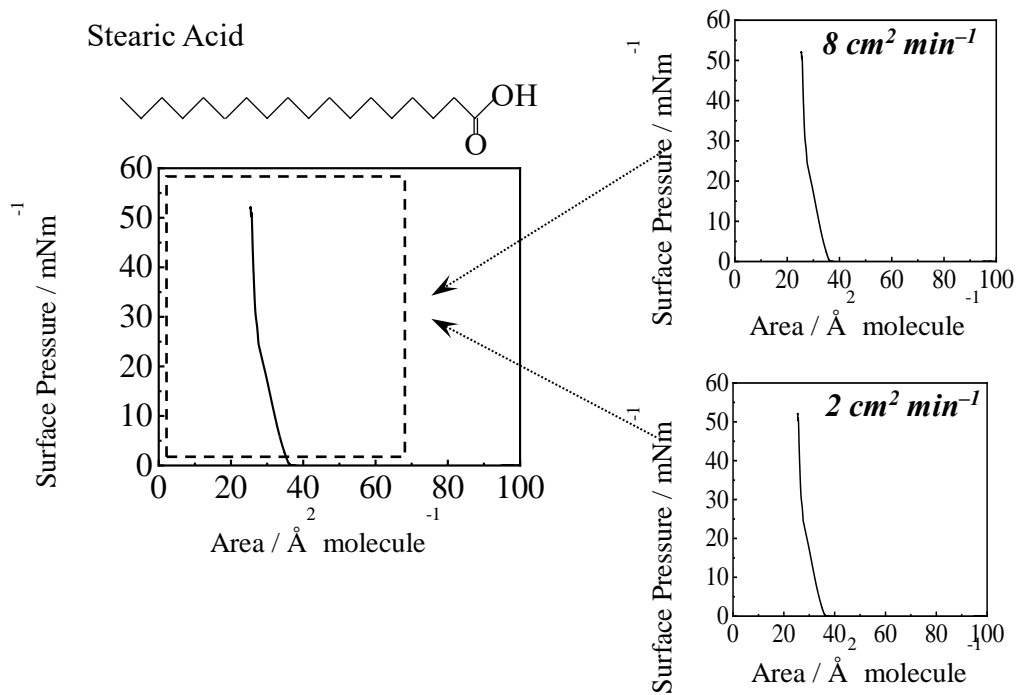


Figure 3-5. Compression rate dependence on π -A isotherms of monolayer on the water surface of stearic acid [119].

3-5. Characterization of Morphology and Arrangement of Organized Particle Films of Organo-Modified ND on Solid Substrate

Figure 3-6 is an AFM image of the surface morphology of a single particle layer formed at standard and low compression rates, and a histogram of the observed particle aggregation size. This figure clearly shows the origin of the compression rate dependence in this system. That is to say, at the standard compression rate, the aggregation size of the secondary particles becomes remarkably large. The height also increases, and three-dimensional stacking behavior is expected. In other words, in order to form a homogeneous monolayer of organo-modified NDs with high dispersibility in solution, sufficient retention time at the air/water interface is necessary.

Figure 3-7 shows the results of out-of-plane XRD for these 20 layered multilayers adjusted by the LB method. The multilayers formed by low compression rate shows that the order is higher than that of the multilayers usually formed by the compression rate. The results of the calculation of D_{001} microcrystal size by Scherrer equation are shown in Table 3-4. An increase in the 30–100 nm crystallite diameter is confirmed. Although ODP-ND is affected by the presence of impurities, an obscure d_{001} diffraction peak at standard compression clearly appears under the condition of slow compression rate.

Figure 3-8 shows the results of in-plane XRD of LB multilayers of organo-modified NDs. In all of the hydrocarbon-based modified ND, it was found that the modified chain forms a crystalline two-dimensional hexagonal packing structure. Changes in the modified chain packing mode due to differences in compression rate are not significant. However, it is obviously a system of fluorocarbon chains. The value of $d_{100} = 4.1 \text{ \AA}$ found in the case of standard compression rate is rather narrow for fluorocarbon chains [123]. Since it is a premature compression rate, there is a possibility that super-compression may form an unreasonable packing structure. In the case of low compression rate, this changes to two-dimensional triclinic

packing structure including a period of 5 Å, which is appropriate for packing fluorocarbon chains. The compression rate dependence of this system could induce structural transitions in two dimensions.

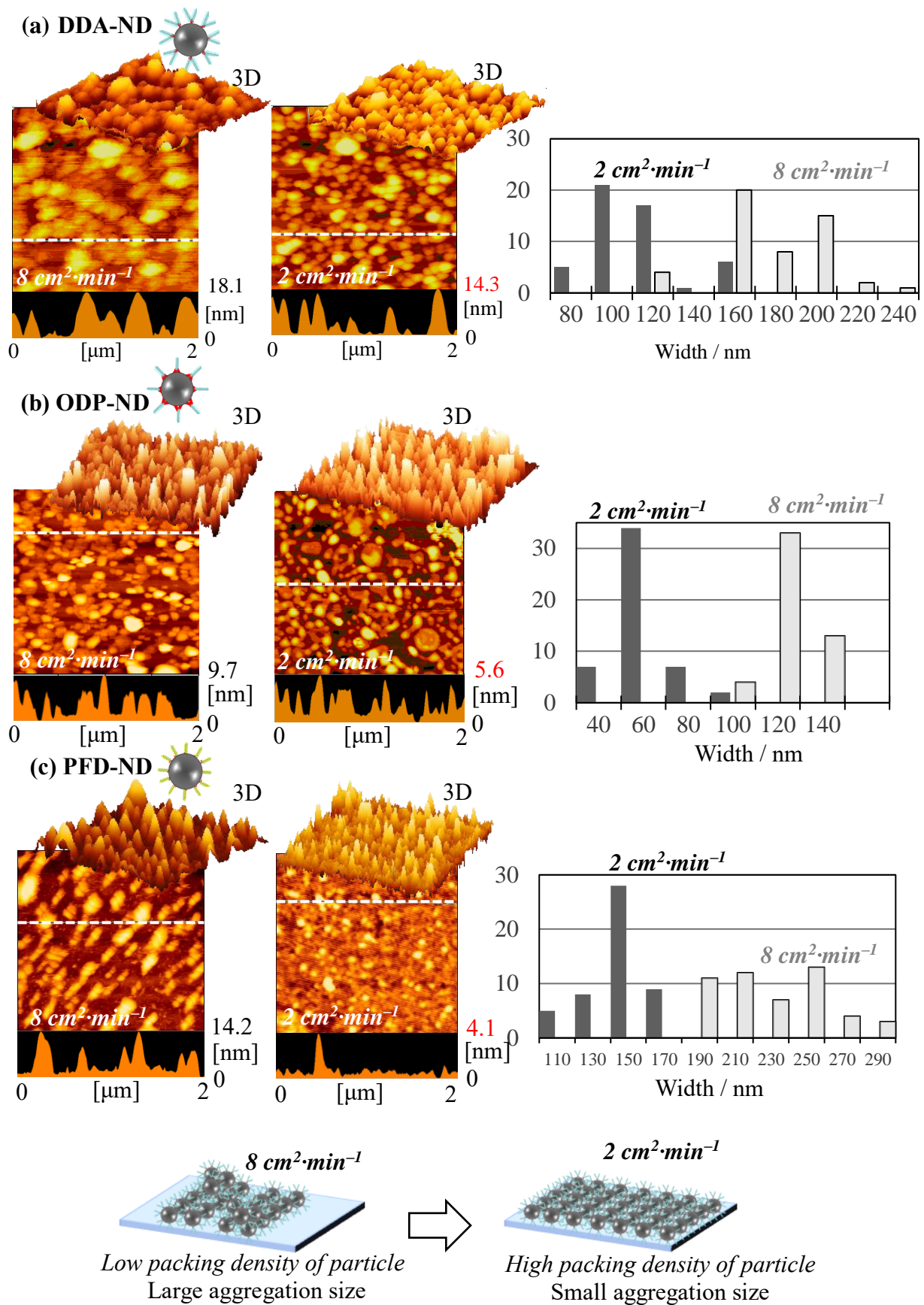


Figure 3-6. AFM images of single particle layers on solid of organo-modified NDs formed by different compression rates, and histograms of their secondary aggregated particles (black: $2 \text{ cm}^2 \cdot \text{min}^{-1}$, gray: $8 \text{ cm}^2 \cdot \text{min}^{-1}$). The upper left corner of each figure shows 3D images.

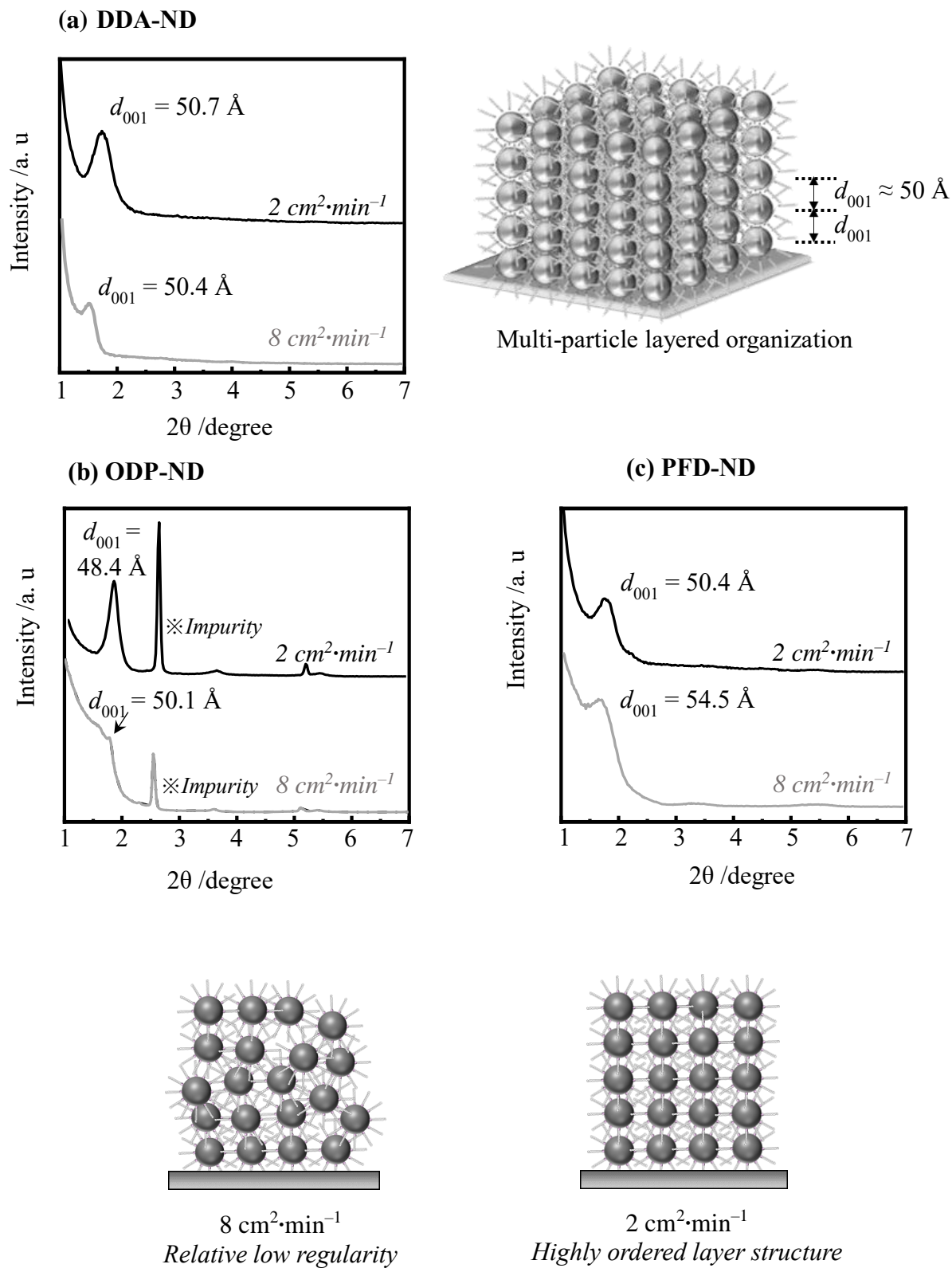


Figure 3-7. Out-of-plane XRD profiles of LB multi-particle layers of organo-modified NDs formed by different compression rates.

Table 3-4. Crystallite size of organo-modified NDs estimated by out-of-plane XRD.

<i>Crystallite sizes</i> - diameter of crystallite at perpendicular direction to the (001) plane -		
Samples	D_{001} (8 cm²·min⁻¹)	D_{001} (2 cm²·min⁻¹)
DDA-ND	197 Å	248 Å
ODP-ND	601 Å	700 Å
PFD-ND	190 Å	226 Å

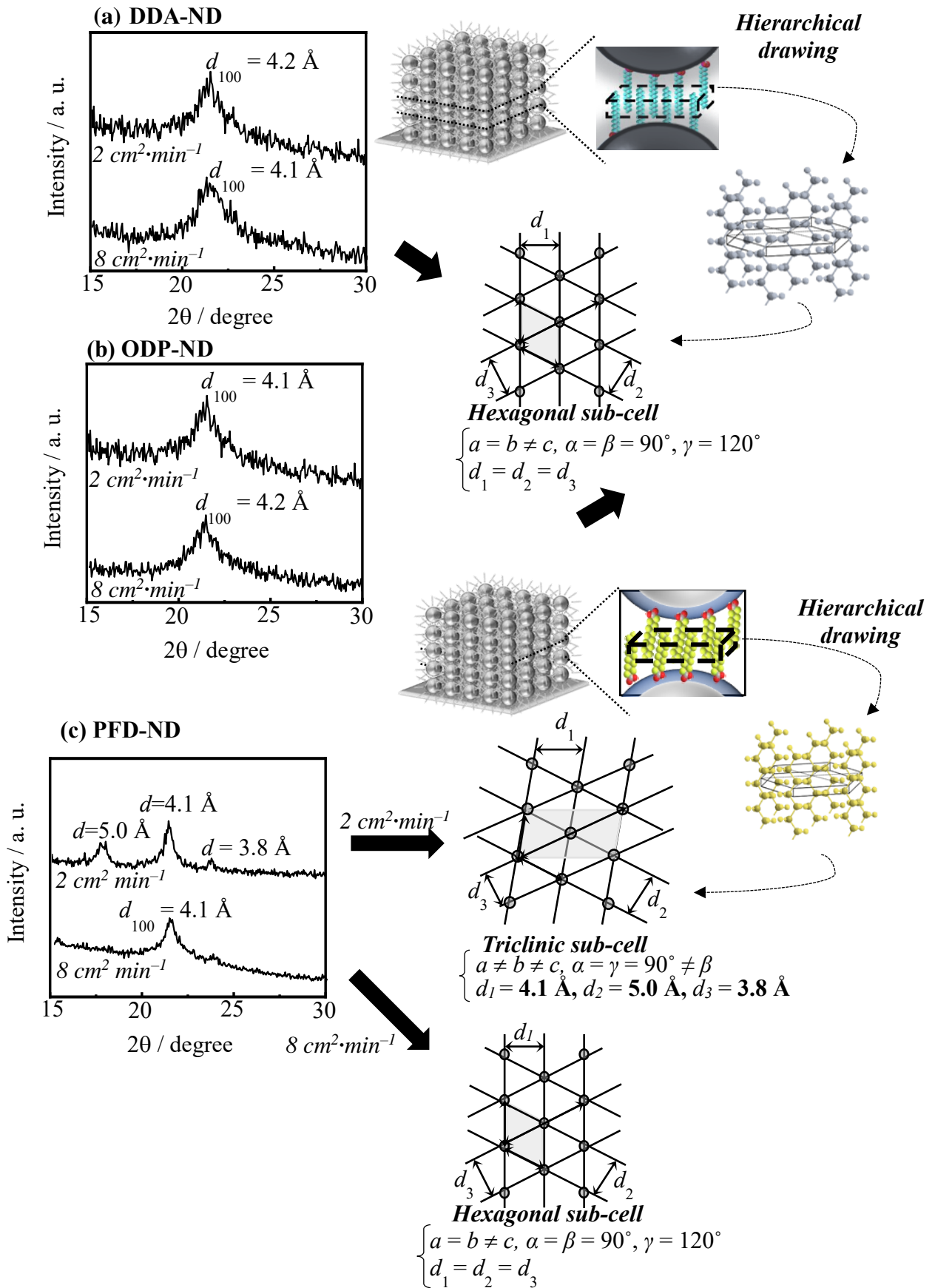


Figure 3-8. In-plane XRD profiles of LB multi-particle layers of organo-modified NDs formed by different compression rates, and schematic models of analyzed their packing system.

3-6. Relation between Condensation Behavior at Air/Water Interface and Dispersibility in Solution of Organo-Modified ND

The contents of this research are summarized in Fig 3-9. The dispersibility of organo-modified ND in solvent is closely related to the condensation behavior of interfacial particle film. As the dispersibility in organic solvent increases, lipophilization progresses such that the stability as a carbon film on the water surface decreases. However, since the modification rates are not 100% under sufficient retention time, the modified nanoparticles direct the relatively low-coated hydrophilic surface to the subphase side, improving the stability as a single layer. This is thought to appear as a difference in secondary particle aggregation size at the air/water interface.

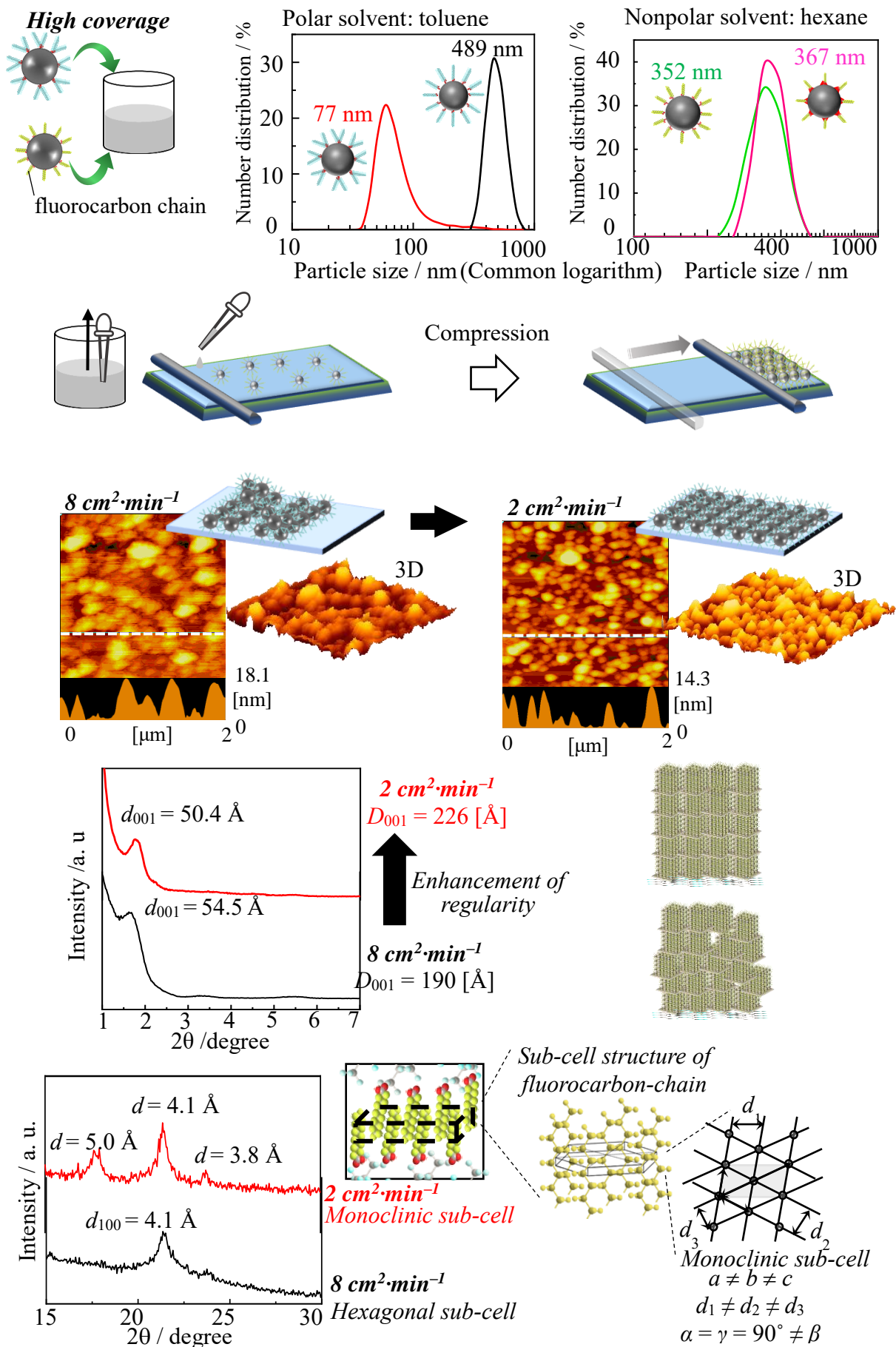


Figure 3-9. Schematic illustration of summary in this study.

3-7. Conclusion

With regard to the above contents, further consideration will be made with reference to Fig S4. In this discussion, the result of the preliminary faster compression speed (32 cm²/min) is also schematically included, and these experimental facts are explained. Nanoparticles with excellent dispersibility in an organic solvent have high lipophilicity. This is consistent with the high degree of coverage with the modifier on the nanoparticle surface. This corresponds to a case where the modification rate is high, or the coverage rate is high due to the existence of a plurality of modified chains. If the modification rate is 100%, nanoparticles completely covered with the hydrophilic part are formed, so this monolayer is unstable on the water surface. It is better to pile up each other in the height direction rather than arrangement in the same plane at the air / water interface. However, if the modification rate is not 100%, the organo-modified nanoparticles will direct the hydrophilic part to the water surface over time and orient the hydrophobic rich modified-chain part as far as possible toward the air. In the case of low modification rate particles, the time for this rearrangement = Retention Time may be short. However, nanoparticles with excellent dispersibility in organic solvents and with high coverage will take longer to rearrange them. Therefore, as shown in Fig. 3-10, it is considered that it needs the sufficient time for rearrangement as a stable single particle layer on water surface at a low compression speed. On the other hand, as the compression speed increases, interfacial aggregation of the particles and piled-up in the height direction are promoted. Such discussion never occurred unless "organo-modified nanoparticles" themselves were produced. Now, the purpose of utilizing nanoparticles in organic solvents is born, and when this is actually produced, the academic theory concerning its behavior will be constructed. This research is a challenge to an extremely new system, and it will be the first step in attempts to create new theories.

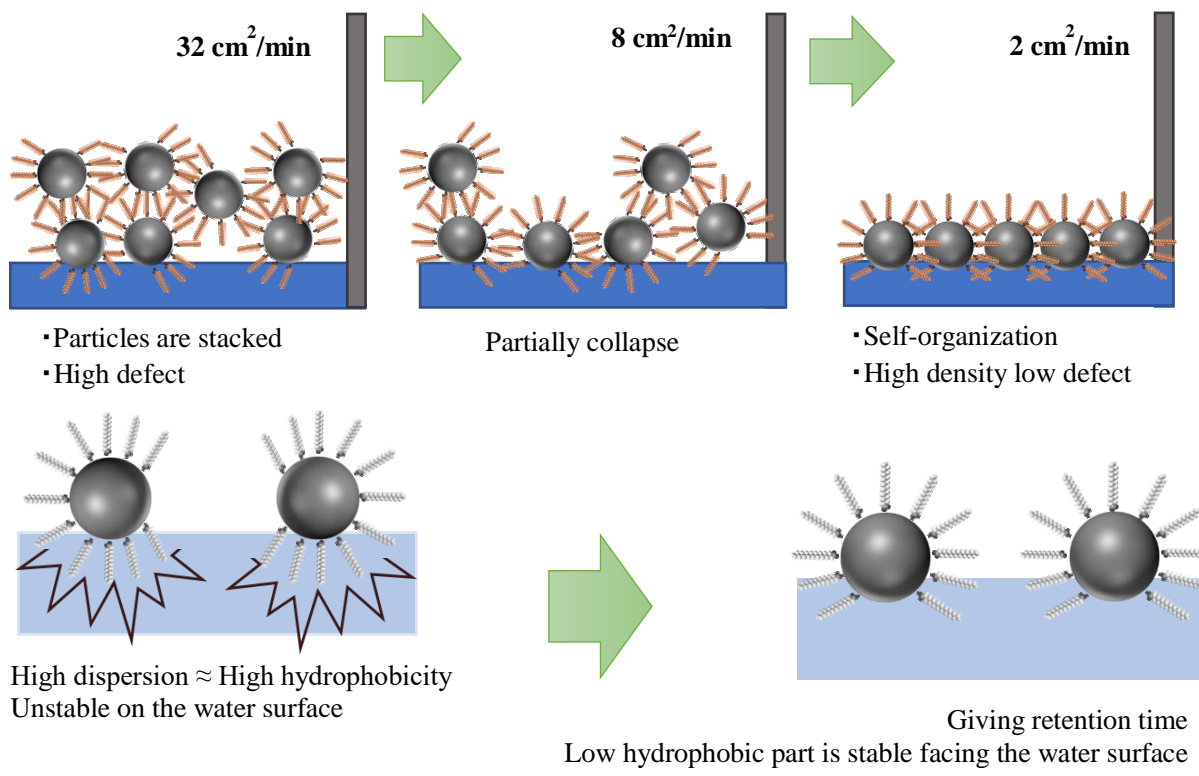


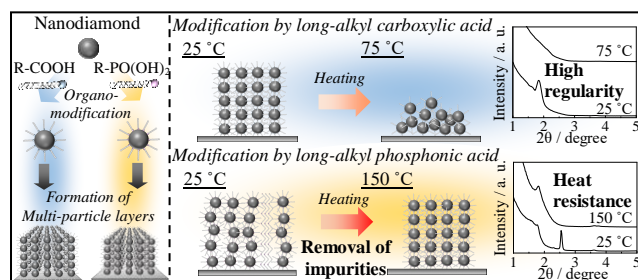
Figure 3-10. Schematic illustration of compression rate dependence of condensation behavior at air / water interface of organio-modified ND.

Chapter 4. Thermal stability of ordered multi-particle layers of long-chain phosphonate-modified nanodiamond with superior heat-resistance

4-1. Abstract

The maintenance properties of the layered regularity in organized films of heat-resistant, organo-modified nanodiamond upon heating were investigated. In long-chain phosphonic acid-modified nanodiamond, desorption of the modified-molecular chain due to temperature elevation was suppressed until 350 °C. This innovative improvement is compared to the desorption behavior at 155 °C of chains of stearic acid-modified nanodiamond. When two-dimensional films with layered organization were formed, clear layered periods were observed, and it was simultaneously confirmed that unmodified-chain impurities could not be removed. Temperature-controlled X-ray diffraction and IR measurements showed that impurities could be fired and removed. Due to the annealing effect during heating above 100 °C, the layered order was enhanced owing to rearrangement of the organo-nanodiamonds. The layered regularity of the organo-particle layers during heating was maintained up to 175 °C, far exceeding the value of 50 °C of the organized film of stearic acid-modified nanodiamond. This technique is expected to be developed for single-layer coating on the outermost layer of a surface with a nanodiamond, which has excellent antibacterial properties and high refractive index and thermal conductivity.

Keywords: nanodiamond; organo-modification; long-chain phosphonic acid; single-particle layer; maintenance properties of layered regularity under heating



4-2. Solid-State Structure and Monolayer Formation of Organo-Modified ND

Figure 4-1 shows the results of the temperature-controlled powder XRD of the ODPA-modified ND and the ODPA surfactant alone. The first-order reflection of ODPA-ND appears at $d_{001} = 34.6 \text{ \AA}$, and the profile of this compound appeared until the third order reflection. Formation of the developed layer structure is understood, and its periodic structure can be maintained up to 100 °C during heating. At 200 °C, this layer structure disappears. In comparison, the first-order diffraction peak in the profile at 50 °C is sharper than that measured at room temperature. This may be caused by rearrangement due to the annealing effect. The linewidth of the diffraction line at 100 °C appears to be sharper, whereas a slight decrease in the diffraction intensity was observed. It is expected that disorder due to the temperature rise also appears during rearrangement from the annealing effect. Comparing these results with the powder XRD profiles of the modifier alone, the diffraction intensity was nearly ten times greater. The diffraction peaks were also sharp, and the influence of the direct beam was not significant for the first-order reflection. Second- and third-order reflections were also observed. Although the long spacing values of ODPA were almost equal to those of ODPA-ND, the intensity of the high-order reflection was extremely high. The layer period disappeared completely at 100 °C. Therefore, the thermal stability of the periodic structural regularity was excellent in ODPA-ND.

Figure 4-2(a) shows the π -A isotherm of a single particle layer on the water surface of octadecyl phosphonate-modified ND at 15 °C. As shown in the insert model figure, since the layer is not necessarily 100% covered by modified chains, it is thought that the hydrophobic chain-rich side is exposed to the air and the adsorbed water side on the ND surface faces the subphase. The horizontal axis of this figure shows the mean area per particle. On the other hand, Fig. 4-2(b) shows the π -A isotherms of a single particle layer of ODPA-ND and a monolayer of ODPA-modified chain molecules on the water surfaces, with the horizontal axis converted to the compression percentage. The meaning of the notation on these horizontal axes is shown in Figs. 4-2(c) and (d), respectively. Compression percentage corresponds to the reduction rate of a single particle layer surface area covering the LB trough. This expression is useful since the number of modified chains adhering to one particle is not constant. The single particle layer and monolayer formed an extremely stable condensed film.

Figures 4-3(a) and (b) show AFM images of a single particle layer of ODPA-ND and a monolayer of ODPA on solid substrates, respectively, transferred by the upstroke LB method. Transferred surface pressures are commonly 20 mN m⁻¹. The difference between the surface morphologies is clear. On the surface of the modified-ND particle layer, an aggregate of secondary particles was observed. The ODPA surfactant monolayer is dotted as formless domains with 2 nm height. The average height information of the ODPA-ND monolayer was 6.2 nm, which is larger than 5 nm, the diameter of pristine ND (Fig. 4-3(c))

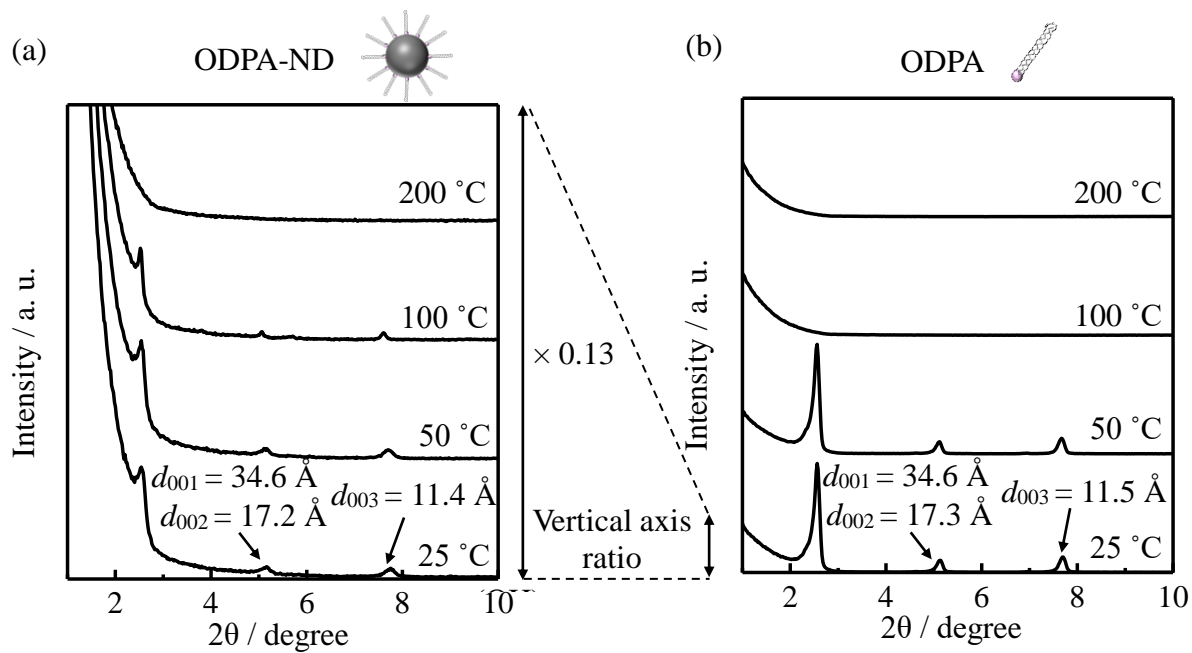


Figure 4-1. *In situ* temperature-controlled powder XRD profiles of (a) ODPA-ND and (b) ODPA in bulk.

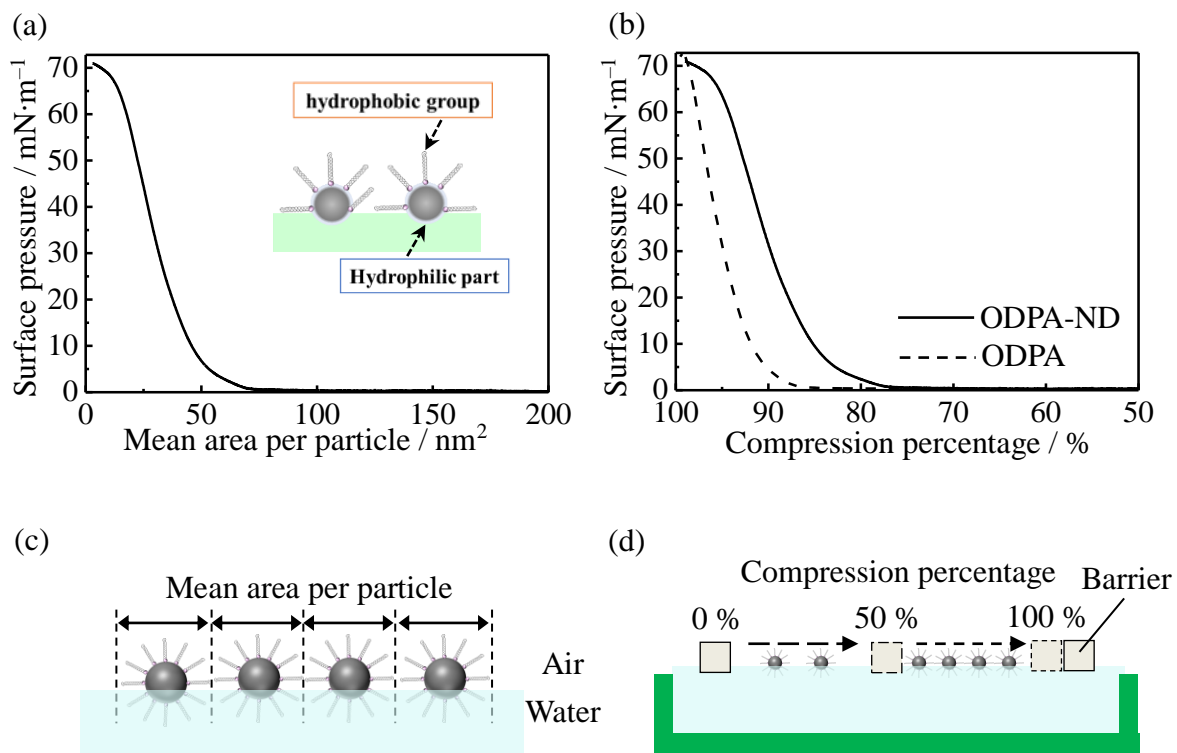


Figure 4-2. (a) Surface pressure-mean area per particle (π -A) isotherm of a monolayer of ODPA-ND on the water surface (15 °C). (b) Surface pressure-compression percentage isotherms of monolayers of ODPA-ND and ODPA on the water surface (15 °C). Schematic illustration of (c) mean area per particle and (d) compression percentage in these measurements.

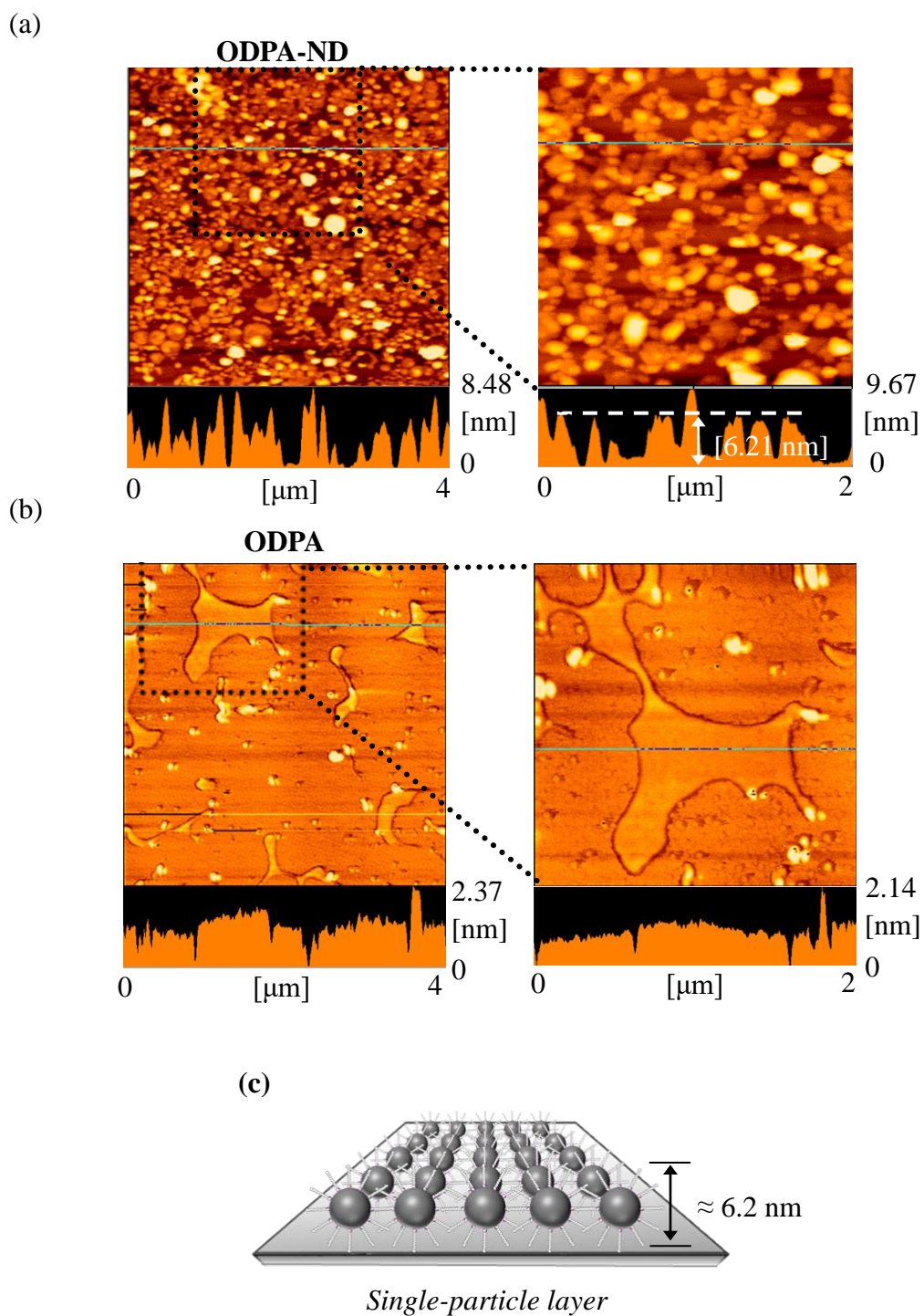


Figure 4-3. Mesoscopic AFM images of Z-type (a) single-particle layer of ODPA-ND and (b) monolayer of ODPA transferred by the LB method at 20 mN m^{-1} ($15 \text{ }^\circ\text{C}$) on a solid. (c) Schematic illustration of the single-particle layer of ODPA-ND.

4-3. Multi-Particle Layer Structure of Organo-Modified ND

Figures 4-4(a)-(c) show the results of temperature-controlled out-of-plane X-ray diffraction of the LB multi-particle layers (20 layers) of ODPA-ND. First, a periodic structure of about 5 nm, which appears to be the first order reflection of organo-modified ND, was observed in the measurement at room temperature (Fig. 4-4(a)). However, the corresponding diffraction peak was not clear at this stage. On the contrary, it was unexpected and undesirable that a diffraction peak originating from the organo-modified agent alone, which can be referred to as an impurity, appeared. Based on corresponding value of the period, multilayers composed of ODPA monolayers were undoubtedly formed. Although purification after the organo-modification reaction was thoroughly performed to eliminate the periodic value derived from this impurity, the impurity was not removed by the chemical treatment. One possibility is that partial desorption occurred during formation of a monolayer. However, a rather interesting phenomenon was also observed. The first-order diffraction peak of the ODPA-ND multilayers became clear and sharp as the *in situ* measured temperature increased from room temperature to 75 °C, and meanwhile, the intensity of the first-order reflection peak due to the impurities was gradually weakened. The ODPA-ND multilayers showed rearrangement due to the annealing effect, and the ODPA multilayers are thought to show decreasing regularity due to increased thermal vibrations. When the measurement temperature was raised to 100 °C, the long period of the multilayers of the ODPA modifier alone

completely disappeared. On the other hand, the first-order periodic value of the ODPA-ND multilayers, which became clearer, continued to be observed at $d_{001} = 49.1 \text{ \AA}$. In the wide-angle XRD, since the certainty of the d value below $2\theta = 2^\circ$ decreased significantly, it cannot be concluded that there was a meaningful difference in the approximately 1 \AA . Essentially, the Bragg's equation is not generally used when $2\theta = 2^\circ$ or less, and small angle X-ray scattering is used in this region. When Bragg's equation is differentiated by θ with respect to d , the influence of the minute change of θ , $\Delta\theta$ on d is clarified. This value jumps from around 2θ value below 2 degrees. That is to say, in the wide-angle X-ray diffraction, the guarantee of "certainty" in the low angle region is markedly reduced as compared with the medium and high angle regions. Since the organo-modifier was a surfactant with a low molecular weight, the measurement temperature was raised to 150°C to remove it by sintering. During this time, the first-order diffraction peak of the ODPA-ND multilayers was maintained. Subsequently, when the temperature was brought down to room temperature, the layered period from the ODPA multilayers as an impurity completely disappeared (Fig. 4-4(b)). It is thought that the impurities may have been fired and removed, or disordering occurred sufficiently to make recrystallization impossible. Furthermore, re-heating of the multilayers occurred and the maintenance characteristic at high temperature of the regularity of the d_{001} spacing was evaluated. As a result, this periodic value was maintained up to 175°C and disappeared at 200°C (Fig. 4-4(c)). The regularity maintaining temperature of 175°C of

the ODP-ND LB multilayers is 20 °C higher than the desorption temperature of the organic chain of ODA-ND in the bulk state. Figure 4-5 shows the result of the in-plane XRD measurement accompanied by the thermal history series of this experiment. Reflections at 4.2 Å in this profile were observed as the d_{100} period of the multilayers before applying the heating and cooling processes. This spacing is associated with the two-dimensional hexagonal packing of an alkyl chain [46]. This periodic value was not observed upon cooling to room temperature after increasing the temperature to 150 °C. This spacing based on the in-plane packing is information derived from the ODP modifier as an impurity. In other words, it can be seen that the ODP-ND multilayers do not form a sub-cell packed with the modifying agent in the two-dimensional plane.

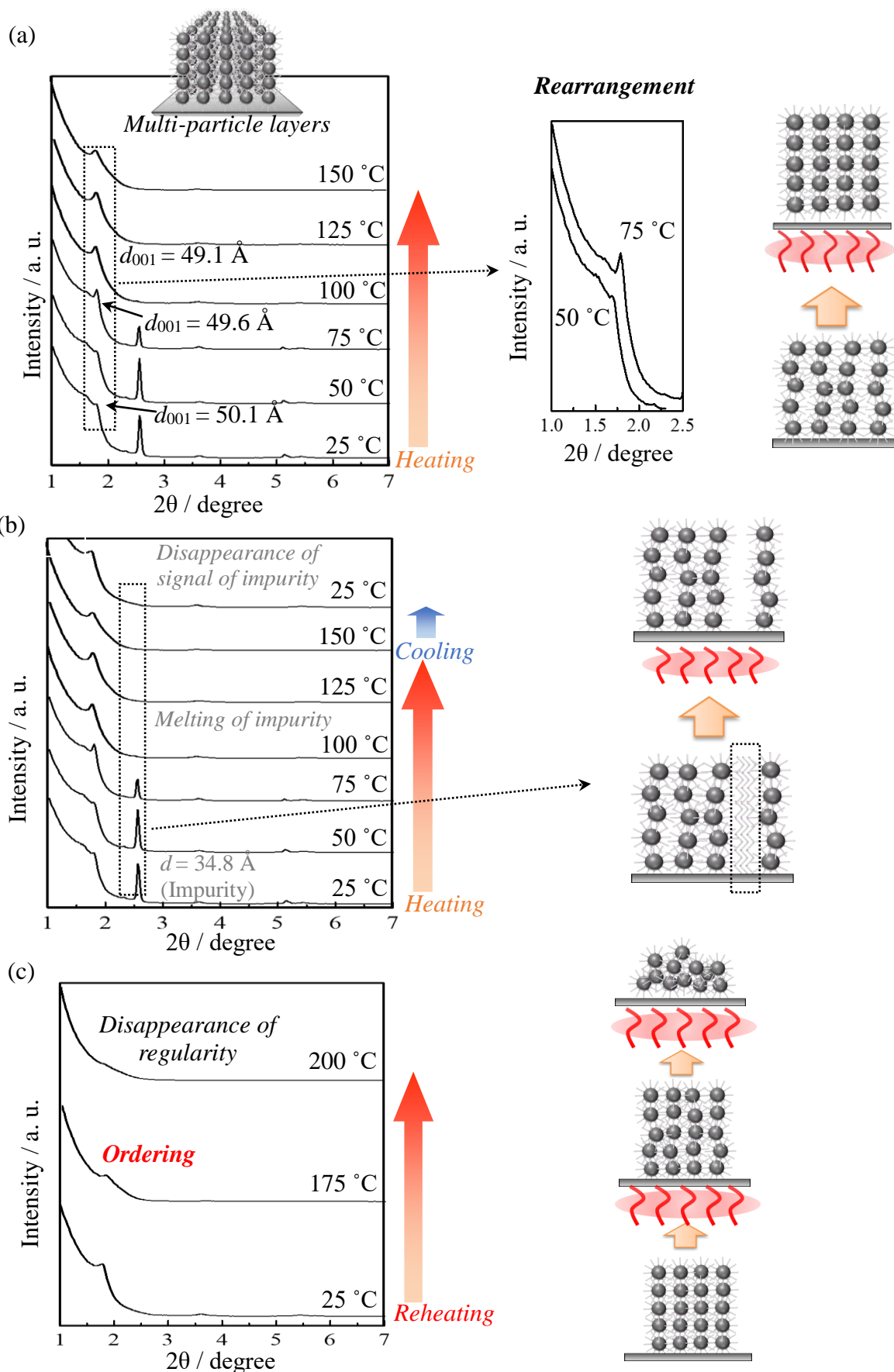


Figure 4-4. *In situ* temperature-controlled out-of-plane XRD profiles of ODPa-ND: (a) Heating process from 25 to 150 °C. (b) Cooling process to room temperature after heating from 25 to 150 °C. (c) Reheating process from room temperature to 200 °C.

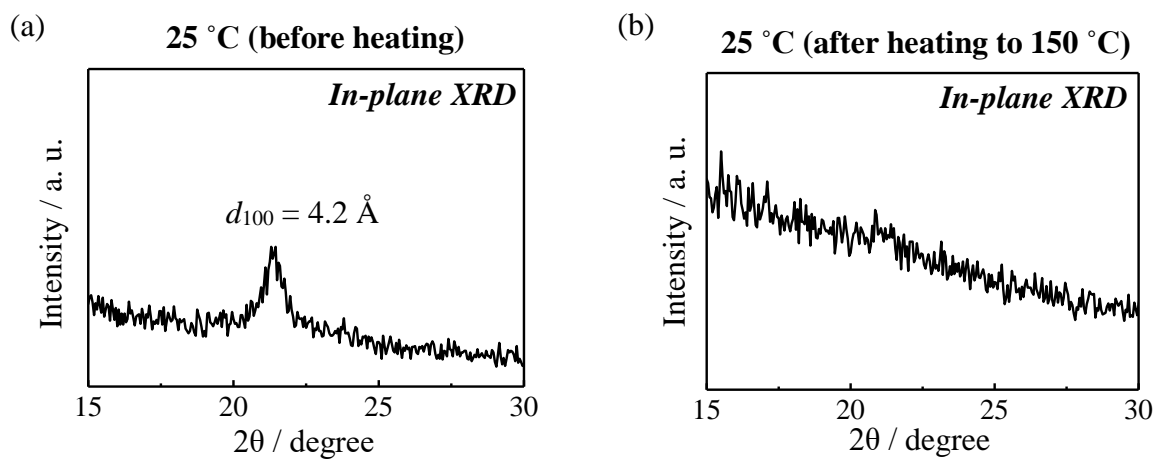


Figure 4-5. *Ex situ* temperature-controlled in-plane XRD of multi-particle layers of ODPA-ND (a) before and (b) after annealing.

4-4. Discussion

For comparison, examples of modified nanoparticles with stearic acid are shown (Fig. 4-6). The ODA-ND multilayers showed a clear layered period of about 4.8 nm in this measurement at both room temperature and 50 °C. However, these multilayers cannot completely maintain layered regularity at only 75 °C. Even if a surface coating with functional nanoparticles were created using this modifying agent, it is likely that the structure and function cannot be maintained when exposed to a temperature of 75 °C or higher. Thus, it was revealed that the thermal stability of the layered periodic structure of the modified nanoparticles was improved by 120 °C or more by merely changing the surface modifying agent.

Next, we performed a verification to determine whether the mixed film state with the modifier alone, which could not be removed by the chemical method, could be removed by firing the multilayers at 150 °C. In Fig. 4-7, changes in the C-H stretching vibration with respect to the ODPA-ND multilayers (these were actually mixed multilayers of ODPA-NA and impurity ODPA) and ODPA multilayers by *ex situ* IR measurement were monitored. Changes in the band area values are shown in Table 4-1. It should be noted that the C-H stretching vibration band appearing in this data comes from both ODPA-ND and ODPA LB films. Also, the state of the mixed film where a small number of ODPA molecules are present in the majority of ODPA-ND cannot be strictly reproduced. Thus, although this measurement

result provides valuable information, it is not conclusive. Here, corresponding consideration will be developed including the results of X-ray diffraction which has been already discussed. The modified chains of ODPA-ND, aside from the impurities in the ODPA-ND multilayers, do not form two-dimensional crystals. Although the layered regularity is less disturbed due to the stability of nanoparticles to thermal vibrations in the high temperature region, the impurity region forming two-dimensional crystals stabilized the structure of ODPA at room temperature. However, as ODPA is an impurity, it is expected that the two-dimensional crystal size cannot be increased as much as a corresponding monolayer, and their crystals were scattered finely. Presumably, even in the LB film of ODPA alone, there should be a two-dimensional microcrystal composed by long alkyl-chain. Even if the order of less than the average size whose microcrystal size could not be increased due to the influence of lattice defects, etc, the lattice spacing of the in-plane XRD would be detectable. The above-mentioned Fig. 4-5 supports this consideration. On the other hand, in Fig. 4-7, both the ODPA-ND and the ODPA multilayers gradually decreased the C-H stretching vibration band area as the temperature rises. However, by detailed comparison, in the ODPA-ND LB film, the band area drastically decreased from 81% at room temperature to 54% at elevated temperatures from 100 to 125 °C. While, in the ODPA LB film, the band area drastically decreased from 76 to 51% at 125 to 150 °C firing. Although there is a difference between a single film and a mixed film, it is thought that the decrease in band area for both is due to

sublimation from the ODPA region with a small two-dimensional crystallite size, which is an effect brought about the calcination treatment at 150 °C, corresponding to removal of ODPA unreacted (or desorbed) raw material. Therefore, from the results of XRD and IR described above, it is expected that there is a high possibility that the ODPA modifier molecule, which is an impurity having the ability to form a two-dimensional crystal, is sublimated/eliminated by heat treatment.

The above results and discussion are summarized in the schematic diagram shown in Fig. 4-8. Figure 4-8(a) shows the results of the model diagram accompanied by the thermal history obtained in this study. A mixed film state containing modified chains and modified nanoparticles was formed at room temperature. The layered period value of the unreacted modified chain was 3.5 nm, and a two-dimensional hexagonal packing formed with a 0.4 nm lattice spacing. Presumably, during firing up to 150 °C, trace amounts of impurities were calcined away and the layered structure of the organo-modified microparticles rearranged. However, it is hard to assert whether impurities were completely removed or whether they were so disturbed that they could not form a two-dimensional crystal/layer structure. The structure was maintained even when cooling was applied from this state, and the layered period was maintained even at elevated temperatures up to 175 °C. Incidentally, as shown in Fig. 4-8(b), the so-called "an interdigitated structure" of the modified chain was not formed between the upper and the lower layers, and it is thought that this structure was maintained by

the interaction between the alkyl chain ends. If the interdigitated structure formed, there is a high likelihood that an in-plane spacing derived from the modified-chain was observed even after removal of impurities (or loss of structure).

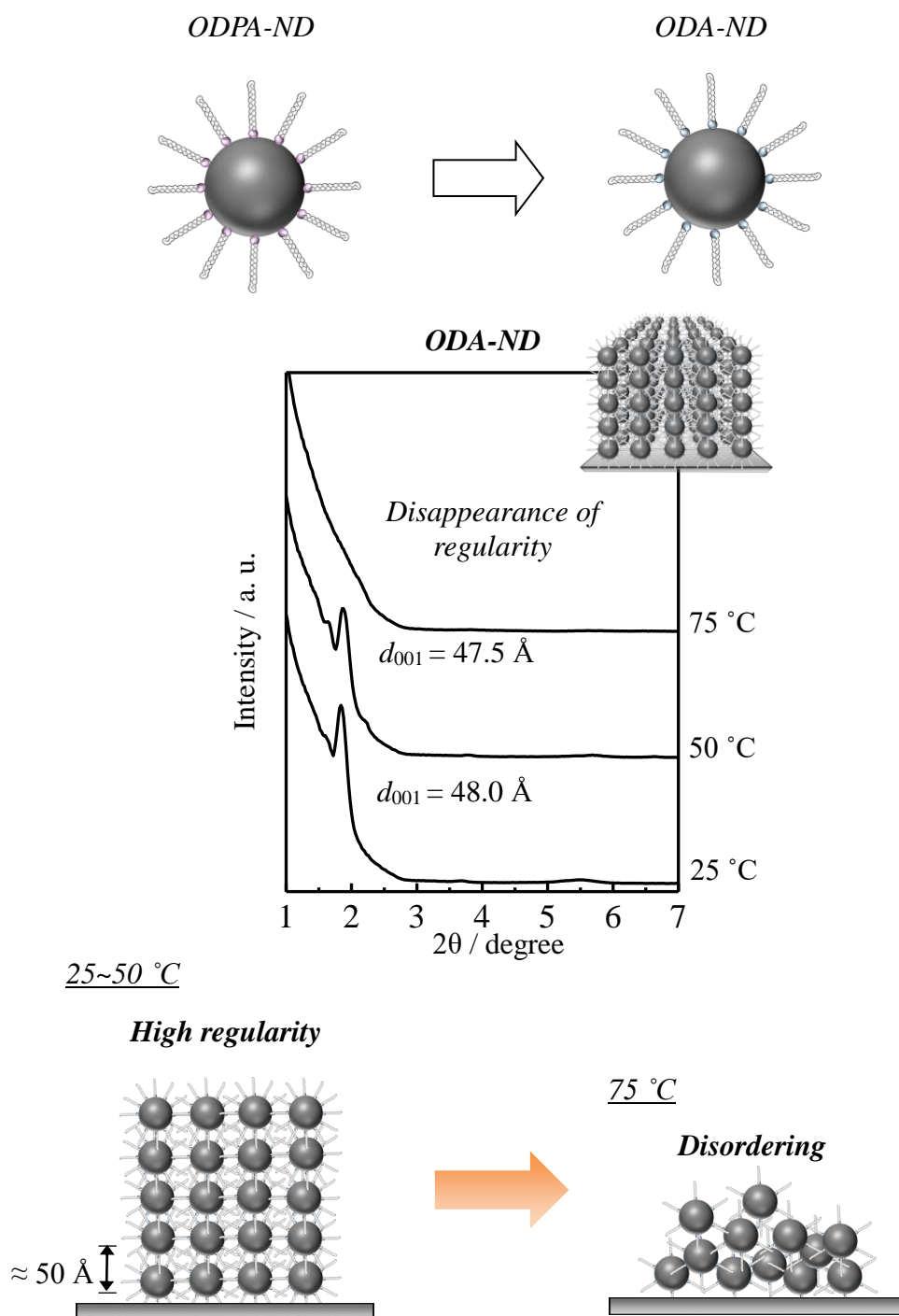


Figure 4-6. *In situ* temperature controlled out-of-plane XRD profiles and schematic illustration of the layered structure of multi-particle layers of ODA-ND transferred at 30 mN m^{-1} (15 °C).

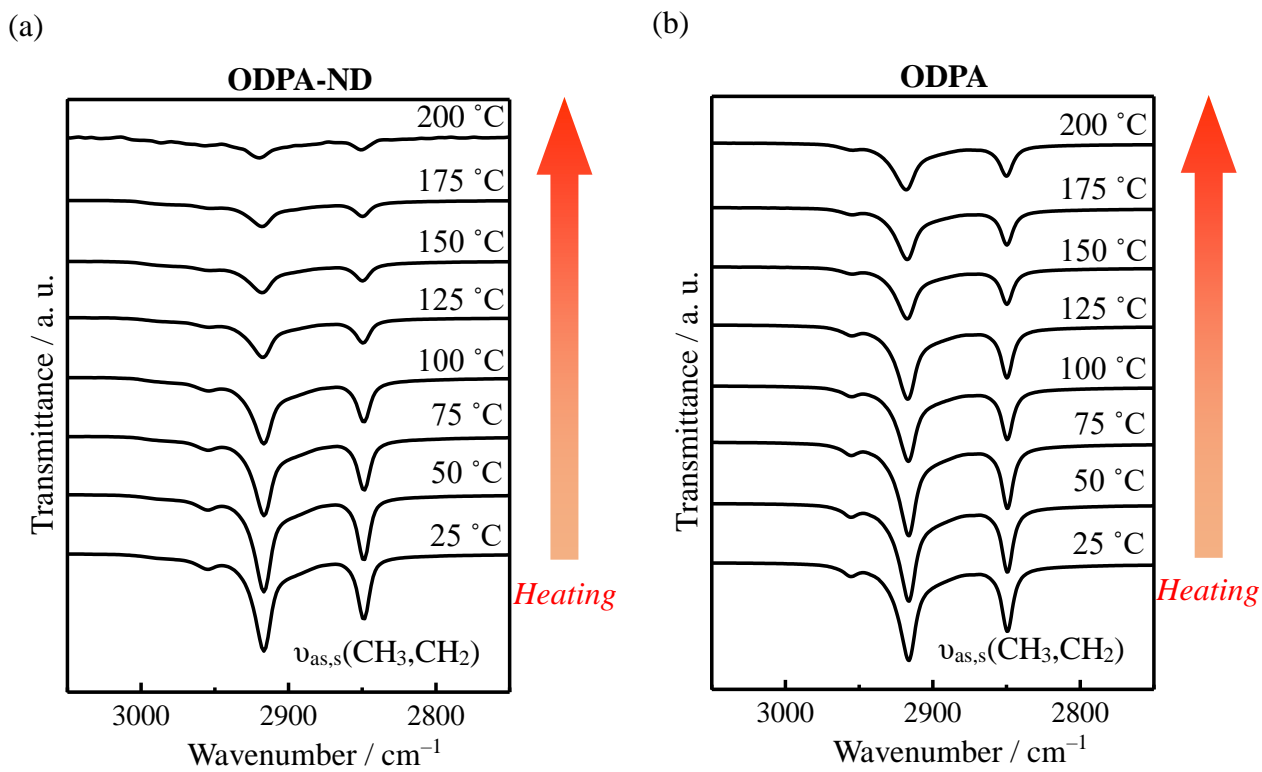


Figure 4-7. *Ex situ* temperature-controlled IR spectrum of multilayers of ODPA-ND and ODPA transferred at 40 mN m⁻¹ (15 °C).

Table 4-1. Changes in absorbance peak areas of symmetric and asymmetric C-H stretching vibrations for the LB multilayers of ODPA-ND and ODPA.

Peak area of absorbance for C-H stretching bands [Abs]		
	ODPA-ND	ODPA
25 °C	0.8838	3.6291
50 °C	0.8934	3.4728
75 °C	0.8054	3.3494
100 °C	0.7234	2.7680
125 °C	0.4803	2.7638
150 °C	0.3970	1.8775
175 °C	0.3565	1.4966
200 °C	0.3471	1.6745

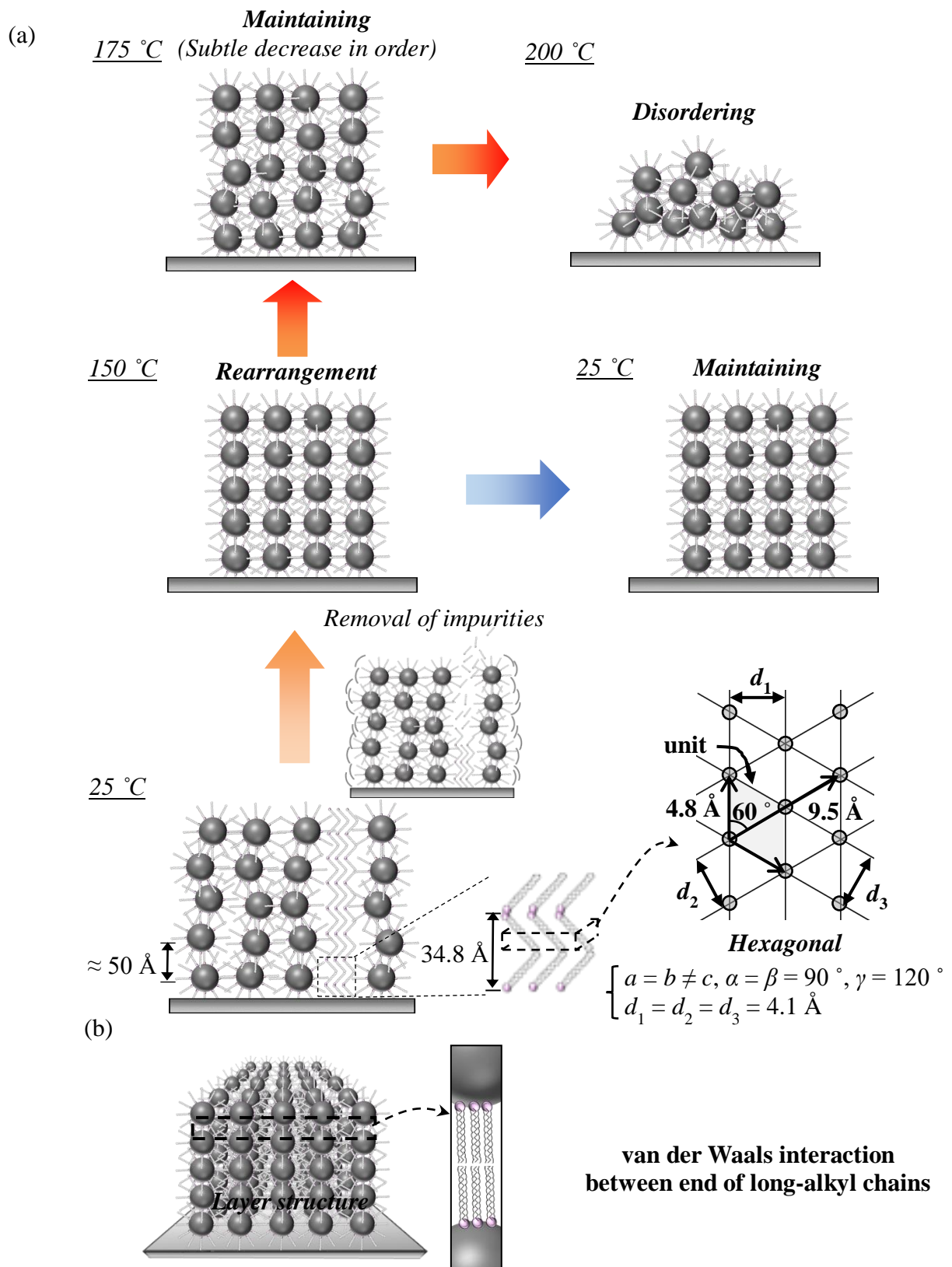


Figure 4-8. (a) Schematic illustration of the structure of multilayers of ODPA-ND with heating. (b) Schematic model of layer structure formation by van der Waals interactions between ends of long-alkyl chains on the ODPA-ND surface.

4-5. Conclusion

Finally, in Fig. 4-9, the structural transitions of the layered structures of a series of modified particles are summarized as a phase diagram. The ordinate indicates the orderliness of the layered structure. The layered structure is thought to be a useful structure for material function due to its exfoliation capability, space utilization between layers, interlayer electron transfer, etc. However, this is a structure limited to graphite, clay, etc. for inorganic materials, and the environmental stability of organic substances/biological substances such as surfactants and cell membranes is low. The technique of surface-modification of such functional inorganic nanoparticles with a heat-resistant organic modifier is highly likely to be utilized as a universal technique, regardless of the selectivity of materials. It is hoped that this work will be expanded and used to develop new technologies in the future.

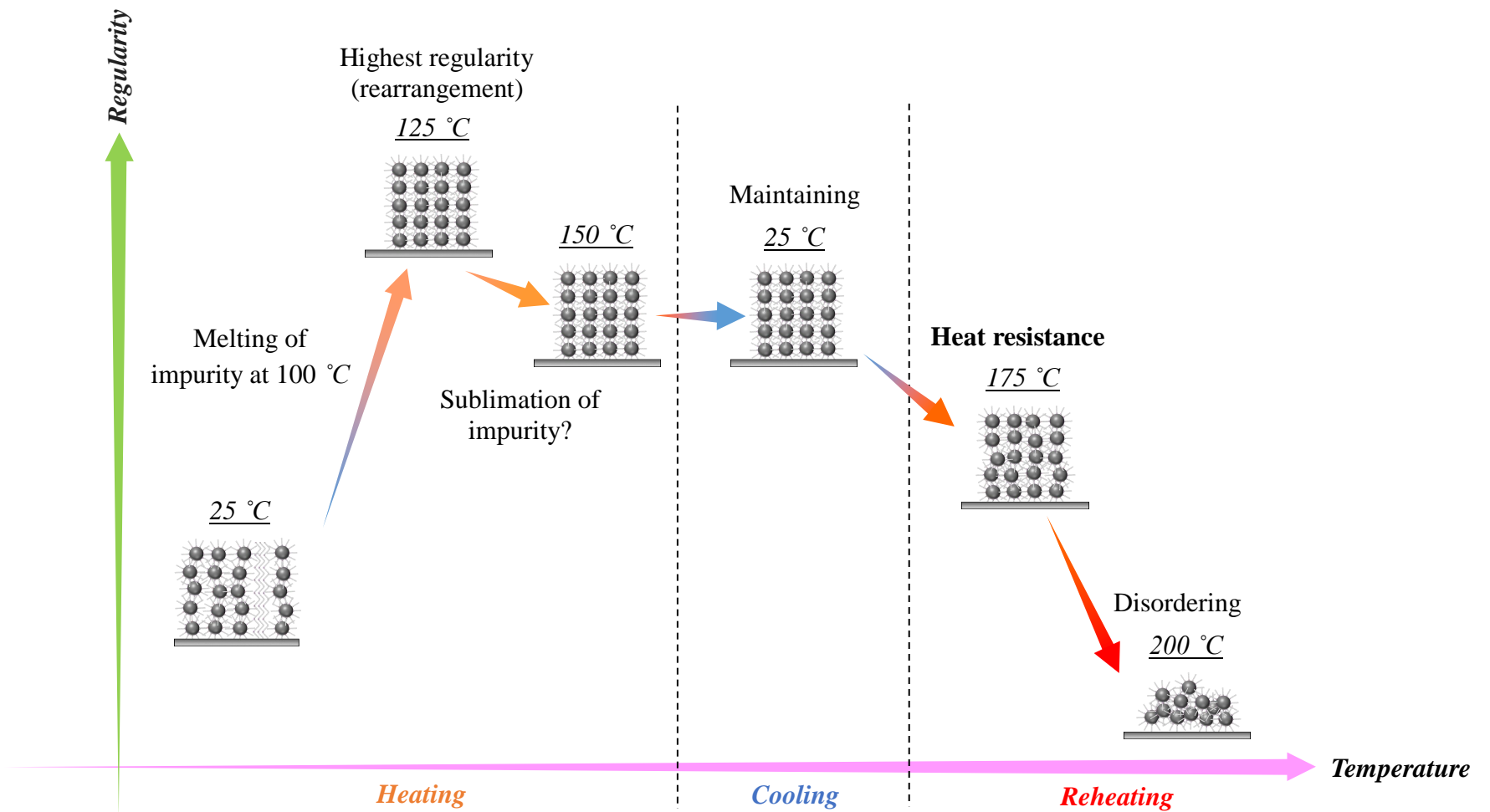


Figure 4-9. Changes in the layered regularity of LB multilayers of ODPa-ND with heating/cooling summarized as a phase diagram.

Chapter 5. Topological "Interfacial" Polymer Chemistry

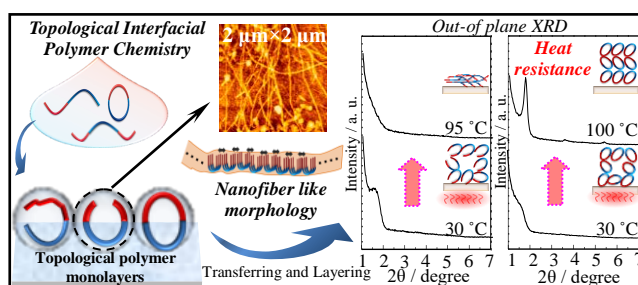
–Dependency of Polymer "Shape" on Surface Morphology and Stability of Layer Structures when Heating Organized Molecular Films of Cyclic and Linear Block Copolymers of n-Butyl Acrylate–Ethylene Oxide–

5-1. Abstract

The “topological polymer chemistry” of amphiphilic linear and cyclic block copolymers at an air/water interface was investigated. A cyclic copolymer and two linear copolymers (AB-type diblock and ABA-type triblock copolymers) synthesized from the same monomers were used in this study. Relatively stable monolayers of these three copolymers were observed to form at an air/water interface. Similar condensed-phase temperature-dependent behaviors were observed in surface pressure–area isotherms for these three monolayers. Molecular orientations at the air/water interface for the two linear block copolymers were similar to that of the cyclic block copolymer. Atomic force microscopic observations of transferred films for the three polymer types revealed the formation of monolayers with very similar morphologies at the mesoscopic scale at room temperature and constant compression speed. ABA-type triblock linear copolymers adopted a fiber-like surface morphology via two-dimensional crystallization at low compression speeds. In contrast, the cyclic block copolymer formed a shapeless domain. Temperature-controlled out-of-plane X-ray diffraction (XRD) analysis of Langmuir–Blodgett (LB) films fabricated from both amphiphilic linear and cyclic block copolymers was performed to estimate the layer regularity at higher temperatures. Excellent heat-resistant properties of organized molecular films created from the cyclic copolymer were confirmed. Both copolymer types showed clear diffraction peaks at room temperature, indicating the formation of highly ordered layer structures. However, the layer structures of the linear copolymers gradually disordered when heated. Conversely, the regularity of cyclic copolymer LB multilayers did not change with heating up to 50 °C.

Higher-order reflections (d_{002} , d_{003}) in the XRD patterns were also unchanged, indicative of a highly ordered structure.

Keywords: Block copolymer, Cyclic polymer, Molecular orientation, Topological polymer chemistry, Monolayer at air/water interface



5-2. Monolayer Formation of Topological Polymers at Air/Water Interface

Figure 5-1(a) shows the π -A isotherms describing the monolayer behaviors of the three block-copolymer shapes examined, in which the compression percentage to the area of LB trough is expressed on the horizontal axis. A "Mean area per repeating monomer unit" as the horizontal axis of isotherms are conveniently indicated in Figure 5-2. The temperature of the subphase was maintained at 15 °C. At first glance, all three polymers showed similar isotherms, with limiting condensed phase areas of about 20 Å² and collapsed surface pressures below 30 mNm⁻¹. Since the values of the horizontal axis were considerably smaller than the limiting area per monomer, these values seemed unusual. (The horizontal axis values are twice the value they should be because two hydrophobic polymer chains cross the air/water interface, as illustrated in the diagram at the bottom of Fig. 5-1.) The reason for this can be seen in the analogous illustrations of the three polymers, which show, to some extent, that there is no preference for any of the cyclic polymer conformations at the air/water interface, as indicated by the similar results of their individual isotherms. Linear AB-type, linear ABA-type, and cyclic-type polymers are expected to have similar interfacial conformations since different topological polymers show similar isotherms. In other words, it appears that the two types of linear polymers adopt a conformation similar to that of the cyclic polymer at the interface. At this stage, the expansion behavior of the linear polymers having unconnected termini is more remarkable than that of the cyclic polymers. The upper part of the illustration of the interfacial model of the linear AB-type polymer in condensed phase of this figure might be exaggerated (see Fig. 5-1). Indeed, the hydrophobic chains exposed to air as shown in the lower part of this figure, seem to be covering the monolayer surface.

The results of π -A isotherm measurements with rising subphase temperatures are shown in Figs. 5-1(b), and 5-1(c) in which changes in the isotherms at subphase temperatures of 25 °C and 35 °C can be observed. All isotherms indicated an expansion tendency concomitant

with an increase in subphase temperature. As a supplement to this figure, from which a full understanding of the characteristic differences of each polymer might be difficult, actual values of the measurements are summarized in Table 5-1. Table 5-1 summarizes the limiting area of condensed and expansion phases as the surface pressure collapses. This data quantitatively indicates that the three polymer types also adopted behaviors and surface conformations similar to linear polymers, with no significant disturbance observed up to 35 °C. Further, the crossing point of the extrapolation lines between the expansion phase and the condensed phase have defined as the transition point. In Figure 5-3, the plots of surface pressure and the molecular area of transition points *vs.* subphase temperature are shown, respectively. Value of the limiting area of transition from the expanded phase to the condensed phase reasonably increases with the rising of subphase temperature. It shows the expansion trend in high subphase temperature conditions. Value of the surface pressure of the transition from the expanded phase to the condensed phase decreases with the rising of the subphase temperature. It finds that the phase transition at relative low surface pressure occurs under the high subphase temperature conditions in this system. In this case, thermal behavior in the bulk is worthy of consideration. DSC thermograms of these topological polymers are shown in Fig. 5-4. PEO units as hydrophilic group in the bulk are crystalline, and hydrophobic n-butyl acrylate corresponds amorphous state. Here, only the melting peak derived from PEO unit is detected. Since the melting point of monolayer on the water surface is generally lower than that in the bulk, it is expected to indicate an expansion trend of these polymers with relative low melting point in the high subphase temperature conditions.

Surprisingly, amphiphilic polymers having different shapes, but identical polymer components exhibited very similar monolayer behaviors and a dependence on subphase temperature. Such behavior is rare among the recent reviews of polymer LB film [61, 62].

Figure 5-5 also shows the π -A isotherms of copolymer monolayers with systematically extended hydrophobic chain lengths for each of the three kinds of polymers. In the case of linear AB-type and cyclic copolymers with long hydrophobic chains, the isotherms showed almost no change. In contrast, linear ABA-type copolymers with short hydrophilic and long hydrophobic groups showed a relatively small limiting area. Therefore, it was found that the shortening of hydrophilic groups influenced the limiting area of isotherms for these polymers. From the results discussed above, it is expected that the formation of this type of interfacial conformation would be represented by the diagram at the top of Fig. 5-1.

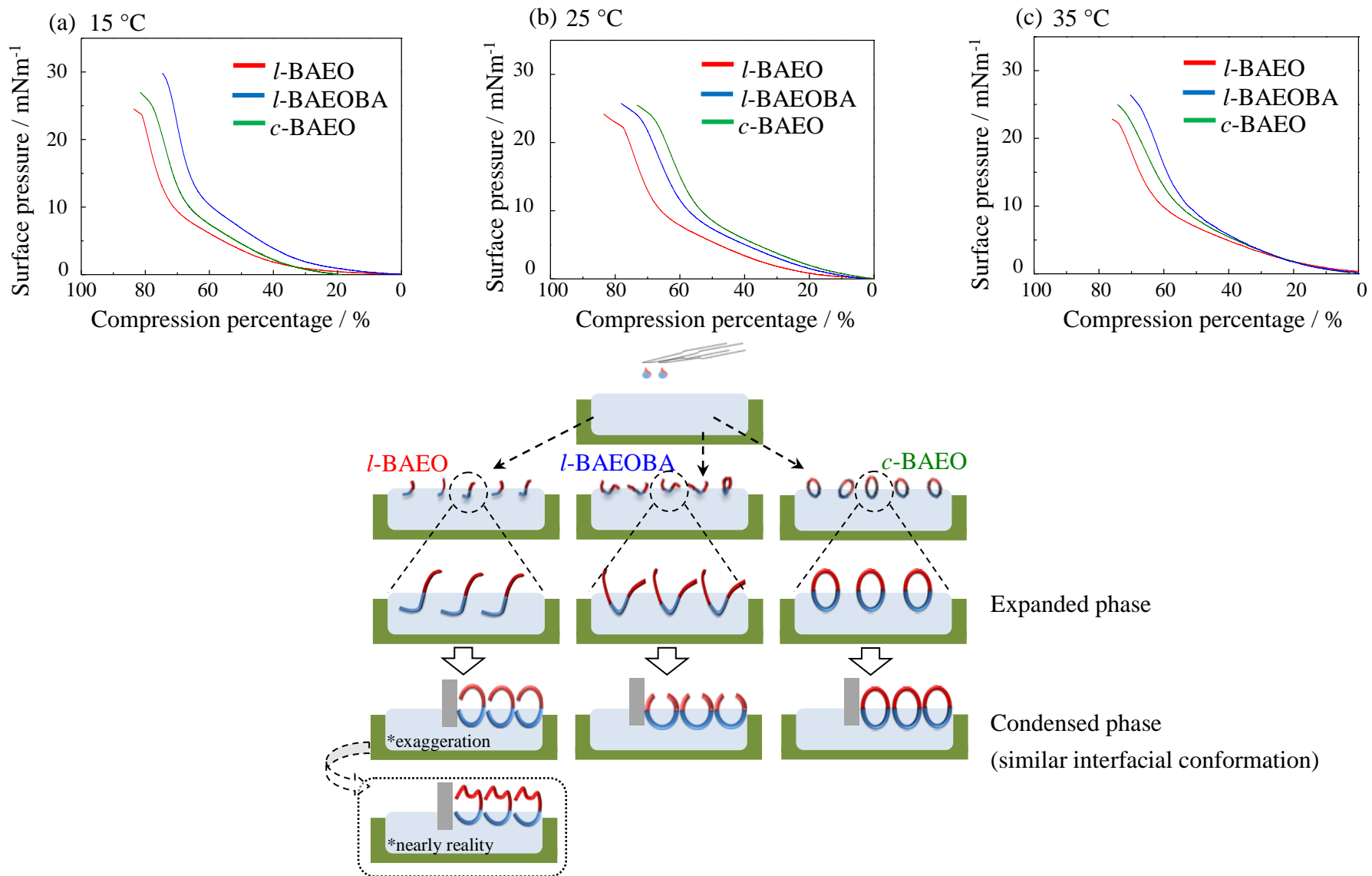


Figure 5-1. π -A isotherms of monolayers on the water surface for *l*-BAEO, *l*-BAEOBA and *c*-BAEO at (a) 15, (b) 25, and (c) 35 °C. (Insert: Schematic illustration of formation mechanism of interfacial conformation)

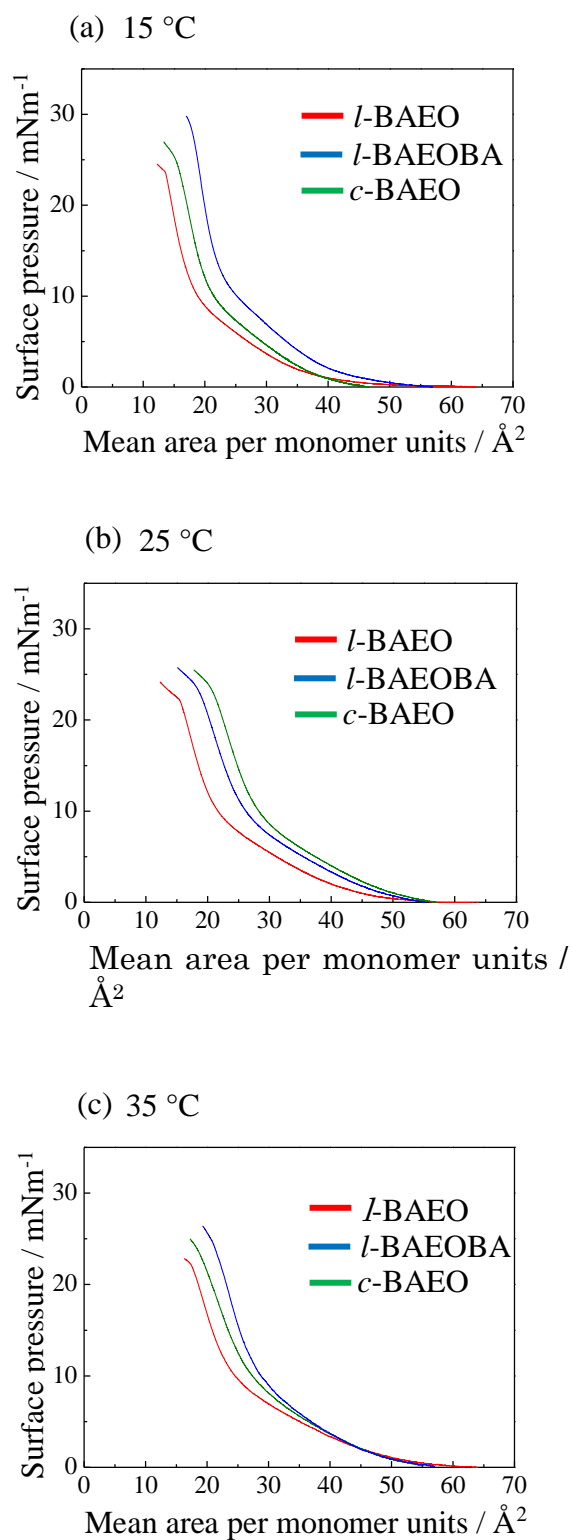
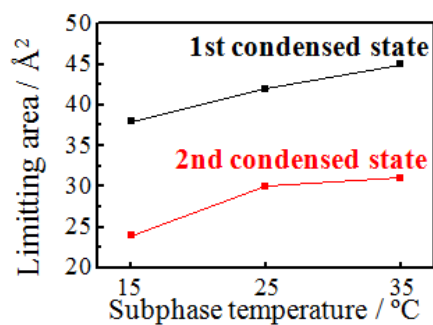


Figure 5-2. π -A isotherms of monolayer on the water surface for (a) *l*-BAEO, (b) *l*-BAEOBA and (c) *c*-BAEO with mean area per monomer units as lateral axis.

Table 5-1. Limiting areas and collapsed pressures for (a) *l*-BAEO, (b) *l*-BAEOBA and (c) *c*-BAEO.

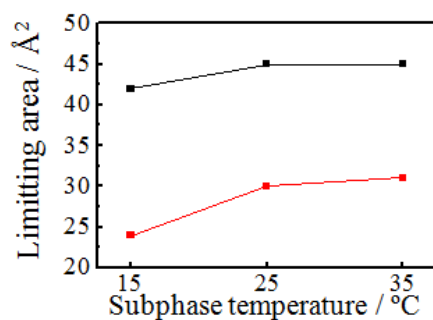
***l*-BAEO**

	First condensed state (\AA^2)	Second condensed state (\AA^2)	Collapsed surface pressure (mNm^{-1})
15 °C	38	24	23
25 °C	42	30	22
35 °C	45	31	22



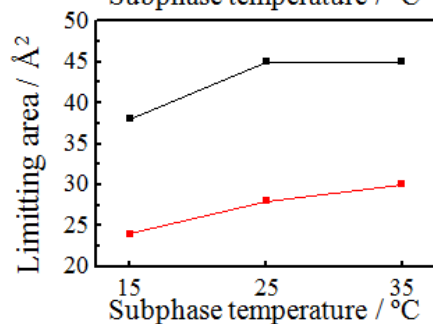
***l*-BAEOBA**

	First condensed state (\AA^2)	Second condensed state (\AA^2)	Collapsed surface pressure (mNm^{-1})
15 °C	42	24	28
25 °C	45	30	24
35 °C	45	31	25



***c*-BAEO**

	First condensed state (\AA^2)	Second condensed state (\AA^2)	Collapsed surface pressure (mNm^{-1})
15 °C	38	24	25
25 °C	44	28	24
35 °C	45	30	24



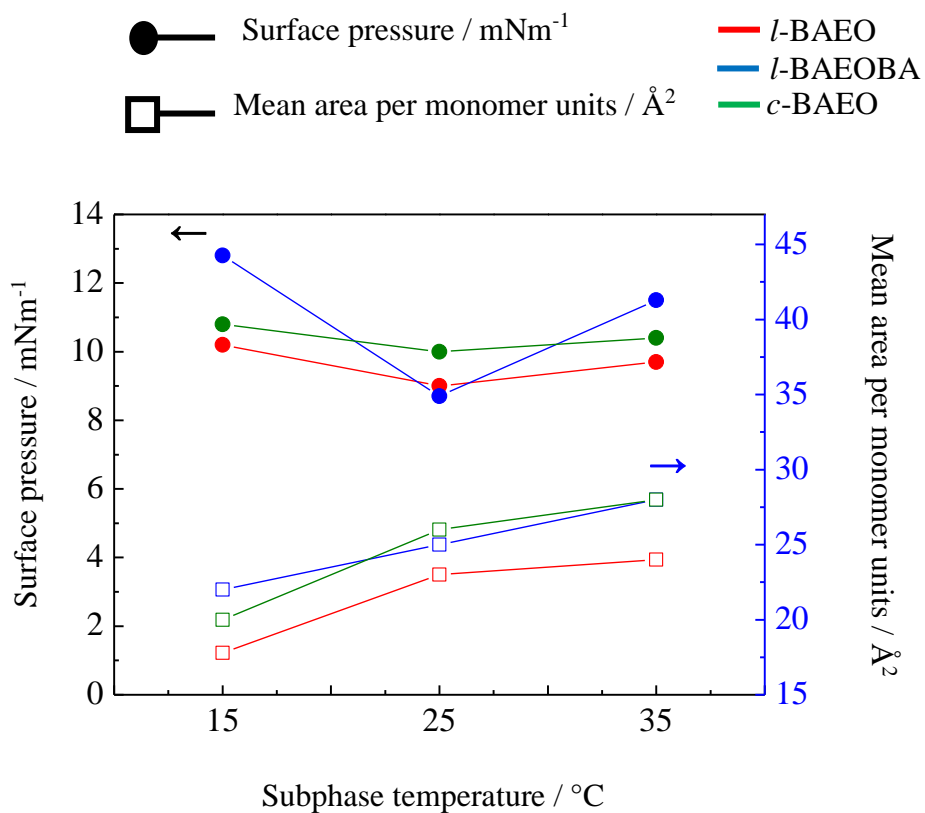


Figure 5-3. Plots of subphase temperature vs. transition surface pressure and transition area of monolayer on the water surface of *l*-BAEO, *l*-BAEOBA and *c*-BAEO.

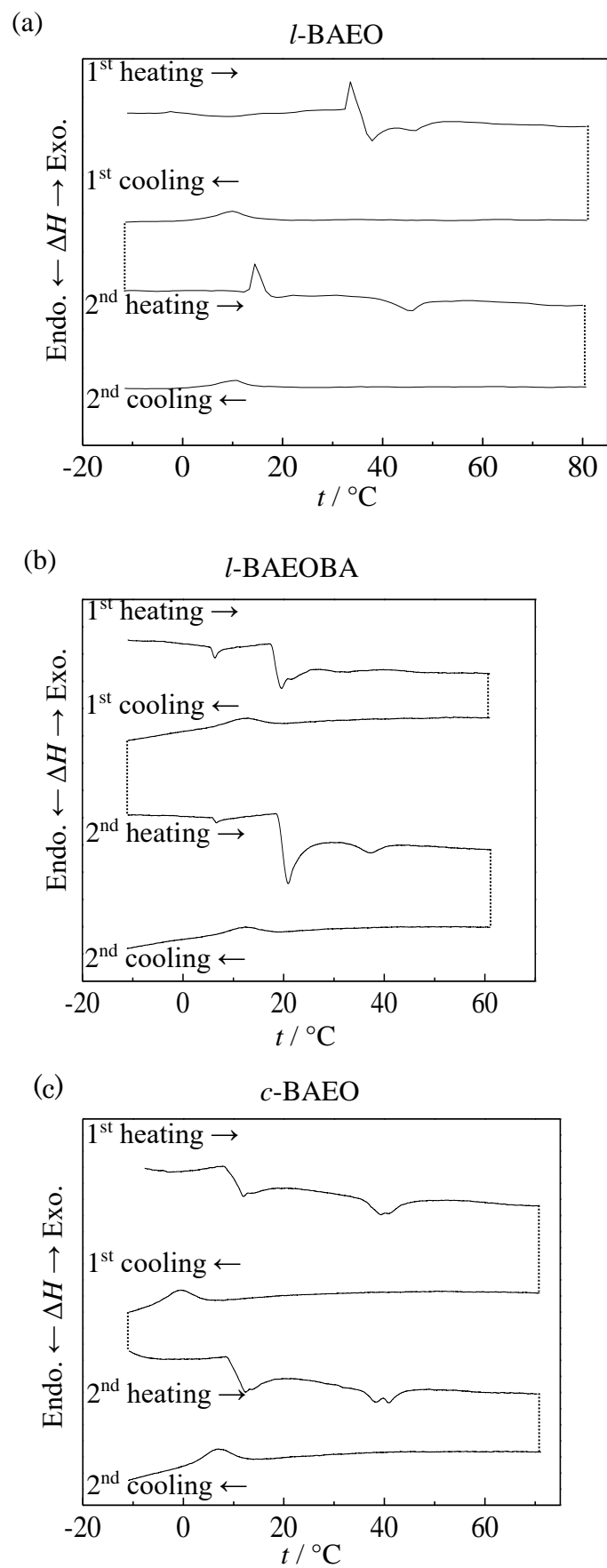


Figure 5-4. DSC thermograms of (a) *l*-BAEO, (b) *l*-BAEOBA and (c) *c*-BAEO.

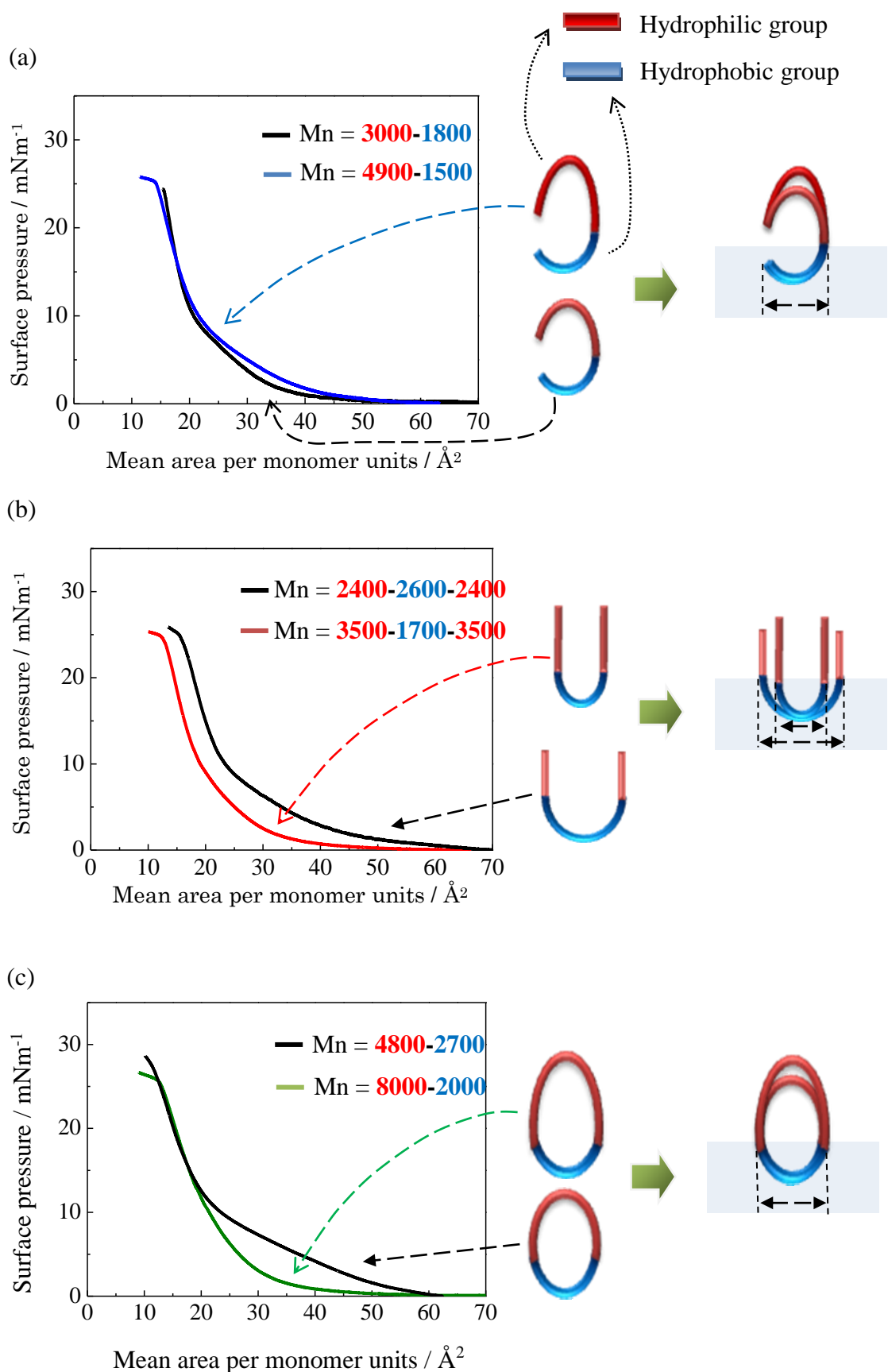


Figure 5-5. π -A isotherms of monolayer on the water surface for (a) *l*-BAEO, (b) *l*-BAEOBA and (c) *c*-BAEO with different molecular weight.

5-3. Monolayer Morphology of Topological Polymers on Solid Substrate

The morphological changes at the mesoscopic scale of the monolayers on solid substrates transferred by the upstroke of the LB method are shown in Figs. 5-6 and 5-7. All figures in fig. 5-6 are shown with a scale of $2\ \mu\text{m} \times 2\ \mu\text{m}$. Figure 5-6(a) shows AFM images of Z-type monolayers of the three block copolymers that were observed in the liquid expanded phase at $15\ \text{mNm}^{-1}$, $9.6\ \text{cm}^2/\text{min}^{-1}$ compression speed, and $15\ ^\circ\text{C}$ subphase temperature. The morphology of the *l*-BAEO monolayer suggested the presence of a domain structure. Both *l*-BAEOBA and *c*-BAEO showed bent line-shaped structures at a $15\ ^\circ\text{C}$ subphase temperature. The aggregation tendencies of the AB-type diblock copolymers appeared quite remarkable at first glance, however, significant differences were not observed in the formation processes for any of the monolayers at the mesoscopic scale. The existence of a significant defect part in these AFM images was expected at a very low transferring ratio. The calculated average transferring ratio for these conditions was 0.35. Therefore, acceleration of the morphological growth at the air/water interface by increasing the transferring surface pressure to $20\ \text{mNm}^{-1}$ induced the modification of the transferring ratio to 0.8. Thus, in order to promote the morphological growth at the air/water interface, spontaneous morphological growth in the two-dimensional plane was performed by the process of reducing the compression rate by 1/8.

Figure 5-7 shows AFM images of Z-type monolayers for each of the three block amphiphilic copolymers at slow compression speeds, in which obvious differences were confirmed. In all the systems, it can be seen that the transferring ratio significantly improved. The ABA-type triblock copolymer monolayer spontaneously grew at a slow rate to form a fibrous domain at the air/water surface, yielding nanofibers. For the AB-type diblock linear copolymer, spontaneous structural growth could not be confirmed, and film quality was rather reduced. Compared with the analogous linear copolymers, the cyclic polymer initially formed monolayer precursors in which domains were connected to each other after formation of

individual nuclear domains. Since the two terminal hydrophobic chains of the ABA-type triblock copolymer were oriented to air, it is suggested that a two-dimensional morphology can be easily produced via inter-terminal van der Waals chain interactions, as illustrated in Figure 5-8.

It is important to note that the two kinds of linear copolymers in this study have a configuration similar to the cyclic polymer at the air/water interface. However, the formation of nanofibers, as shown for the ABA triblock linear copolymer, could not be confirmed in the other polymer films. This fact may be attributed to the influence of compression rate-dependent spontaneous structural formation (1st order spontaneous growth) at the air/water interface. In this study, although much information was gained from preliminary experiments, the dependence of polymer shape, as found in archaea and lipids of other organisms. It becomes a factor influenced by the form and functionality in the two-dimensional organization. Indeed, in the case of multilayer formation by stacking of monolayers, it is easy to form periodic structures based on their interfacial configurations. In addition, the experimental estimation of heat-resistance in a multilayer tells us that the layer structure of a cyclic polymer is quite stable to heat.

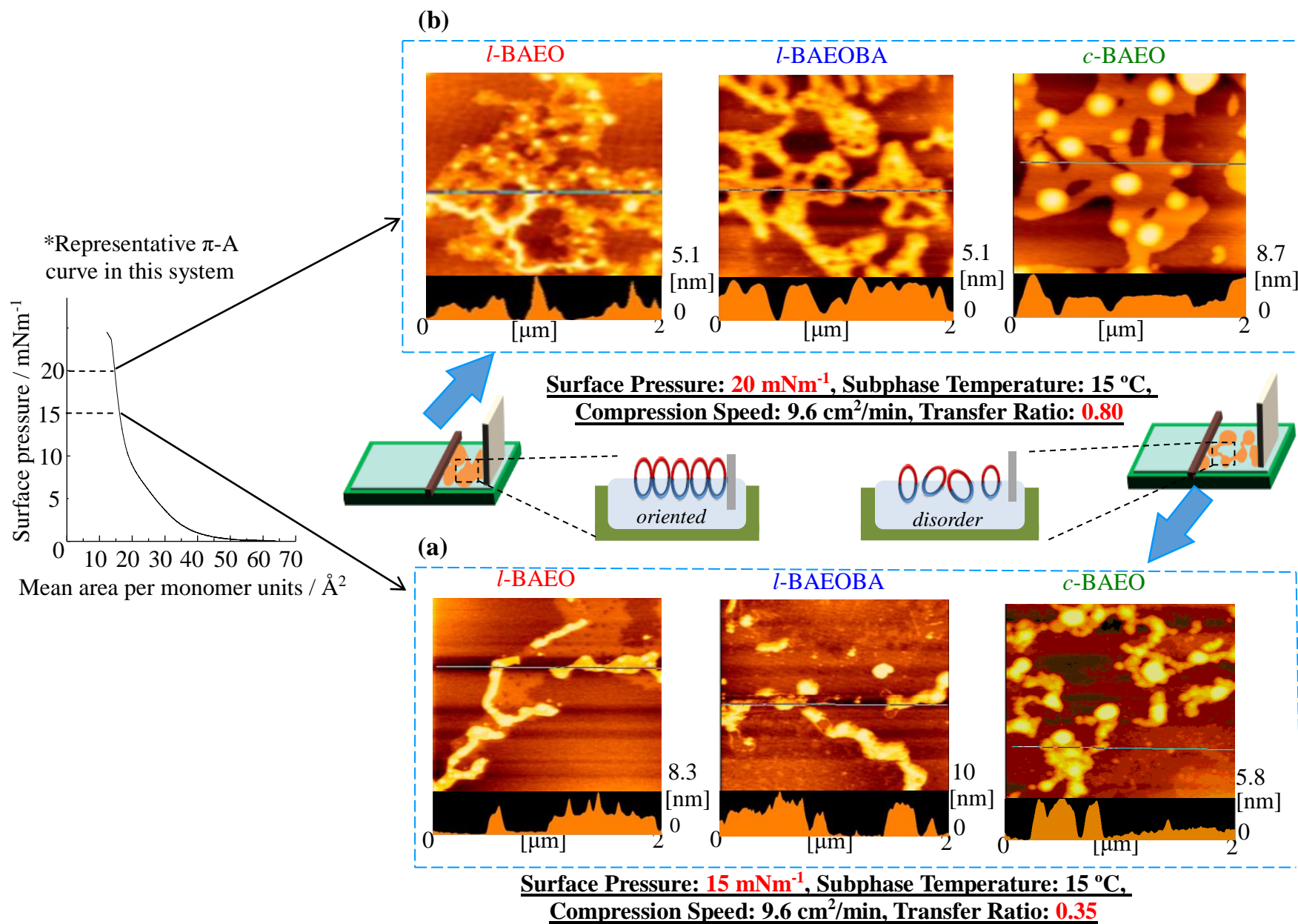
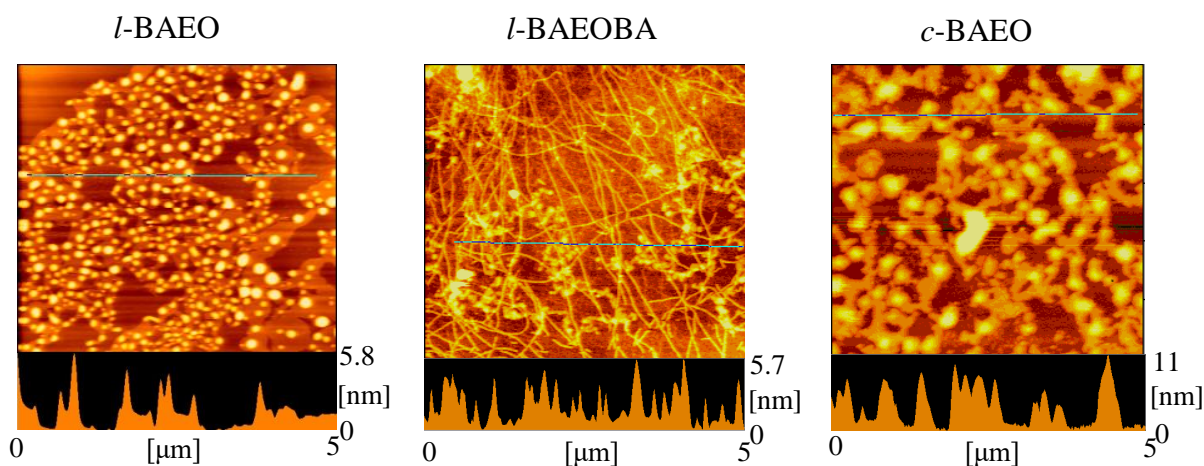
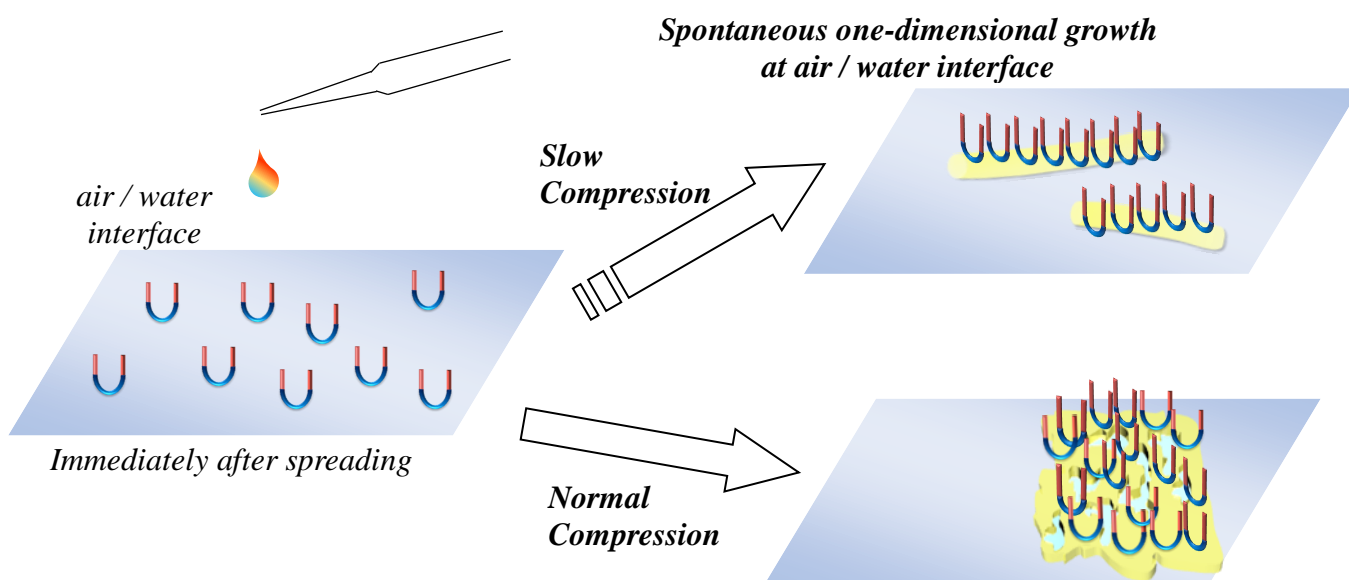


Figure 5-6. AFM images of Z-type monolayers for *l*-BAEO, *l*-BAEOBA and *c*-BAEO: (a) 15 °C, 15 mNm⁻¹, 9.6 cm²/min, and (b) 15 °C, 20 mNm⁻¹, 9.6 cm²/min.



Surface Pressure: 15 mNm⁻¹, Subphase Temperature: 15 °C,
Compression Speed: 1.2 cm²/min

Figure 5-7. AFM images of Z-type monolayers for (a) *l*-BAEO, (b) *l*-BAEOBA, and (c) *c*-BAEO (15 °C, 15 mNm⁻¹, 1.2 cm²/min). (Insert: Conceptual diagram of one-dimensional growth of morphology by slow compression)

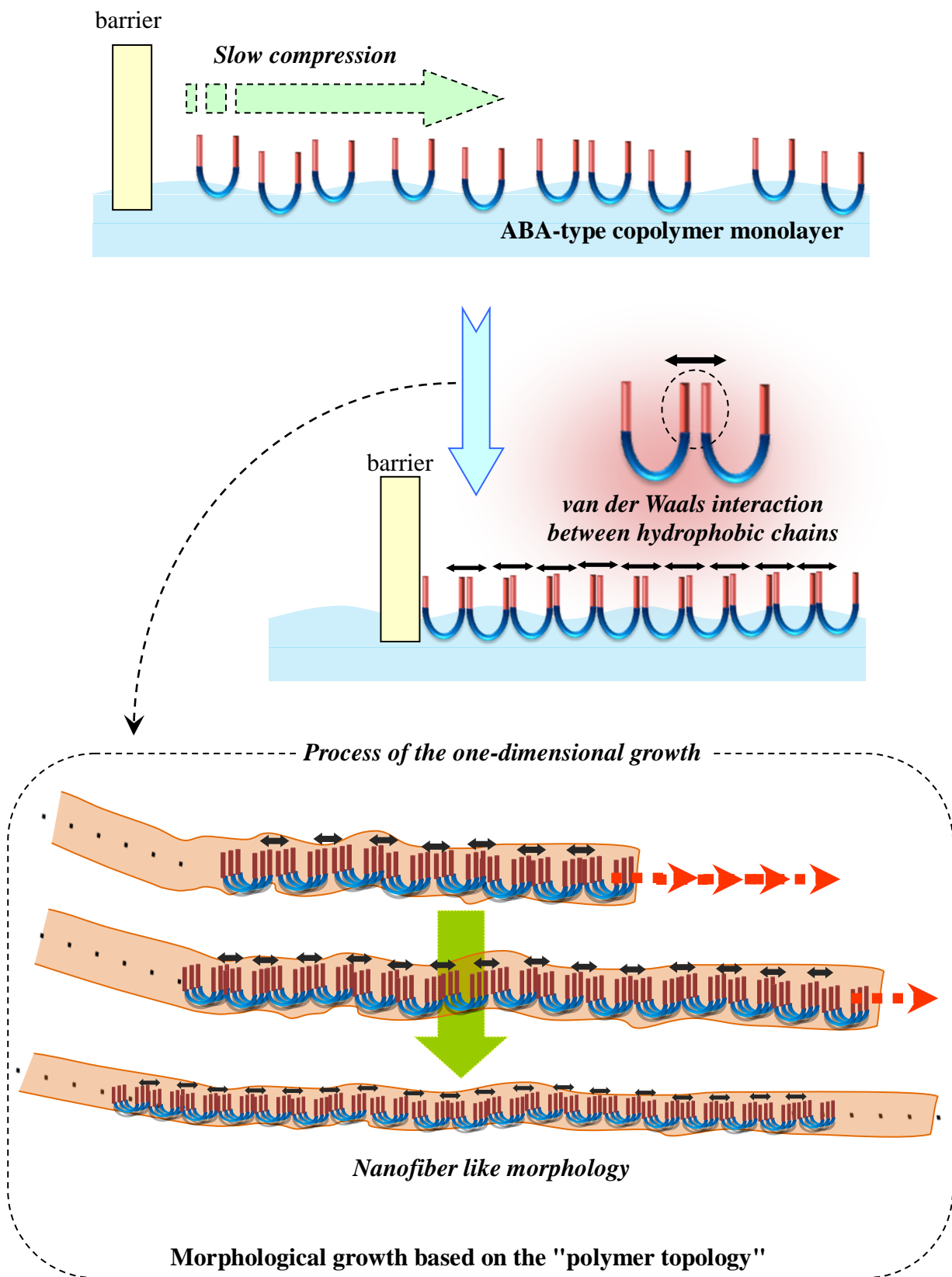


Figure 5-8. Schematic illustration of one-dimensional growth of a fiber-like morphology of a monolayer of *l*-BAEOBA.

5-4. Molecular Arrangement of Topological Polymers in Multilayers

Figure 5-9 shows in-plane XRD profiles of transferred LB multilayers of amphiphilic block copolymers with different shapes. These polymers were presumed to pack hexagonally in multilayered molecular films. In-plane XRD profiles showed crystalline peaks that were attributed to the hexagonal close-packing of long alkyl chains (two-dimensional (100) plane, $d_{100} = 4.1\text{--}4.2 \text{ \AA}$). The upright hydrophobic polymer chains exposed to air were expected to be packed hexagonally in multilayers composed of these amphiphilic block copolymers. However, since the data is not fully consistent with this expectation, there is a possibility that alkyl groups had aggregated and packed in a manner similar to what occurs in microphase separation.

Figure 5-10 shows out-of-plane XRD profiles of transferred LB multilayers of amphiphilic block copolymers with different shapes. Although these profiles showed similar diffraction profiles, the peaks in each profile indicated the formation of a layer structure with a very high degree of order. The layer periodicity value was calculated to be 5.1 nm from three third-order reflections ($d_{003} \times 3$) (since the first-order reflection was observed at an extremely low angle in the XRD). The ring diameter of polymers with a cyclic conformation was about 10 nm as determined from the results of high energy X-ray scattering in a photon factory with synchrotron radiation [95] of block copolymer micellar solutions. These copolymers were not perpendicular and adopted a substantial tilt angle to the substrate as shown in the inserts in Fig. 5-10. The sizes of the crystallites in the direction perpendicular to the layers were also estimated using the Scherrer equation [128]. From the half-width of the first-order reflection, the sizes of the crystallites were calculated to be about 15 nm. Figure 8 shows the *ex situ* out-of-plane XRD profiles observed with heating of *l*-BAEO, *l*-BAEOBA, and *c*-BAEO LB multilayers. These measurements were carried out after annealing the LB multilayers in order to study the differences in the heat-resistance properties between the linear and cyclic

polymers. In the case of AB-type diblock and ABA-type triblock linear copolymers, a reduction and disappearance in diffraction intensity was observed with heating below 100 °C. The layer structures of the LB multilayers of *l*-BAEO and *l*-BAEOBA were gradually disordered, and the regularity of the layer structures completely disappeared after annealing at 50°C and 95 °C, respectively. However, in the case of the cyclic polymer, the diffraction intensity was not reduced after annealing up to a temperature of 110 °C. Not only were first-order reflections observed, but also third-order reflections, indicating that the regularity of the cyclic polymer LB multilayers did not change with heating up to 110 °C. Therefore, it finds that LB film of the cyclic polymer receive significantly the effect of the annealing. The heat-resistant properties of micelles of cyclic polymers in aqueous solution were shown to have excellent heat stability [94].

Figure 5-11 shows the schematic illustration of the disordering behavior of polymers in LB multilayers with heating based on the results of the heated *ex site* out-of-plane XRD analysis shown in Fig. 5-10. In previous studies, these changes in physical properties were attributed to the presence of end groups. Changes in molecular mobility with heating and in the presence of salts influenced the heat-resistance and salt-resistance of the micellar solution. It was found that the presence of the terminal group also induced the disordering of the layer structures in this study. This behavior will be a key to solving the mystery of the heat resistance ability of thermophilic bacteria compared with linear-type lipid systems.

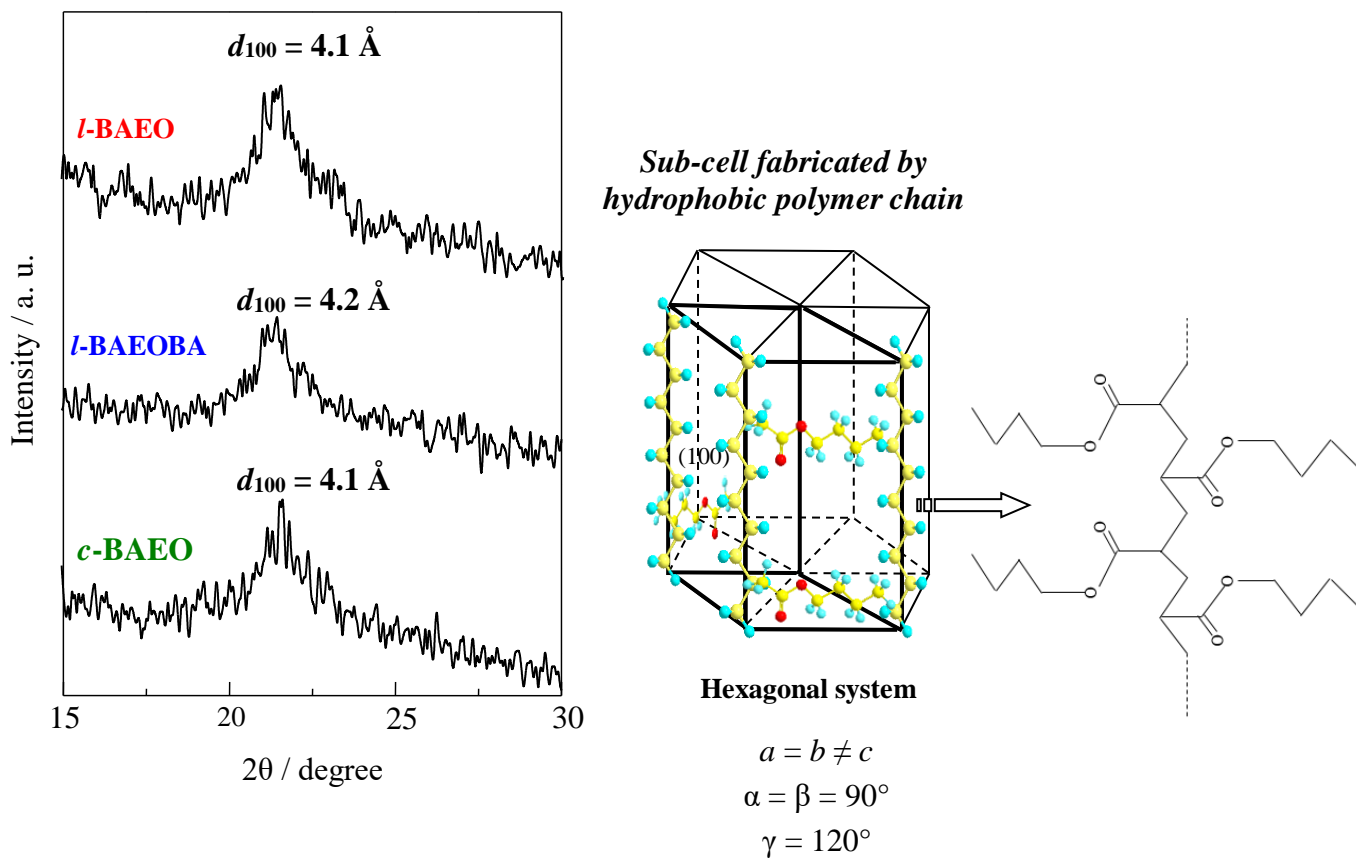


Figure 5-9. In-plane XRD profiles of LB multilayers of *l*-BAEO, *l*-BAEOBA and *c*-BAEO (20 layers, 15 °C, 15 mNm⁻¹).

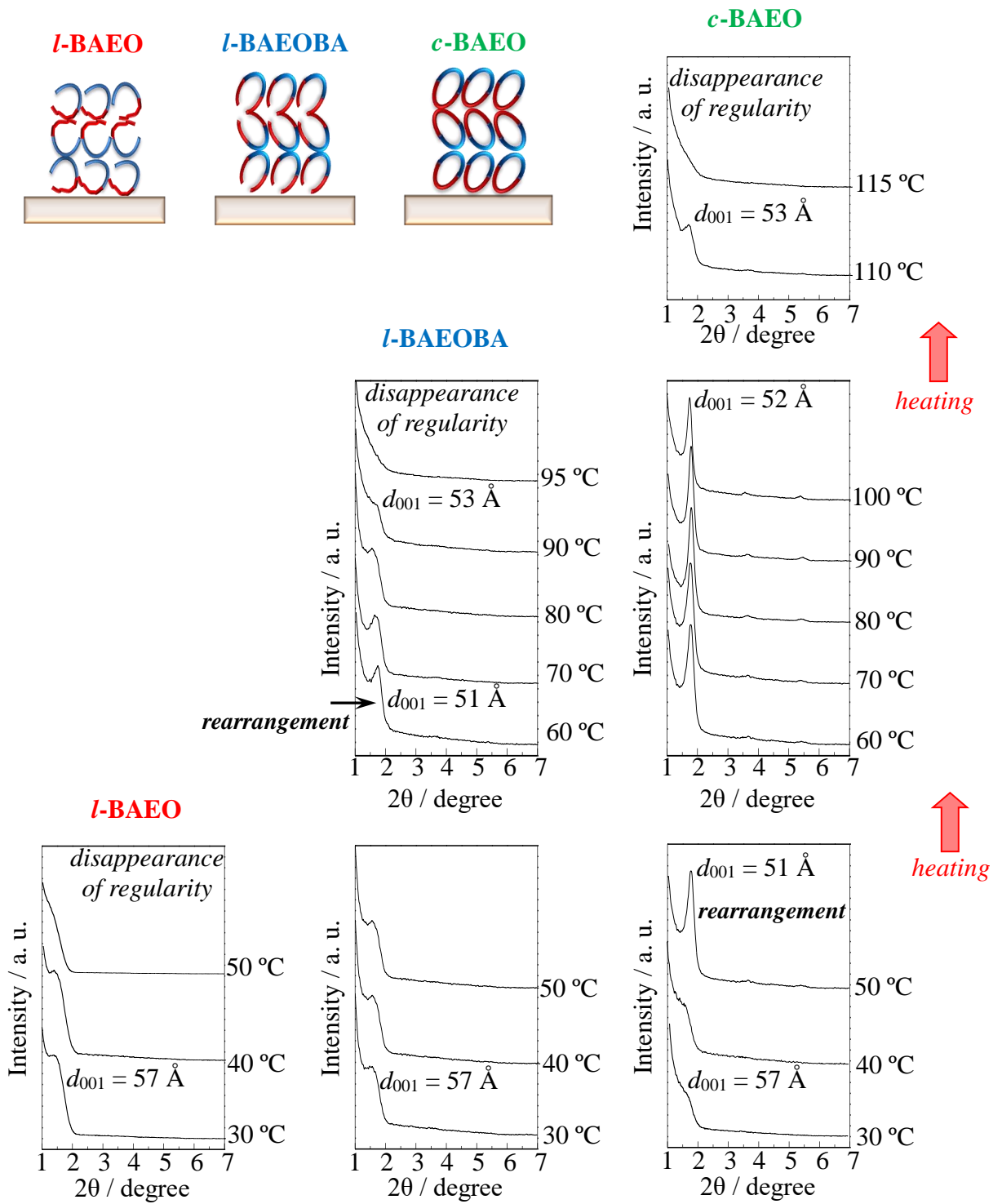


Figure 5-10. *Ex situ* out-of plane XRD profiles at various LB multilayer temperatures for *l*-BAEO, *l*-BAEOBA, and *c*-BAEO.

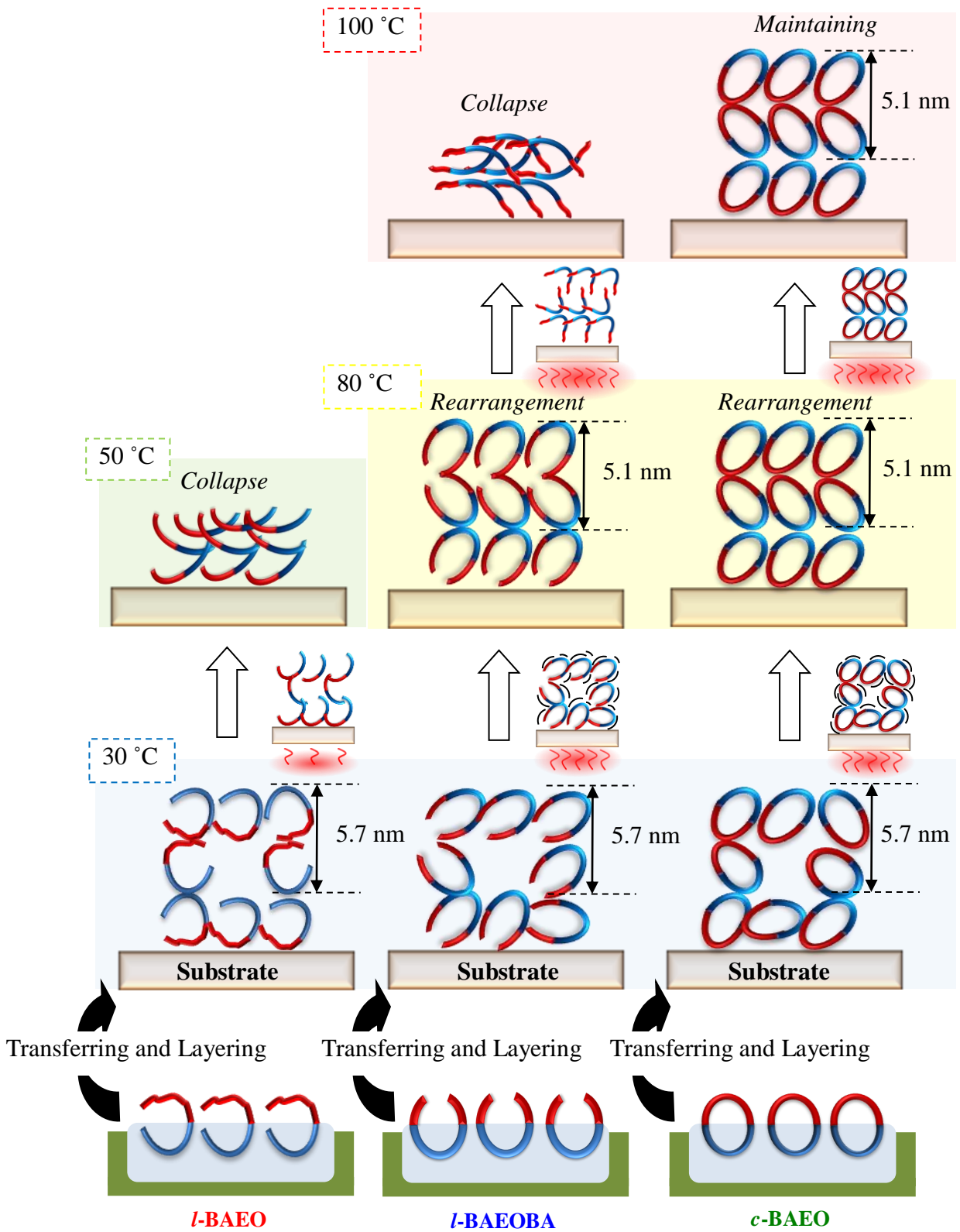


Figure 5-11. Illustration of layer structures of LB multilayers for *l*-BAEO, *l*-BAEOBA and *c*-BAEO.

5-5. Conclusion

Based on a precise structural and morphological analysis, Fig. 5-12 shows an illustration of the hierarchical structural formation reached from "monolayer morphology" to the "built-up layered organization" of topological polymers like *l*-BAEOBA and *c*-BAEO. This figure indicates that polymer topological interfacial chemistry is derived from molecular shape, and that intermolecular interactions comes from the shape and change in molecular mobility. A quite stable hierarchical structure was formed from the layered organization and molecular packing for a mesoscopic morphology such as seen in nanofibers. Such sophisticated molecular techniques with bottom-up technology could introduce new avenues for research and development of new molecular devices. For example, development of heat-resistant molecular devices might be within view using only the end-caps of macromolecules, if the chemical structure of a candidate macromolecule is similar to the polymers discussed in this paper. The outcome of this study might then be recognized as a significant development toward new molecular devices and an understanding of new properties of biomolecules.

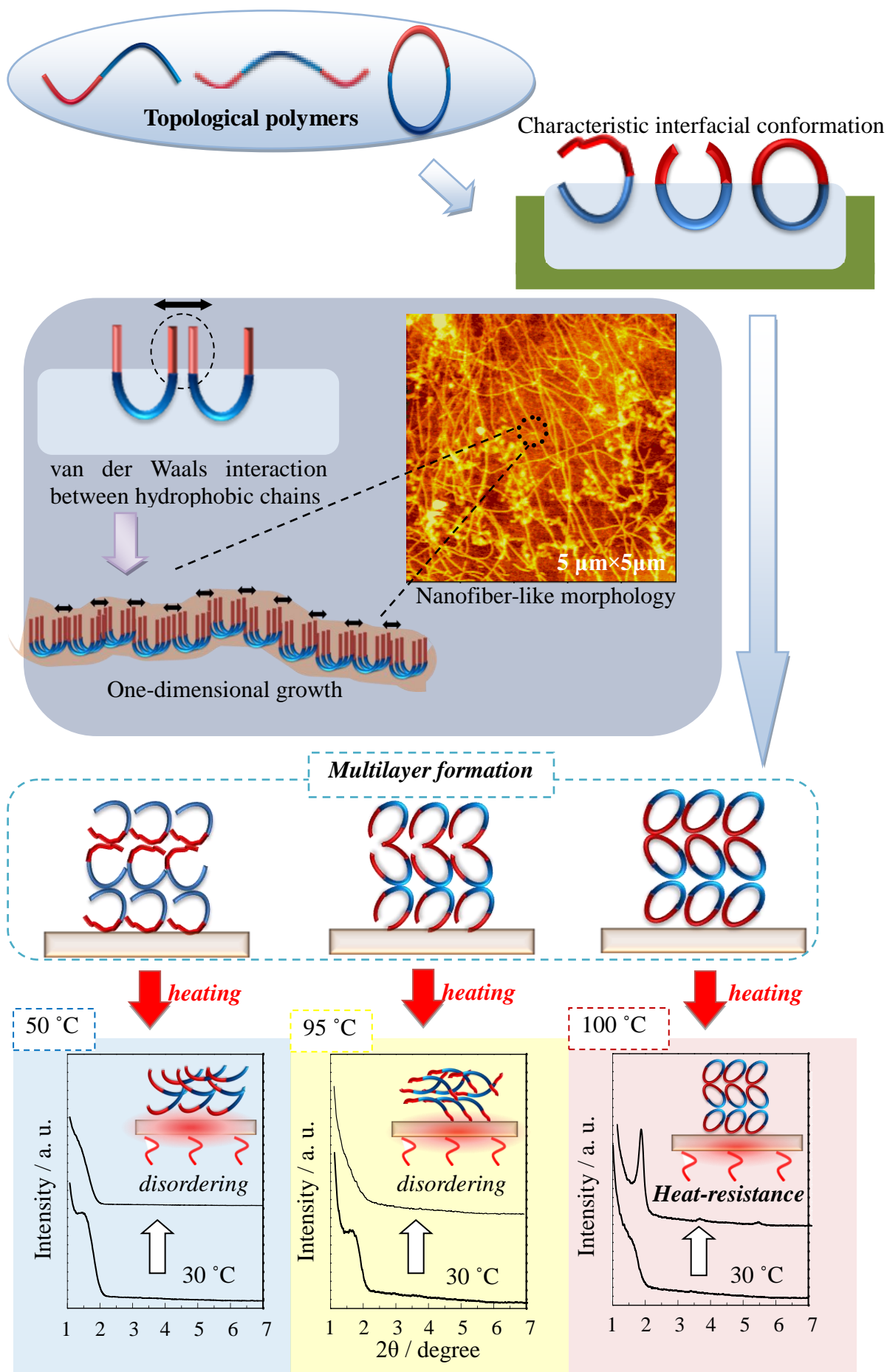


Figure 5-12. Schematic illustration of the topological polymer interfacial chemistry proposed in this study.

6. Concluding Remarks

The doctoral thesis has been reported the following three contents.

Organo-modified NDs by outermost surface treatment using several long-chain compounds have attained nanodispersion in general organic solvents as if these NDs were dissolved. A high surface coverage/high modification ratio decreased the particle agglomerate size of organo-modified NDs in the polar solvent, and their modification by fluorinated hydrophobic chain also attained a well-dispersed state in nonpolar solvents like *n*-hexane. It seems that the helical conformation peculiar to fluorinated chains cancels the polarization of the C-F bond and attains a low-polarity state. Therefore, since the miscibility between the organo-NDs with low polarity surface and the surrounding nonpolar solvent is remarkable, fluorinated organo-NDs might be easily dispersed. The resultant dispersed solution can be used as a spreading solvent of monolayers at the air/water interface of organo-modified NDs. These experiments show that there is close relationship between the dispersion properties of organo-modified inorganic fine particles in organic solvent and their condensation/expansion behavior in the interfacial monolayer on the water surface. Organo-modified NDs with excellent dispersion ability in organic solvent do not have superior interfacial condensability as single particle layers at the air/water interface. Sufficient retention time is needed to form the homogeneous monolayer of organo-particles at the air/water interface. The reasons for this peculiar behavior correspond to the secondary aggregation tendency of organo-NDs on the

water surface. Since lipophilicized nanoparticles are not necessarily advantageous to monolayer formation at the air/water interface, the enhancement of aggregated ND particle size was observed in the case where the compression rate during single particle layer formation was standard.

Further, maintenance properties of layered regularity under heating in the organized particle films of heat-resistant organo-modified ND were investigated. A comparison of the phosphonate-modification of the bidentate bond and the stearate-modification of the monodentate electrostatic bond have been performed. In long-chain phosphonate-modified ND, desorption of the modified-molecular chains by temperature elevation was suppressed until 350 °C. This is an innovative improvement compared to the desorption behavior at 155 °C of chains of stearate-modified ND. Both organo-modified NDs were well-dispersed in general organic solvents. Nano-dispersion has been achieved even in a dispersion medium having a concentration at two orders of magnitude higher than that of a spreading solution for a single particle layer on the water surface. The monolayer on the water surface of the organo-modified ND formed an extremely stable condensed film. When layered organization is formed during the formation of two-dimensional molecular films, a clear layered period is observed, and the existence of unmodified-chain impurities that cannot be removed was simultaneously confirmed. However, it was no doubt that the organo-modified ND formed a highly developed layered structure in the LB film. Further, temperature-controlled XRD and IR measurements

showed that impurities can be fired and removed. Due to the annealing effect upon heating above 100 °C, the layered regularity was enhanced by rearrangement of the organo-modified NDs. The layered regularity of the organo-particle layers during heating was maintained up to 175 °C, far exceeding the value of 50 °C for the organized particle film of stearate-modified ND. As a result of this study, it was possible to obtain a phase diagram in the heat treatment condition of the organo-modified ND layered structure. This technique is expected to be developed for technology that utilizes a single layer coating at the outermost layer with ND, which has excellent antibacterial properties and a high refractive index and thermal conductivity due to functional nanocarbons.

In addition, the topological properties of polymers at an air/water interface were investigated using amphiphilic linear and cyclic block copolymers. A cyclic AB-type diblock linear copolymer and two ABA-type triblock copolymers with the same monomer components were newly synthesized and used in this study. All copolymers were observed to form relatively stable monolayers at an air/water interface. Similar tendencies for the condensed phase as well as temperature-dependent behaviors were observed in the π -A isotherms of all three monolayers examined. The molecular orientations at the air/water interface of the two linear block copolymers were found to be quite similar to that of the cyclic block copolymer. As determined by AFM observations of monolayers on solid substrates, the monomolecular films of the three

copolymers adopted a morphology similar to that of the mesoscopic scale under room temperature and constant compression speed conditions. The ABA-type triblock linear copolymer was observed to form a fibril structure upon two-dimensional crystallization at a low compression speed, while the cyclic block copolymer formed an aggregated domain. The LB multilayers of these block copolymers formed highly ordered layer structures with a layer periodicity of 5.1 nm. In the case of the cyclic polymer, the diffraction intensity was not reduced after annealing up to 110 °C, indicating that the regularity of the cyclic polymer LB multilayers were unchanged with heating. The excellent heat stability of cyclic polymers was also demonstrated and discussed.

References and Notes

1. M. Choi, K. Na, J. Kim, Y. Sakamoto, O. Terasaki, R. Ryoo, Stable single-unit-cell nanosheets of zeolite MFI as active and long-lived catalysts, *Nature* **461** (2009) 246–249.
2. B. Oregan, M. Gratzel, A low-cost, high-efficiency solar-cell based on dye-sensitized colloidal TiO₂ films, *Nature* **353** (1991) 737–740.
3. Y. Chisti, Biodiesel from microalgae, *Biotechnol. Adv.* **25** (2007) 294–306.
4. J.P. Perdew, K. Burke, M. Ernzerhof, Generalized gradient approximation made simple, *Phys. Rev. Lett.* **77** (1996) 3865–3868.
5. T.L. Greaves, C.J. Drummond, Protic ionic liquids: properties and applications, *Chem. Rev.* **108** (2008) 206–237.
6. M.S. Wang, T.J. Pinnavaia, Clay polymer nanocomposites formed from acidic derivatives of montmorillonite and an epoxy-resin, *Chem. Mater.* **6** (1994) 468–474.
7. M.M. Gui, K.T. Lee, S. Bhatia, Feasibility of edible oil vs. non-edible oil vs. waste edible oil as biodiesel feedstock, *Energy* **33** (2008) 1646–1653.
8. G.T. Rochelle, Amine scrubbing for CO₂ capture, *Science* **325** (2009) 1652–1654.
9. F. Yang, R. Murugan, S. Wang, S. Ramakrishna, Electrospinning of nano/micro scale poly(L-lactic acid) aligned fibers and their potential in neural tissue engineering, *Biomater.* **26** (2005) 2603–2610.
10. Q. Xiang, J. Yu, M. Jaroniec, Synergetic effect of MoS₂ and graphene as cocatalysts for enhanced photocatalytic H₂ production activity of TiO₂ nanoparticles, *J. Am. Chem. Soc.*

134 (2012) 6575–6578.

11. F.J. Ulm, M. Vandamme, C. Bobko, J. A. Ortega, Statistical indentation techniques for hydrated nanocomposites: Concrete, bone, and shale, *J. Am. Chem. Soc.* **90** (2007) 2677–2692.
12. Y.Y. Wu, W.C. Tsui, T. C. Liu, Experimental analysis of tribological properties of lubricating oils with nanoparticle additives, *Wear* **262** (2007) 819–825.
13. Y. Xu, Y. Peng, X. Zheng, K.D. Dearn, H. Xu, X. Hu, Synthesis and tribological studies of nanoparticle additives for pyrolysis bio-oil formulated as a diesel fuel, *Energy* **83** (2015) 80–83.
14. R.A.E. Wright, K. Wang, J. Qu, B. Zhao, Oil-Soluble polymer brush grafted nanoparticles as effective lubricant additives for friction and wear reduction, *Angew. Chem. Int. Ed.* **55** (2016) 8656–8660.
15. Official web site of "nano car race", <http://nanocar-race.cnrs.fr/indexEnglish.php>.
16. D. Ishikawa, T. Mori, Y. Yonamine, W. Nakanishi, D.L. Cheung, J.P. Hill, K. Ariga, Mechanochemical tuning of the binaphthyl conformation at the air-water interface, *Angew. Chem. Int. Ed.* **54** (2015) 8988–8991.
17. H. Itoh, A. Takahashi, K. Adachi, H. Noji, R. Yasuda, M. Yoshida, K. Kinoshita, Mechanically driven ATP synthesis by F-1-ATPase, *Nature* **427** (2004) 465–468.
18. M.A. Meyers, A. Mishra, D.J. Benson, Mechanical properties of nanocrystalline materials,

- Prog. Mater. Sci.* **51** (2006) 427–556.
19. N. V. Mochalin, O. Shenderova, D. Ho, Y. Gogotsi, The properties and applications of nanodiamonds, *Nat. Nanotechnol.* **7** (2012) 11–23.
 20. S. Osswald, G. Yushin, V. Mochalin, S.O. Kucheyev, Sergei Y. Gogotsi, Control of sp(2)/sp(3) carbon ratio and surface chemistry of nanodiamond powders by selective oxidation in air, *J. Am. Chem. Soc.* **128** (2006) 11635–11642.
 21. O.A. Williams, J. Hees, C. Dieker, W. Jaeger, L. Kirste, C. E. Nebel, Size-dependent reactivity of diamond nanoparticles, *ACS Nano* **4** (2010) 4824–4830.
 22. C. Miao, J.C. Lambropoulos, S. D. Jacobs, Process parameter effects on material removal in magnetorheological finishing of borosilicate glass, *Appl. Opt.* **10** (2010) 1951–1963.
 23. E. Piorkowska, Z. Kulinski, A. Galeski, R. Masirek, Plasticization of semicrystalline poly(L-lactide) with poly(propylene glycol), *Polymer* **47** (2006) 7178–7188.
 24. E.P. Giannelis, Polymer layered silicate nanocomposites, *Adv. Mater.* **8** (1996) 29–35.
 25. X. Zhao, T. Jiao, X. Ma, H. Huang, J. Hu, Y. Qu, J. Zhou, L. Zhang, Q. Peng, Facile fabrication of hierarchical diamond-based AuNPs-modified nanocomposites via layer-by-layer assembly with enhanced catalytic capacities, *J. Taiwan I. Chem. Eng.* **80** (2017) 614–623.
 26. X. Zhao, K. Ma, T. Jiao, R. Xing, X. Ma, J. Hu, H. Huang, L. Zhang, X. Yan, Fabrication of hierarchical layer-by-layer assembled diamond-based core-shell nanocomposites as

- highly efficient dye absorbents for wastewater treatment, *Sci. Rep.* 44076 (2017) DOI: 10.1038/srep44076.
27. S. Huo, P. Duan, T. Jiao, Q. Peng, M. Liu, self-assembled luminescent quantum dots to generate full-color and white circularly polarized light, *Angew. Chem. Int. Ed.* **7** **56** (2017) 12174-12178.
28. K. Chen, J. Li, L. Zhang, R. Xing, T. Jiao, F. Gao, Q. Peng, Facile synthesis of self-assembled carbon nanotubes/dye composite films for sensitive electrochemical determination of Cd(II) ions, *Nanotechnol.* **29** (2018) 445603.
29. A. Fujimori, Y. Kasahara, N. Honda, S. Akasaka, The Role of modifying molecular chains in the formation of organized molecular films of organo-modified nanodiamond. – construction of a highly-ordered low defect particle layer, and evaluation of desorption behavior of organic chains–, *Langmuir* **31** (2015) 2895–2904.
30. A. Fujimori, K. Ohmura, N. Honda, K. Kakizaki, Creation of high-density and low-defect single-layer film of magnetic nanoparticles by method of interfacial molecular films, *Langmuir* **31** (2015) 3254–3261.
31. Q. Meng, N. Honda, S. Uchida, K. Hashimoto, H. Shibata, A. Fujimori, Giant two-dimensional zinc oxide nanodisc crystal creation using single-particle layer of organo-modified inorganic fine particles, *J. Colloid Interf. Sci.* **453** (2015) 90–99.
32. F. Schreiber, Structure and growth of self-assembling monolayers, *Prog. Sur. Sci.* **65** (2000)

151–256.

33. R. Waugh, E. A. Evans, Thermoelasticity of red blood-cell membrane, *Biophys. J.* **26** (1979)

115–131.

34. P. Uetz, L. Giot, G. Cagney, T.A. Mansfield, R.S. Judson, J.R. Knight, D. Lockshon, V.

Narayan, M. Srinivasan, P. Pochart, A. Qureshi-Emili, Y. Li, B. Godwin, D. Conover, T.

Kalbfleisch, G. Vijayadamodar, M.J. Yang, M. Johnston, S. Fields, J.M. Rothberg, A

comprehensive analysis of protein-protein interactions in *Saccharomyces cerevisiae*, *Nature*

403 (2000) 623–627.

35. H. Sirringhaus, P.J. Brown, R.H. Friend, M.M. Nielsen, K. Bechgaard, B.M.W. Langeveld-

Voss, A.J.H. Spiering, R.A.J. Janssen, E.W. Meijer, P. Herwig, D.M. de Leeuw, Two-

dimensional charge transport in self-organized, high-mobility conjugated polymers, *Nature*

401 (1999) 685–688.

36. Y. Zhang, Yan-Wen Tan, H.L. Stormer, P. Kim, Experimental observation of the quantum

Hall effect and Berry's phase in graphene, *Nature* **438** (2005) 201–204.

37. P.C. LeBaron, Z. Wang, T.J. Pinnavaia, Polymer-layered silicate nanocomposites: an

overview, *Appl. Clay Sci.* **15** (1999) 11–29.

38. I. Vermes, C. Haanen, H. Steffens-Nakken, C. Reutelingsperger, A novel assay for apoptosis

Flow cytometric detection of phosphatidylserine early apoptotic cells using fluorescein

labelled expression on Annexin V, *J. Immunol. Methods* **184** (1995) 39–51.

39. J.L. Sussman, M. Harel, F. Frolov, C. Oefner, A. Goldman, L. Toker, I. Silman, Atomic structure of acetylcholinesterase from *Torpedo californica*: a prototypic acetylcholine-binding protein, *Science* **253** (1991) 872–879.
40. D. Zhao, Q. Huo, J. Feng, B.F. Chmelka, G.D. Stucky, Nonionic Triblock and Star Diblock Copolymer and Oligomeric Surfactant Syntheses of Highly Ordered, Hydrothermally Stable, Mesoporous Silica Structures, *J. Am. Chem. Soc.* **120** (1998) 6024–6036.
41. Q. Zhang, E.E. Remsen, K.L. Wooley, Shell Cross-Linked Nanoparticles Containing Hydrolytically Degradable, Crystalline Core Domains, *J. Am. Chem. Soc.* **122** (2000) 3642–3651.
42. M.S. Wang, T.J. Pinnavaia, Clay-Polymer Nanocomposites Formed from Acidic Derivatives of Montmorillonite and an Epoxy Resin, *Chem. Mater.* **6** (1994) 468–474.
43. A.L. Plant, Supported Hybrid Bilayer Membranes as Rugged Cell Membrane Mimics, *Langmuir* **15** (1999) 5128–5135.
44. D.M. Spencer, T.J. Wandless, S.L. Schreiber, G.R. Crabtree, Controlling signal transduction with synthetic ligands, *Science* **262** (1993) 1019–1024.
45. A. Tolentino, S. Leon, A. Alla, A. Martínez de Ilarduya, S. Muñoz-Guerra, Comblike Ionic Complexes of Poly(γ -glutamic acid) and Alkanoylcholines Derived from Fatty Acids, *Macromolecules* **46** (2013) 1607–1617.
46. V. Vand, I.P. Bell, A Direct Determination of the Crystal Structure of the β Form of Trilaurin,

- Acta. Cryst.* **4** (1951) 465–469.
47. W. Su, M. Hong, J. Weng, R. Cao, S. Lu, A Semiconducting Lamella Polymer $[\{\text{Ag}(\text{C}_5\text{H}_4\text{NS})\}_n]$ with a Graphite-Like Array of Silver(I) Ions and Its Analogue with a Layered Structure, *Angew. Chem., Int. Ed.* **39** (2000) 2911–2914.
48. C.T. Kresge, M.E. Leonowicz, W.J. Roth, J.C. Vartuli, J.S. Beck, Ordered mesoporous molecular sieves synthesized by a liquid-crystal template mechanism, *Nature* **359** (1992) 710–712.
49. K.B. Blodgett, Films Built by Depositing Successive Monomolecular Layers on a Solid Surface, *J. Am. Chem. Soc.* **57** (1935) 1007–1022.
50. K.B. Blodgett, I. Langmuir, Built-Up Films of Barium Stearate and Their Optical Properties, *Phys. Rev.* **51** (1937) 964–982.
51. I. Langmuir, V.J. Schaefer, Improved Methods of Conditioning Surfaces for Adsorption, *J. Am. Chem. Soc.* **59** (1937) 1762–1763.
52. A. Cossaro, R. Mazzarello, R. Rousseau, L. Casalis, A. Verdini, A. Kohlmeyer, L. Floreano, S. Scandolo, A. Morgante, M.L. Klein, G. Scoles, X-ray Diffraction and Computation Yield the Structure of Alkanethiols on Gold(111), *Science* **321** (2008) 943–946.
53. K. Larsson, Molecular Arrangement in Glycerides, *Eur. J. lipid. Sci. Technol.*, **74** (1972) 136–142.
54. E.S. Lutton, The identity and polymorphism of oleyldistearin from kokum butter, *J. Am.*

- Chem. Soc.* **68** (1946) 676–679.
55. H. Moshino, Y. Koyano, S. Mouri, Y.F. Miura, M. Sugi, Kinetics of Thermal Dissociation–Restoration Processes of J-Aggregate, *Jpn. J. Appl. Phys.* **48** (2009) 051504.
56. Y.F. Miura, M. sano, T. Sugimoto, Generation of disk-like domains with nanometer scale thickness in merocyanine dye LB film induced by hydrothermal treatment, *Nanoscale Res. Lett.* **8** (2013) 429.
57. Q. Meng, S. Honda, Y. Tezuka, T. Yamamoto, A. Fujimori, Topological “Interfacial” Polymer Chemistry -Dependency of Polymer "Shape" on Surface Morphology and Stability of Layer Structures when Heating Organized Molecular Films of Cyclic and Linear Block Copolymers of n-Butyl Acrylate-Ethylene Oxide-. *J. Polym. Sci. B, Polym. Phys.* **54** (2016) 486–498.
58. M. Morga, Z. Adamczyk, M. Ocwieja, E. Bielanska, Hematite/silver nanoparticle bilayers on mica - AFM, SEM and streaming potential studies, *J. Colloid Interf. Sci.* **424** (2014) 75–83.
59. M. Morga, Z. Adamczyk, D. Kosior, M. Ocwieja, Hematite/silica nanoparticle bilayers on mica: AFM and electrokinetic characterization, *Phys. Chem. Chem. Phys.* **20** (2018) 15368–15379.
60. V.N. Mochalin, O. Shenderova, D. Ho, Y. Gogotsi, The properties and applications of nanodiamonds, *Nat. Nanotechnol.* **7** (2012) 11–23.

61. M. Chen, Xue-Qing Zhang, H.B. Man, R. Lam, E.K. Chow, D. Ho, Nanodiamond Vectors Functionalized with Polyethylenimine for siRNA Delivery, *J. Phys. Chem. Lett.* **1** (2010) 3167–3171.
62. M. Shamsa, W.L. Liu, A.A. Balandin, C. Casiraghi, W.I. Milne, A.C. Ferrar, Thermal conductivity of diamond-like carbon films, *Appl. Phys. Lett.* **89** (2006) 161921.
63. K. Tsugawa, M. Ishihara, J. Kim, M. Hasegawa, Y. Koga, Large-Area and Low-Temperature Nanodiamond Coating by Microwave Plasma Chemical Vapor Deposition, *New Diamond Front. Carbon Technol.* **16** (2006) 337–346.
64. H. Etemadi, R. Yegani, V. Babaeipour, Study on the reinforcing effect of nanodiamond particles on the mechanical, thermal and antibacterial properties of cellulose acetate membranes, *Diamond Relat. Mater.* **69** (2016) 166–176.
65. Y. Liang, M. Ozawa, A. Krueger, A General Procedure to Functionalize Agglomerating Nanoparticles Demonstrated on Nanodiamond, *ACS Nano*, **3** (2009) 2288–2296.
66. Yu-Jun Zhai, Zhi-Cai Wang, W. Huang, Jie-Juan Huang, Yan-Yan Wang, Yong-Qing Zhao, Improved mechanical properties of epoxy reinforced by low content nanodiamond powder, *Mater. Sci. Eng., A*, **528** (2011) 7295–7300.
67. K. Enomoto, M. Kikuchi, A. Narumi, S. Kawaguchi, Surface Modifier-Free Organic–Inorganic Hybridization To Produce Optically Transparent and Highly Refractive Bulk Materials Composed of Epoxy Resins and ZrO₂ Nanoparticles, *ACS Appl. Mater.*

- Interfaces* **10** (2018) 13985–13998.
68. E. Osawa, Recent progress and perspectives in single-digit nanodiamond, *Diamond Relat. Mater.* **16** (2007) 2018–2022.
69. P. Salarizadeh, M. Javanbakht, M. Abdollahi, L. Naji, Preparation, characterization and properties of proton exchange nanocomposite membranes based on poly(vinyl alcohol) and poly(sulfonic acid)-grafted silica nanoparticles, *Int. J. Hydrogen Energy* **38** (2013) 5473–5479.
70. K.A.D. Guzman, M.P. Finnegan, J.F. Banfield, Influence of Surface Potential on Aggregation and Transport of Titania Nanoparticles, *Environ. Sci. Technol.*, **40** (2006) 7688–7693.
71. K. Ariga, M.V. Lee, T. Mori, Xiao-Yan Yu, J.P. Hill, Two-dimensional nanoarchitectonics based on self-assembly, *Adv. Colloid Interface Sci.* **154** (2010) 20–29.
72. S. Kangoa, S. Kalia, A. Celli, J. Njuguna, Y. Habibi, R. Kumar, Surface modification of inorganic nanoparticles for development of organic–inorganic nanocomposites—A review, *Prog. Polym. Sci.* **38** (2013) 1232–1261.
73. A. Fujimori, S. Arai, J. Kusaka, M. Kubota, K. Kurosaka, Formation and Structure of Langmuir–Blodgett Films of Organo-modified Aluminosilicate with High Surface Coverage, *J. Colloid Interface Sci.* **392** (2013) 256–265.
74. A. Fujimori, N. Honda, H. Iwashita, Y. Kaneko, S. Arai, M. Sumita, S. Akasaka, Formation

- and Structure of Fine Multi-particle Layered Organo-modified Zirconium Dioxides Fabricated by Langmuir–Blodgett Technique, *Colloids Surf. A*, **446** (2014) 109–117.
75. S. R. Batten, R. Robson, Interpenetrating Nets: Ordered, Periodic Entanglement, *Angew. Chem., Int. Ed.* **37** (1998) 1460–1494.
76. L. Carlucci, G. Ciani, D. M. Proserpio, A. A. Sironi, A Three-Dimensional, Three-Connected Cubic Network of the SrSi₂ Topological Type in Coordination Polymer Chemistry: [Ag(hmt)](PF₆).nH₂O (hmt = Hexamethylenetetraamine), *J. Am. Chem. Soc.* **117** (1995) 12861–12862.
77. J. Kumaki, Y. Nishikawa, T. Hashimoto, Visualization of Single-Chain Conformations of a Synthetic Polymer with Atomic Force Microscopy, *J. Am. Chem. Soc.* **118** (1996) 3321–3322.
78. K. Fukuda, Y. Shibasaki, H. Nakahara, M.H. Liu, Spontaneous formation of polypeptides in the interfacial thin films of amphiphilic amino acid esters: acceleration of the polycondensation and control of the structure of resultant polymers, *Adv. Colloid Interf. Sci.* **87** (2000) 113–145.
79. T. Kunitake, Y. Okahata, M. Shimomura, S. Yasunami, K. Takarabe, Formation of stable bilayer assemblies in water from single-chain amphiphiles. Relationship between the amphiphile structure and the aggregate morphology, *J. Am. Chem. Soc.* **103** (1981) 5401–5413.

80. H. Klok, J. Langenwalter, S. Lecommandoux, Self-Assembly of Peptide-Based Diblock Oligomers, *Macromolecules* **33** (2000) 7819–7826.
81. H. Huber, M. J. Hohn, R. Rachel, T. Fuchs, V. C. Wimmer, A new phylum of Archaea represented by a nanosized hyperthermophilic symbiont, *Nature* **417** (2002) 63–67.
82. M. Könneke, A. E. Bernhard, J. R. de la Torre, C. B. Walker, J. B. Waterbury, Isolation of an autotrophic ammonia-oxidizing marine archaeon, *Nature* **437** (2005) 543–546.
83. A. Bouchereau, A. Aziz, F. Larher, J. Martin-Tanguy, Polyamines and environmental challenges: recent development, *Plant Sci.*, **140** (1999) 103–125.
84. K. C. Lyons, W. D. Comper, Diffusion of tritiated water in chondroitin sulfate solutions, *Biophys. Chem.* **47** (1993) 61–66.
85. F. X. Zhang, H. Y. Low, Ordered three-dimensional hierarchical nanostructures by nanoimprint lithography, *Nanotechnology* **17** (2006) 1884–1890.
86. H. Oike, Y. Yaguchi, Y. Tezuka, Tailored synthesis of branched polymers with poly(tetrahydrofuran) having an azetidinium salt end group, *Macromol. Chem. Phys.* **200** (1999) 768–773.
87. K. Adachi, H. Irie, T. Sato, A. Uchibori, M. Shiozawa, Y. Tezuka, Electrostatic Self-Assembly and Covalent Fixation with Cationic and Anionic Telechelic Precursors for New Loop and Branch Polymer Topologies, *Macromolecules* **38** (2005) 10210–10219.
88. H. Oike, H. Imamura, Y. Tezuka, Synthesis of Poly(tetrahydrofuran) Polymacromonomers

- Having Mixed Branch Segments through Reshuffling in Electrostatic Self-Assembly and Subsequent Covalent Fixation, *Macromolecules* **32** (1999) 8816–8820.
89. T. Yamamoto, Y. Tezuka, Topological polymer chemistry: a cyclic approach toward novel polymer properties and functions *Polym. Chem.* **2** (2011) 1930–1939.
90. C. P. Higgins, R. G. Luthy, Sorption of perfluorinated surfactants on sediments, *Environ. Sci. Technol.* **40** (2006) 7251–7256.
91. R. Tourir, N. Dkhireche, T.M. Ebn M. Sfaira, O. Senhaji, J.J. Robin, B. Boutevin, M. Cherkaoui, Study of phosphonate addition and hydrodynamic conditions on ordinary steel corrosion inhibition in simulated cooling water, *Mater. Chem. Phys.* **122** (2010) 1–9.
92. S. Park, K. Lian, Y. Gogotsi, Pseudocapacitive behavior of carbon nanoparticles modified by phosphomolybdic acid, *J. Electrochem. Soc.* **156** (2009) A921–A926.
93. Y. Xu, Y. Peng, X. Zheng, K. D. Dearn, H. Xu, X. Hu, Synthesis and tribological studies of nanoparticle additives for pyrolysis bio-oil formulated as a diesel fuel, *Energy* **83** (2015) 80–88.
94. (a) S. Honda, T. Yamamoto, Y. Tezuka, Topology-Directed Control on Thermal Stability: Micelles Formed from Linear and Cyclized Amphiphilic Block Copolymers, *J. Am. Chem. Soc.* **132** (2010) 10251–10253. (b) K. Adachi, S. Honda, S. Hayashi, Y. Tezuka, ATRP–RCM Synthesis of Cyclic Diblock Copolymers, *Macromolecules* **41** (2008) 7898–7903.
95. K. Y. Heo, Y. Y. Kim, Y. Kitazawa, M. Kim, K. S. Jin, T. Yamamoto, M. Ree, Structural

- Characteristics of Amphiphilic Cyclic and Linear Block Copolymer Micelles in Aqueous Solutions, *ACS Macro Lett.* **3** (2014) 233–239.
96. Q. Meng, M. Hashimoto, S. Honda, Y. Tezuka, T. Yamamoto, A. Fujimori, Molecular Arrangement of Organized Molecular Films of Linear and Cyclic Amphiphilic Block Copolymers with Different Shapes, *Trans. Mat. Res. Soc. Jpn.* **39** (2014) 79–83.
97. C. Dietrich, L. A. Bagatolli, Z. N. Volovyk, N. L. Thompson, Lipid rafts reconstituted in model membranes, *Biophys. J.* **80** (2001) 1417–1428.
98. H. J. Kim, E. Chatani, Y. Goto, S. R. Paik, Seed-dependent accelerated fibrillation of alpha-synuclein induced by periodic ultrasonication treatment, *J. Microbiol. Biotechnol* **2007**, *17*, 2027–2032.
99. Y. B. Zhang, Y. W. Tan, H. L. Stormer, P. Kim, Experimental observation of the quantum Hall effect and Berry's phase in graphene, *Nature* **438** (2005) 201–204.
100. T. Yamamoto, Y. Umemura, O. Sato, Y. Einaga, Observation of the Anisotropic Photoinduced Magnetization Effect in Co–Fe Prussian Blue Thin Films Fabricated by Using Clay Langmuir–Blodgett Films as a Template, *J. Am. Chem. Soc.* **127** (2005) 16065–16073.
101. Y. Yin, A. P. Alivisatos, Colloidal nanocrystal synthesis and the organic-inorganic interface, *Nature* **437** (2005) 664–670.
102. K. Ariga, Y. Yamauchi, T. Mori, J. P. Hill, What can be done with the Langmuir-Blodgett

- method? Recent developments and its critical role in materials science, *Adv. Mater.* **25** (2013) 6477–6512.
103. N. Crawford, R. M. Leblanc, CdSe and CdSe(ZnS) quantum dots in 2D: a Langmuir monolayer approach, *Coord. Chem. Rev.* **263-264** (2014) 13-24.
104. M. C. Petty, *Langmuir-Blodgett Films*. Cambridge Univ. Press: New York (1996).
105. K. Ariga, Y. Yamauchi, G. Rydzek, Q. Ji, Y. Yonamine, K. C.-W. Wu, J. P. Hill, Layer-by-layer nanoarchitectonics: invention, innovation, and evolution, *Chem. Lett.* **43** (2014) 36–38.
106. J. Lee, K.-P. Hong, K. Shin, Studies of Nanostructured Polymer Thin Films by Using Neutron Reflection, *Sci. Adv. Mater.* **7** (2015) 830–841.
107. A. Fujimori, H. Hoshizawa, S. Kobayashi, K. Kanai, Y. Ouchi, K. Seki, Layer Structure Estimation of Three-dimensional Crystal and Two-dimensional Molecular Film for Fluorinated Comb Copolymers, *J. Polym. Sci. B, Polym. Phys.* **46** (2008) 534–546.
108. J. B. Peng, G. T. Barnes, I. R. Gentle, The structures of Langmuir-Blodgett films of fatty acids and their salts, *Adv. Colloid Interf. Sci.* **91** (2001) 163–219.
109. Y. Kim, F. Zhao, M. Mitsuishi, A. Watanabe, T. Miyashita, Photoinduced High-Quality Ultrathin SiO₂ Film from Hybrid Nanosheet at Room Temperature, *J. Am. Chem. Soc.* **130** (2008) 11848–11849.
110. M. Ishifuji, M. Mitsuishi, T. Miyashita, Bottom-up Design of Hybrid Polymer

- Nanoassemblies Elucidates Plasmon-Enhanced Second Harmonic Generation from Nonlinear Optical Dyes, *J. Am. Chem. Soc.* **131** (2009) 4418–4424.
111. M. Osada, T. Sasaki, Two-Dimensional Dielectric Nanosheets: Novel Nanoelectronics From Nanocrystal Building Blocks, *Adv. Mater.* **24** (2012) 210–228.
112. F. F. Xu, Y. Ebina, Y. Bando, T. Sasaki, Structural Characterization of (TBA, H)Ca₂Nb₃O₁₀ Nanosheets Formed by Delamination of a Precursor-Layered Perovskite, *J. Phys. Chem. B* **107** (2003) 9638–9645.
113. M. Muramatsu, K. Akatsuka, Y. Ebina, K. Wang, T. Sasaki, T. Ishida, K. Miyake, M. Haga, Fabrication of densely packed titania nanosheet films on solid surface by use of Langmuir-Blodgett deposition method without amphiphilic additives, *Langmuir* **21** (2005) 6590–6595.
114. A. Fujimori, H. Hoshizawa, S. Kobayashi, N. Sato, K. Kanai, Y. Ouchi, Highly Ordered and Stable Layered “Polymer Nanosheets” Constructed with Amorphous Side-Chains and π - π Stacking of Functional Groups in Ternary Comb Copolymers, *J. Phys. Chem. B* **114** (2010) 2100–2110.
115. A. Fujimori, Y. Kaneko, T. Kikkawa, S. Chiba, Y. Shibasaki, Fabrication and Structure of "Polymer Nanosphere Multilayered Organization", *J. Colloid Interf. Sci.* **418** (2014) 338–349.
116. A. Fujimori, N. Sato, S. Chiba, Y. Abe, Y. Shibasaki, Surface Morphological Changes in

- Monolayers of Aromatic Polyamides Containing Various N-alkyl Side-Chains, *J. Phys. Chem. B* **114** (2010) 1822–1835.
117. N. R. Greiner, D. S. Phillips, J. D. Johnson, F. Volk, Diamonds in detonation soot, *Nature* **333** (1988) 440–442.
118. Y. Kasahara, Y. Guo, T. Tasaki, Q. Meng, M. A. A. Mamun, M. Iizuka, S. Akasaka, A. Fujimori, Nano-dispersion in transparent polymer matrix with high melting temperature contributing to hybridization of heat-resistant organo-modified nanodiamond, *Polym. Bull.* **75** (2018) 4145–4163.
119. A. Fujimori, N. Honda, H. Iwashia, Y. Kaneko, S. Arai, M. Sumita, S. Akasaka, Formation and structure of fine multi-particle layered organo-modified zirconium dioxides fabricated by Langmuir-Blodgett technique, *Colloids Surf. A* **446** (2014) 109–117.
120. G.L. Gaines, Jr., Insoluble monolayers at liquid gas interfaces, Wiley, New York, (1966).
121. K. Blodgett, Monomolecular films of fatty acids on glass, *J. Am. Chem. Soc.* **56** (1934) 459–460.
122. A. Fujimori, T. Araki, H. Nakahara, E. Ito, M. Hara, H. Ishii, Y. Ouchi, K. Seki, In-plane X-ray diffraction and polarized NEXAFS spectroscopic studies on the organized molecular films of fluorinated amphiphiles with vinyl groups and their comb-polymers, *Chem. Phys. Lett.* **349** (2001) 6–12.
123. A. Fujimori, Y. Sugita, H. Nakahara, E. Ito, M. Hara, N. Matsuie, K. Kanai, Y. Ouchi, K.

- Seki, Change of molecular packing and orientation from monolayer to multilayers of hydrogenated and fluorinated carboxylate studied by in-plane X-ray diffraction together with NEXAFS spectroscopy at C K-edge, *Chem. Phys. Lett.* **387** (2004) 345–351.
- 124 T. Tasaki, Y. Guo, H. Machida, Q. Meng, S. Akasaka, A. Fujimori, Nano-dispersion of Fluorinated Phosphonate-Modified Nanodiamond in Crystalline Fluoropolymer Matrix of Polymer/Nanofiller Transparent Hybrid, *Polym. Compos.*, **39** (2018) in press. (DOI: 10.1002/pc.25047)
125. R. Matsuno, K. Yamamoto, H. Otsuka, A. Takahara, Polystyrene- and poly(3-vinylpyridine)-grafted magnetite nanoparticles prepared through surface-initiated nitroxide-mediated radical polymerization, *Macromolecules* **37** (2004) 2203–2209.
126. T. Hasegawa, T. Shomoaka, N. Shioya, K. Morita, M. Sonoyama, T. Takagi, T. Kanamori, Stratified dipole-arrays model accounting for bulk properties specific to perfluoroalkyl compounds, *ChemPlusChem* **79** (2014) 1421–1425.
127. N. Aiba, Y. Sasaki, J. Kumaki, Strong compression rate dependence of phase separation and stereocomplexation between isotactic and syndiotactic poly(methyl methacrylate)s in a Langmuir monolayer observed by atomic force microscopy, *Langmuir* **26** (2010) 12703–12708.
128. H. P. Klug, L. E. Alexander, *X-ray Diffraction Procedures*. John Wiley and Sons: New York (1974).

<< Publication Lists >>

1. Original Papers (11 papers)

- 1) H. Machida, Y. Abiko, S. Hirayama, Q. Meng, S. Akasaka, A. Fujimori,* “Correlation Between Nanodispersion of Organo-Modified Nanodiamond in Solvent and Condensed Behavior of Their Organized Particle Films.”, *Colloids Surf. A*, **2018**, in press.
- 2) Y. Guo, K. Fukushi, S. Hirayama, H. Machida, Q. Meng, S. Akasaka, A. Fujimori,* “Thermal stability of ordered multi-particle layers of long-chain phosphonate-modified nanodiamond with superior heat-resistance.”, *Colloids Surf. A*, **2018**, 556, 227–238.
- 3) Y. Kasahara, Y. Guo, T. Tasaki, Q. Meng, M. Iizuka, S. Akasaka, A. Fujimori,* “Nano-dispersion in Transparent Polymer Matrix with High Melting Temperature Contributing to Hybridization of Heat-resistant Organo-modified Nanodiamond.”, *Polym. Bull.* **2018**, 75(9), 4145–4163.
- 4) T. Tasaki, Y. Guo, Q. Meng, M. A. A. Mamun, Y. Kasahara, S. Akasaka, A. Fujimori,* “Dependency of Nanodiamond Particle Size and Outermost-Surface Composition on Organo-Modification - Evaluation by Formation of Organized Molecular Films and Nano-Hybridization with Organic Polymers -”, *ACS Appl. Mater. Interf.*, **2017**, 9(16), 14379–14390.
- 5) Q. Meng, S. Honda, Y. Tezuka, T. Yamamoto, A. Fujimori, “Topological "Interfacial" Polymer Chemistry -Dependency of Polymer "Shape" on Surface Morphology and Stability of Layer Structures when Heating Organized Molecular Films of Cyclic and Linear Block Copolymers of Butyl Acrylate-Ethylene Oxide-”, *J. Polym. Sci. B, Polym. Phys.*, **2016**, 54, 486–498.
- 6) A. Fujimori,* T. Kikkawa, Q. Meng, Y. Shibasaki, “Control of Fine Structure in "Polymer Nanosphere Multilayered Organization" and Enhancement of Its Optical Property”, *Langmuir*, **2015**, 31, 9177–9181.

- 7) M. A. A. Mamun, Y. Soutome, Q. Meng, A. Fujimori,* “Flexible Transparent Fluorinated Nanohybrid with Innovative Heat-resistance Property -New Technology Proposal for Fabrication of Transparent Materials using "Crystalline" Polymer-”, *J. Polym. Sci. B, Polym. Phys.*, **2015**, 53(23), 1674–1690.
- 8) M. A. A. Mamun, Y. Soutome, Y. Kasahara, Q. Meng, S. Akasaka, A. Fujimori,* “Fabrication of Transparent Nanohybrids with Heat Resistance using High-density Amorphous Formation and Uniform Dispersion of Nanodiamond.”, *ACS Appl. Mater. Interf.*, **2015**, 7(32), 17792–17801.
- 9) Q. Meng, N. Honda, S. Uchida, K. Hashimoto, H. Shibata, A. Fujimori,* “Giant Two-dimensional Zinc Oxide Nanodisc Crystal Creation Using Single-Particle Layer of Organo-modified Inorganic Fine Particles.”, *J. Colloid Interf. Sci.*, **2015**, 453, 90–99.
- 10) Q. Meng, M. Hashimoto, S. Honda, Y. Tezuka, T. Yamamoto, A. Fujimori*, “Molecular Arrangement of Organized Molecular Films of Linear and Cyclic Amphiphilic Block Copolymers with Different Shapes.”, *Trans. Mat. Res. Soc. Jpn.*, **2014**, 39(1), 79–82.
- 11) M. Hashimoto, Q. Meng, S. Honda, Y. Tezuka, T. Yamamoto, A. Fujimori*, “Dependency of the Molecular "Shape" on Surface Morphology of Organized Molecular Films of Cyclic and Linear Block Copolymer of Polyethylene Oxide – Butyl Acrylate.”, *Trans. Mat. Res. Soc. Jpn.*, 39(1), **2014**, 83–86.
- *12) Q. Meng, S. Honda, Y. Tezuka, T. Yamamoto, A. Fujimori, “Fabrication of Phase diagrams of Organized Molecular Films of "Topological" Cyclic and Linear Block Copolymers of Butyl Acrylate-Ethylene Oxide.”, **2018**, in preparation.

Review Article

1. 孟起, 藤森厚裕, ” Dependency of Polymer "Shape" on Morphology and Stability of Layer Structures of Organized Molecular Films of Cyclic and Linear Block Copolymers of

Butyl Acrylate–Ethylene Oxide”(高分子トポロジー"界面"化学の提案), *Annual Report, The 120th Committee, Japan Society for the Promotion of Science*, (Japanese), **2015**, 66, 65-68.

2. Conference Presentation 【24 件】

International Conference 【1 件】

1. 「Molecular Arrangement of Organized Molecular Films of Linear Cyclic Amphiphilic Block Copolymers with Different Shapes 」
Qi Meng, Msamichi Hashimoto, Satoshi Honda, Takuya Yamamoto, Yasuyuki Tezuka, Atsuhiko Fujimori, The 15th IUMRS International Conference in Asia, Fukuoka University, 28 August 2014(poster)

Domestic Conference 【23 件】

1. 「表面有機化ナノダイヤモンドの溶剤中ナノ分散と その界面粒子膜形成」
町田 大樹, 孟 起, 藤森 厚裕, 平成 30 年度 繊維学会秋季研究発表会, 福井大学, 2018 年 11 月 1 日(poster)
2. 「有機化ナノダイヤモンド粒子の溶媒中ナノ分散と組織粒子膜凝集挙動の相関」
町田 大樹, 孟 起, 多田 亜喜良, 山本 拓海, 中島 達貴, 設楽 裕治, 藤森 厚裕, 第 69 回コロイドおよび界面化学討論会, 筑波大学, 2018 年 9 月 18 日(oral)
3. 「表面修飾有機化無機ナノ粒子の溶剤中ナノ分散とその単粒子膜形成挙動：潤滑剤応用に向けて」
町田 大樹, 孟 起, 藤森 厚裕, 第 67 回高分子討論会, 北海道大学, 2018 年 9 月 13 日(oral)
4. 「種々の表面改質鎖を用いたナノダイヤモンドの溶液中分散性と水面上単分子膜挙動」
町田 大樹, 孟 起, 郭 毅飛, 藤森 厚裕, 日本化学会第 98 春季年会, 日本大学理工学部, 2018 年 3 月 21 日(oral)
5. 「潤滑油応用を志向した無機ナノ粒子の表面改質効果—溶媒中定常ナノ分散の試

- みと単粒子層化キャラクターゼーション」
孟起, 町田 大樹, 多田 亜喜良, 山本 拓海, 中島 達貴, 設楽 裕治, 藤森 厚裕,
第 68 回コロイドおよび界面化学討論会, 神戸大学鶴甲第一キャンパス, 2017 年
9 月(poster).
6. 「耐熱性表面改質ナノダイヤモンドによる組織粒子膜化と高分子マトリックス中におけるナノ分散」
郭 毅飛, 田崎 平, 孟起, 赤坂 修一, 藤森 厚裕, 第 66 回高分子年次大会, 幕張メッセ, 2017 年 5 月(poster)
 7. 「含高密度非晶鎖・結晶性透明ポリマー/ナノカーボン複合体創出に資する粒子表面の耐熱性表面修飾」
田崎 平, 孟起, 郭 毅飛, 赤坂 修一, 藤森 厚裕, 第 66 回高分子年次大会, 幕張メッセ, 2017 年 5 月(oral)
 8. 「表面改質ナノダイヤモンドの機能革新 –溶媒中ナノ分散と単粒子膜形成–」
孟起, 田崎 平, 赤坂 修一, 藤森 厚裕, 第 66 回高分子年次大会, 幕張メッセ, 2017 年 5 月(poster)
 - 9 「高融点透明樹脂とのナノ複合化を志向した耐熱性有機化ナノダイヤモンドの開発と組織化膜の手法によるそのキャラクターゼーション」
郭 毅飛, 田崎 平, 孟起, 赤坂 修一, 藤森 厚裕, 日本化学会第 97 春季年会, 慶応大学日吉キャンパス, 2017 年 3 月(oral)
 10. 「高密度非晶鎖を含む結晶性透明ポリマー/ナノカーボン複合体創出に資するナノダイヤモンドの耐熱性表面改質」
田崎 平, 郭 毅飛, 孟起, 赤坂 修一, 藤森 厚裕, 日本化学会第 97 春季年会, 慶応大学日吉キャンパス, 2017 年(oral)
 11. 「有機化ナノダイヤモンド界面単粒子膜形成に資する汎用有機溶媒中へのナノ分散化技術の確立」
孟起, 田崎 平, 赤坂 修一, 藤森 厚裕, 第 97 春季年会, 3B4-32, 慶応義塾大学 日吉キャンパス, 2017 年 3 月.(oral)
 12. 「ナノダイヤモンドの表面改質に基づく結晶性高分子中へのナノ分散挙動」
田崎 平, Muhammad Abdullah Al Mamun, 孟起, 郭 毅飛, 赤坂 修一, 藤森 厚裕, 第 65 回高分子討論会, 神奈川大学, 2016 年 9 月(oral)

13. 「高分子トポロジー”界面”化学の提案」
孟起, 本多 智, 手塚 育志, 山本 拓矢, 藤森 厚裕, 第 25 回日本 MRS 年次大会, 横浜開港記念会館 2015 年 12 月 9 日(oral)
14. 「トポロジカル高分子の組織膜における層状秩序の熱変化」
孟起, 手塚 育志, 山本 拓矢, 藤森 厚裕, 第 64 回 高分子学会年次大会 札幌コンベンションセンター 2015 年 5 月 28 日(oral)
15. 「直鎖状, 並びに環状両親媒性ブロック共重合体組織化膜の層状秩序に対する疎水鎖長依存性」
孟起, 手塚 育志, 山本 拓矢, 藤森 厚裕, 日本化学会 第 95 春季大会, 日本大学理工学部 船橋キャンパス, 2015 年 3 月 26 日(oral)
16. 「超薄分子組織膜の高分子トポロジー化学」
孟起, 橋本 真道, 手塚 育志, 山本 拓矢, 藤森 厚裕, 第 63 回高分子討論会, 長崎大学 文教キャンパス, 2014 年 9 月 24 日(oral)
17. 「二次元分子膜の形態と分子配列に及ぼす“高分子トポロジー”効果」
孟起, 橋本 真道, 手塚 育志, 山本 拓矢, 藤森 厚裕, 第 65 回コロイドおよび界面化学討論会, 東京理科大学 神楽坂キャンパス, 2014 年 9 月 3 日(oral)
18. 「界面組織膜に機能性変化をもたらす方法論: 高分子トポロジー効果に基づいて」
孟起, 橋本 真道, 手塚 育之, 山本 拓矢, 藤森 厚裕, 第 63 回 高分子学会年次大会, 名古屋国際会議場, 2014 年 5 月 28 日(poster)
19. 「界面分子膜における高分子トポロジー効果 —分子の「かたち」が組織膜形成に及ぼす影響—」
孟起, 橋本 真道, 本多 智, 手塚 育之, 山本 拓矢, 藤森 厚裕, 第 63 回 日本化学会 第 94 春季年会, 名古屋大学 東山キャンパス, 2014 年 3 月 29 日 (oral)
20. 「両親媒性環状, ならびに直鎖状高分子組織化膜の分子配列と耐熱挙動の相関性評価」
孟起, 橋本 真道, 本多 智, 手塚 育之, 山本 拓矢, 藤森 厚裕, 第 23 回日本 MRS 年次大会, 横浜開港記念会館 2013 年 12 月(poster)
21. 「高分子トポロジー効果を二次元界面膜で議論する-分子配向と単分子膜形態の視点から-」
橋本 真道, 孟起, 本多 智, 手塚 育之, 山本 拓矢, 藤森 厚裕, 第 62 回高分子

討論会，金沢大学角間キャンパス，2013年9月(oral)

22. 「ポリエチレンオキシド-ブチルアクリレート環状，並び直鎖状ブロック共重合体組織化膜中の分子配向における「かたち」の依存性」

橋本 真道，孟 起，本多 智，手塚 育之，山本 拓矢，藤森 厚裕，第 23 回日本 MRS 年次大会，横浜開港記念会館，2013 年 12 月(oral)

23. 「ポリエチレンオキシド-ブチルアクリレート環状，並び直鎖状ブロック共重合体組織化膜中の分子配向における「かたち」の依存性」

橋本 真道，孟 起，本多 智，手塚 育之，山本 拓矢，藤森 厚裕，第 64 回コロイドおよび界面化学討論会，名古屋工業大学，2013 年 9 月(oral)

Acknowledgements

～ 謝 辞 ～

本博士論文を完成するにあたり、6年間ご指導賜りました、藤森 厚裕 准教授に厚く御礼申し上げます。加えまして、副査として本論文をご審査頂きました、松岡 浩司 教授、本多 善太郎 准教授、鈴木 美穂 准教授に心からお礼申し上げます。

ナノダイヤモンドサンプルをご提供頂きました、株式会社ダイセル 主任研究員の梅本 浩一 氏、城 大輔 博士に感謝申し上げます。加えまして、有機修飾ナノダイヤモンドの溶媒中ナノ分散の研究に於いて、有効な議論をして頂いた JXTG エネルギー株式会社の設楽 裕治 博士、多田 亜喜良 博士、山本 拓海 氏、中島 達貴 氏に心からお礼申し上げます。加えまして、DLS 測定でご助力賜りました、東洋大学 鶴飼 智史 准教授にお礼を申し上げます。

また、トポロジカル高分子試料を頂戴しました、北海道大学 山本 拓矢 准教授、東京工業大学 手塚 育志 教授、東京大学 本多 智 博士に感謝申し上げます。

研究の進行に於いて、特にお世話になりました、藤森研究室の町田 大樹さん、郭 毅飛さん、平山 周平さんに心からのお礼を申し上げます。また、共に研究に励んだ藤森研究室の皆さん、OB、OGの皆さんに感謝申し上げます。

最後になりますが、私を日本に送り出し、就学を支えて下さいました、両親と親族に心からの感謝を送ります。この日本での学習と研究生活の経験を活かし、今後の社会人生活を充実したものにしていきたいと思っております。

ありがとうございました.

平成 31 年 3 月 浅春

(初稿提出・平成 30 年 12 月)

孟 起